Physics – Uspekhi **42** (9) 887 – 916 (1999) ©1999 Uspekhi Fizicheskikh Nauk, Russian Academy of Sciences

REVIEWS OF TOPICAL PROBLEMS PACS numbers: 61.72.Bb, 62.20.Fe, **83.50.–v**

Dislocation self-organization processes and crystal plasticity

G A Malygin

Contents

1. **Introduction** **887**
2. **Equations of evolution of a dislocation ensemble** **889**
   2.1 Basic equations; 2.2 Microscopic equations; 2.3 Problem of averaging a dislocation ensemble; 2.4 Equations of evolution of the density of dislocations
3. **Strain-hardening curves of crystals** **892**
   3.1 Multistage nature of strain-hardening curves; 3.2 Size, orientational, and surface effects
4. **Slip lines and bands** **897**
   4.1 Correlation effects; 4.2 Double cross slip and equations of evolution of dislocation density; 4.3 Slip lines; 4.4 Slip bands; 4.5 Annihilation channels
5. **Cellular dislocation structure** **906**
   5.1 Equation of evolution of dislocation density in the case of multiple slip; 5.2 Cellular structure and its parameters; 5.3 Self-similarity of cellular structures; 5.4 Formation of a cellular structure in polycrystalline materials
6. **Conclusion** **911**

Appendices **912**
I. Statistical averaging of a dislocation ensemble; II. Correlation stress

References **913**

Abstract. The theoretical treatment of the evolution of a dislocation ensemble in a plastically deformed real crystal is discussed. Kinetic equations for the dislocation density are formulated which include elementary dislocation processes (source generation, immobilization, multiplication, annihilation, and diffusion) and on the basis of which the first three stages of the crystal's strain-hardening curves are quantitatively analyzed. Dislocation self-organization processes leading to slip localization and various nonuniform dislocation structures are considered. Mechanisms of the formation of slip lines, slip bands, defect-free (annihilation) channels in neutron-irradiated or quenched crystals, and dislocation cellular structures are discussed in detail based on the equations obtained. A comparison of theoretical results with experimental data is made.

1. Introduction

The modern physics of strength and plasticity of crystals is based on the discoveries made in 1920 – 30s, the time when the concepts were formulated of the elementary carriers of plastic deformation and defects determining (reducing) the strength of crystals: dislocations [1, 2], microcracks [3, 4], and vacancies [5]. In the 1970s these were supplemented by the concept of disclinations [6 – 8]. The results of intensive experimental and theoretical studies of the properties of defects, dating back to the 1950s and 60s, formed the substance of the new chapters of solid state physics: the physics of the strength and plasticity of crystals, and the physics of defects in crystals.

These studies have been summarized in a large number of monographs [8 – 16] and reviews [17 – 25], as well as important publications in *Usp. Fiz. Nauk* [26 – 33]. They provided physical validation for the widely used methods for improving the strength of structural materials, and for the theoretical basis for creating new materials with better deformation and strength properties.

By the mid-1970s, however, it became clear that a theory that is based on the properties of individual defects and simple models of their interactions is not capable of explaining the entire diversity of strength and deformation properties of real materials, and cannot account for such features as the multistage nature of strain-hardening curves [17, 19 – 22, 34], localization of plastic deformation as a system of slip lines and bands [34 – 42], formation of various dislocation structures (cells [43 – 49], blocks [50, 51], disoriented structures [52 – 55], fragmented structures [56], annihilation structures [57 – 59], and structures specific to the mechanical fatigue of crystals [60 – 62]).

This list ought to be supplemented by the formation (on the macroscopic level) of Lüders [63, 64] and Portevin – Le Châtelier [65, 66] regions (bands) of inhomogeneous plastic deformation, Danilov – Zuev deformation waves [67, 68], adiabatic shear bands in the case of low-temperature deformation and high-strain-rate deformation [71, 72], super-localization of deformation in the form of coarse slip lines when the crystal is loaded at elevated temperatures [34, 73], unstable (serrated) stress – strain diagrams [65, 66, 69, 70],

G A Malygin A F Ioffe Physico-Technical Institute,
Russian Academy of Sciences,
ul. Politekhnicheskaya 26, 194021 St. Petersburg, Russian Federation
Tel. (7-812) 247 91 57
E-mail: malygin.ga@pop.ioffe.rssi.ru

Received 5 April 1999, revised 4 June 1999
Uspekhi Fizicheskikh Nauk **169** (9) 979 – 1010 (1999)
Translated by A S Dobroslavskiĭ; edited by S N Gorin

which are an indication of the spatial and temporal instability of plastic deformation and the development of regimes of critical self-organization and deterministic chaos [74 – 76].

Along with the traditional optical techniques [34 – 40], extensively used were various microscopic techniques (replicas [37, 38], selective etching [41, 42], and transmission electron microscopy [43 – 49]. The results lead to the conclusion that the observed diversity of deformation and dislocation structures derives from the natural evolution of the dislocation ensemble, dependent on the crystal structure and the deformation conditions, and the development of collective, cooperative phenomena.

This necessitated the construction of the theory of dislocation ensembles in crystals subjected to plastic deformation, and the formulation of the kinetic equations for describing the space – time evolution given the real deformation condition. The first attempts to express such equations as a kinetic equation for homogeneous density of dislocations as function of time [77 – 79] or current strain [80 – 82] date back to the 1960s. Although these equations were rather heuristic, and based on intuitive assumptions, they demonstrated the existence of a fundamental relationship between the evolution of the density of dislocations (the processes of multiplication and annihilation of dislocations) with the kinetics of high-temperature creep [77], with the shape of the curve of strain hardening [82], and with the 'tooth' (yield point) in the deformation diagrams of low-dislocation crystals [80].

Subsequently these equations were augmented with terms accounting for the spatially inhomogeneous distribution of dislocations in crystals. Such extended equations were used for analyzing the emergence of spatially inhomogeneous dislocation structures (cells [84], tangles [85 – 87]), and the localization of deformation in the form of bands of adiabatic shear and heating when the crystals were stressed at helium temperatures (~ 4.2 K) [88, 89].

Concurrently with the model treatment, a theoretically more consistent approach to the formulation of dislocation kinetic equations based on the statistical averaging of dynamic and kinematic relations that describe the state and motion of dislocations in the dislocation ensemble [90 – 97] was also developed. The results will be discussed in Section 2.1.

The next major step in formulating the equations of evolution of a dislocation ensemble was made in the mid-1980s. Following the recognition of the synergetic nature of self-organization of thermodynamically nonequilibrium (dissipative) structures in various physical [98 – 100], chemical [101] and biological [102 – 104] systems, the synergetic approach was also applied to the dislocation ensemble. The equations of evolution were expressed as a system of nonlinear reaction – diffusion equations in the densities of mobile and immobile dislocations [105 – 113]. The kinetic interaction between these resulted in the loss of spatial stability by the dislocation ensemble, and gave rise to inhomogeneous dislocation structures in the crystal [114 – 118].

Equations of this type were formulated for the densities of dislocations of different signs [106, 119 – 123], dislocations in intersecting slip systems [116, 124], and for a dislocation–disclination ensemble [125 – 128]. Although the equations took into account the processes of multiplication, diffusion, immobilization, and annihilation of dislocations that control the actual evolution of a dislocation ensemble, the main purpose of most authors was to announce the possibility of analyzing some or other of the above-mentioned phenomena from the standpoint of synergetics. Because of this, most of the theoretical results are qualitative by nature, and cannot be used for making direct comparisons with experiment.

Such comparison, however, is very important, inasmuch as it may help us to understand to what extent it is the kinetic processes, including the processes of self-organization of dislocations, that determine the formation of various dislocation and deformation structures in crystals, as well as the character and the multistage nature of curves of strain hardening of crystals.

In this review we build on the works where such a comparison has been made, and critically evaluate the available results of statistical averaging of dislocation ensembles, to demonstrate that the kinetic processes are definitive for the phenomena discussed here.

The review is formatted as follows. In Section 2, we give the main equations and relations of the continuum theory of dislocations, and outline the procedure for statistical averaging of dislocation ensembles. A simplified procedure is then used for expressing the kinetic equations for the density of dislocations, which cover the principal elementary processes involved in the space – time evolution of a dislocation ensemble in real crystals.

In Section 3, under the assumption of homogeneous distribution of dislocation density, we see how these equations agree with the typical three-stage curve of strain hardening of crystals at the temperatures $T < 0.5T_{\mathrm{m}}$, where T_{m} is the melting temperature.

In Section 4, we use the equations of Section 2 for analyzing the process of formation of slip lines and bands at the initial stage of plastic deformation of crystals (in the case of single slip). We also consider the special cases of localization of deformation in the form of coarse slip lines resulting from the dislocation-free and defect-free channels in the case of plastic deformation of metal crystals subjected to irradiation, quenching, or deformation at a low temperature.

In Section 5, we use our equations for analyzing the mechanism of formation of a cellular dislocation structure in the case of multiple slip, and consider the particular features of formation of dislocation structures in polycrystalline materials.

In this discussion, we assume that the dislocation ensemble contains an equal number of dislocations with opposite signs of the Burgers vector. Because of space limitations, we do not discuss here the mechanism of formation of misoriented and fragmented dislocation structures associated with the presence of excess (noncompensated) density of dislocations of one sign. To take into account the effects of incomplete plastic rotations, the equations of the continuum theory of dislocations must be supplemented by equations and relations of the continuum theory of disclinations [6, 94, 129, 130].

In the Conclusion, we summarize our discussion and outline the directions of further study. We also discuss the common features of certain ensembles that, like a dislocation ensemble, consist of linear objects — for example, vortex filaments in hard superconductors [131, 132], or thermal vortices in superfluid helium [133, 134].

To facilitate comparison between theory and experiment, the review contains illustrative material drawn from published results, as well as original results obtained by the author or derived from the experimental data found in literature.

2. Equations of evolution of a dislocation ensemble

On the microscopic level, the plastic deformation of crystals is the result of motion of linear defects — dislocations, and in the more general case dislocations and disclinations. The former are the boundaries of those regions of a crystal where one part of the crystal has experienced a translational shear with respect to another by the Burgers vector **b**, whereas the latter are the boundaries of regions where one part of crystal has experienced a plastic rotation with respect to another by the Frank vector $\mathbf{\Omega}$.

In this way, dislocations are the boundaries of regions of incomplete plastic shear, and disclinations are those of incomplete plastic rotation. The continuum theory of dislocations and disclinations [6, 16, 94, 129, 130], given the distribution of defects in crystal, allows the distribution of fields of stress σ_{ik}, strain ε_{ik}, and strain rate $\dot{\varepsilon}_{ik}$ to be found — that is, the parameters that determine the strength and deformation of the material.

2.1 Basic equations

In the case of a purely dislocation ensemble, there are the following equations and relations:

for the external σ_{ik}^{ext} and internal σ_{ik}^{in} stress

$$\frac{\partial \sigma_{ik}}{\partial x_k} = 0\,, \qquad \sigma_{ik} = \sigma_{ik}^{\text{ext}} + \sigma_{ik}^{\text{in}}\,,$$

$$\sigma_{ik}^{\text{in}} = \int A_{iksp}(r'-r)\,\alpha_{sp}(r',t)\,\mathrm{d}r'\,, \qquad F_l = \epsilon_{lpq} v_p b_s \sigma_{qs}\,; \quad (2.1)$$

for the tensor density of dislocations α_{sp} and its flux J_{lp}

$$\frac{\partial \alpha_{sp}}{\partial t} + \epsilon_{sql}\frac{\partial J_{lp}}{\partial x_q} = 0\,, \qquad \frac{\partial \alpha_{sp}}{\partial x_p} = 0\,, \qquad J_{lp} = \epsilon_{lqs}\alpha_{sp} u_q\,; \quad (2.2)$$

for strains and strain rates (elastic and plastic)

$$\varepsilon_{ik} = \varepsilon_{ik}^{\text{el}} + \varepsilon_{ik}^{\text{pl}}\,, \qquad \varepsilon_{ik}^{\text{el}} = \int B_{iksp}(r'-r)\,\alpha_{sp}(r',t)\,\mathrm{d}r'\,,$$

$$\varepsilon_{ik}^{\text{pl}} = \int \dot{\varepsilon}_{ik}^{\text{pl}}\,\mathrm{d}t\,, \qquad \dot{\varepsilon}_{ik} = \dot{\varepsilon}_{ik}^{\text{el}} + \dot{\varepsilon}_{ik}^{\text{pl}}\,,$$

$$\dot{\varepsilon}_{ik}^{\text{el}} = \int C_{ikml} J_{ml}\,\mathrm{d}r'\,, \qquad \dot{\varepsilon}_{ik}^{\text{pl}} = \frac{1}{2}(J_{ik} + J_{ki})\,. \quad (2.3)$$

In Eqns (2.1)–(2.3), $A_{iksp} = -c_{ikmn}\epsilon_{njs}c_{pjql}G_{qm,l}$, $B_{iksp} = [\epsilon_{sim}c_{lqmp}G_{qk,l}]_{[ik]}$, $C_{ikml} = -c_{njml}[G_{ij,nk}]_{[ik]}$, $G_{qm}(r'-r)$ is the tensor Green's function of the static theory of elasticity of crystals, c_{ikmn} is the tensor of elastic constants, ϵ_{njs} is the commutation tensor, F_l is the force with which external and internal long-range stresses act on the dislocation, v is the unit vector of the tangent to the dislocation line, u is the dislocation velocity, and $\alpha_{sp} = \sum_a \alpha_{sp}^a$ is the tensor density of dislocations with different Burgers vectors.

In Eqn (2.1), we have neglected the dynamic components of external and internal stress because the movement of dislocations in the case of ordinary plastic deformation is predominantly quasistatic in nature: force F acting on the dislocation is balanced out by the force of friction $\mathbf{F}^{(\text{f})} = \xi b\sigma^{(\text{f})}$ resulting from the interaction of a moving dislocation with the Peierls relief [15], with point obstacles such as the impurity atoms [13], or with the 'dislocation forest' [21, 24]. A dislocation moving at a high (super-barrier) velocity experiences viscous friction due to the interaction with the electron [30] and phonon [32] subsystems of the crystal.

As a result, the equation of balance of stresses applied to the dislocation with Burgers vector b^a is (superscript a is dropped):

$$n_i(\sigma_{ik}^{\text{ext}} + \sigma_{ik}^{\text{in}})b_k = b\sigma^{(\text{f})}\,, \qquad \sigma^{(\text{f})} = \sigma^*(u,T) + \sigma_{\text{f}} + \sigma_\mu\,. \quad (2.4)$$

Here $\mathbf{n} = v \times \xi$ is the unit vector to the slip plane of the dislocation (ξ being the unit vector normal to the direction of motion of the dislocation), $b = |\mathbf{b}|$.

The friction stress $\sigma^{(\text{f})}$ is contributed to by the effective stress σ^* which depends on the velocity of the dislocation and the temperature T, by the athermal component of friction stress σ_{f} resulting from the interaction of dislocation with point obstacles or Peierls relief, and by the deformation (dislocation) hardening of crystal σ_μ which depends on the scalar density of dislocations.

The stress of viscous drag of a dislocation moving at a high velocity ($u > 10^{-3}u_{\text{s}}$) is a linear function of the velocity $\sigma_{\text{v}} = (B/b)u$, where u_{s} is the speed of sound, and B is the coefficient of viscous drag [30, 32]. According to Eqn (2.4), the velocity of thermally activated motion of a dislocation is

$$u = \xi u\,, \qquad u = u_{\text{s}}\exp\left[-\frac{H(\sigma^*)}{kT}\right],$$

$$\sigma^* = n_i(\sigma_{ik}^{\text{ext}} + \sigma_{ik}^{\text{in}})\,b_k|\mathbf{b}|^{-1} - \sigma_{\text{f}} - \sigma_\mu\,, \quad (2.5)$$

where $H(\sigma^*)$ is the activation energy, and k is the Boltzmann constant.

Thus, knowing the distribution of the density of dislocations $\hat{\alpha}(\mathbf{r},t)$, we can use the equations of motion (2.4), (2.5) for finding the flux of dislocations $\hat{J}(\mathbf{r},t)$, and Eqns (2.1) and (2.3) for finding the distribution of stress, strain, and the strain rate.

As pointed out in the Introduction, in the case of plastic deformation of real crystals, the dislocation ensembles undergo a sophisticated evolution that depends on the internal structure of the crystal and on the deformation conditions. Since the equations of continuum theory of dislocations have been derived for a structureless continuum of geometric points, they are not capable of describing this evolution and establishing the physical scale of the phenomena. This requires considering the dislocation ensemble in the crystal as a set of discrete particles (dislocations) possessing individual physical parameters (Burgers vector, velocity, orientation of the dislocation line). The interaction between the particles, or between particles and other important (in the sense of their effect on the evolution of the dislocation ensemble) structural features is definitive for the space and time scales of the processes.

The standard approach to the solution of such a 'many-body problem' is to introduce the distribution function of particles with respect to some principal dynamic parameters (coordinates, velocities), to formulate the kinetic equation, and to perform statistical averaging of the ensemble with the purpose of expressing the equations of motion in the statistical means [134–138]. This obvious method for constructing the equations of evolution of a dislocation ensemble has been employed by some authors. For example, in Ref. [90] the model of a one-dimensional laminar flow of a 'dislocation liquid' and the one-particle function of distribution of dislocations with respect to velocities were used for expres-

sing the equation of evolution of dislocation density which took into account the dynamic effects — that is, the inertial (field) mass of dislocations. A similar result for the three-dimensional 'Coulomb gas' of dislocations was obtained in Refs [91, 94].

Note that, in view of the small mass of dislocations, the inclusion of the dynamic effects is apparently interesting only in the case of high-speed (shock) deformation of materials. Under ordinary loading conditions, the motion of a dislocation is quasistatic in nature. The main contribution to the evolution of a dislocation ensemble comes not from the dynamic but from the kinematic effects related to the processes of generation of dislocations at dislocation sources, multiplication of dislocations, diffusion, annihilation, correlation, and polarization. For example, using the two-particle function of distribution of dislocations with respect to coordinates it was possible to analyze the effect of shielding of dislocations of one sign by dislocations of the opposite sign in a two-dimensional ensemble of screw dislocations [139, 140].

As regards other elementary processes that determine the evolution of a dislocation ensemble, the relevant 'collision terms' were mainly expressed from phenomenological and heuristic considerations, using the two-dimensional statement of the problem. The exception is Ref. [52], where the microscopic approach was used for expressing the 'collision integral' responsible for the multiplication of dislocations on such obstacles as disperse particles and inclusions.

2.2 Microscopic equations

To illustrate the difficulties encountered with the three-dimensional model of the dislocation ensemble and set the guidelines for a consistent expression of kinematic 'collision' terms in the three-dimensional statement of the kinetic problem, let us consider in greater detail Eqn (2.2) for the tensor density of dislocations and its flux.

The first equation in (2.2) is the equation of conservation of the Burgers vector [16]. Since the Burgers vector in crystals is constant along the dislocation line, this equation is simply a kinematic relation that reflects the fact that dislocations move as lines rather than points [141].

Observing that an individual dislocation loop is a dislocation ensemble with the density of dislocations $\alpha^a_{sp} = b^a_s\,\delta_p(\mathbf{l}^a)$ [6], where $\delta(\mathbf{l})$ is the delta function defined on the directional line of a dislocation [142], we rewrite Eqn (2.2) for clarity in vector form, dropping the constant vector b (the 'mechanical charge' of dislocation) and superscript a:

$$\frac{\partial\delta(\mathbf{l})}{\partial t} + \nabla\times\big(\mathbf{u}\times\delta(\mathbf{l})\big) = 0\,, \qquad \nabla\cdot\delta(\mathbf{l}) = 0\,. \tag{2.6}$$

Transforming the triple vector product, we obtain the equation of conservation of density of the directional dislocation line, which includes a transport part and an inhomogeneous part:

$$\frac{\partial\delta(\mathbf{l})}{\partial t} + \nabla\cdot\big(\mathbf{u}\,\delta(\mathbf{l})\big) = \mathbf{u}\nabla\cdot\delta(\mathbf{l}) + \big(\delta(\mathbf{l})\,\nabla\big)\,\mathbf{u}\,, \qquad \nabla\cdot\delta(\mathbf{l}) = 0\,. \tag{2.7}$$

The terms on the right-hand side of this equation account for the change in length and orientation of the dislocation line and its individual segments as it moves along.

The condition $\nabla\cdot\delta(\mathbf{l}) = 0$ implies that the dislocation line either is closed or ends at the surface. If it lands on the Frank – Read dislocation source with a critical length l_{F}, then $\nabla\cdot\delta(\mathbf{l}) = l_{\mathrm{F}}^{-1}\,\delta(l_{\mathrm{F}})$, where $\delta(l)$ is a delta function defined on a nondirectional dislocation line [6, 142]. We may symbolically assume that $\delta_p(\mathbf{l}) = v_p\,\delta(\mathbf{l})$ (where v is the unit vector tangent to the dislocation line, introduced above).

The gradient of velocity of the dislocation in the direction of the tangent to the dislocation line on the right-hand side of the first equation in Eqn (2.7) describes the change in orientation and length of the dislocation owing to the presence of an inhomogeneous external and internal (long-range, local, and stochastic) fields of stresses that affect the direction of motion of dislocation and its velocity: $\big(\delta(\mathbf{l})\,\nabla\big)\,\mathbf{u} = \delta(\mathbf{l})\,\partial\mathbf{u}/\partial l$.

On the strength of Eqn (2.5) and arguments developed above, the equation of evolution of directional segments of a dislocation loop of arbitrary shape may be expressed on the microscopic level in the explicit form [141]:

$$\begin{aligned}\frac{\partial\delta(\mathbf{l})}{\partial t} + \nabla\cdot\big(\mathbf{u}\,\delta(\mathbf{l})\big) &= \frac{\mathbf{u}_{\mathrm{F}}}{l_{\mathrm{F}}}\,\delta(l_{\mathrm{F}}) + \frac{u}{R_v}\,\delta(\mathbf{l}) \\ &\quad + \frac{\partial\ln u}{\partial l}\,\mathbf{u}\,\delta(l) + \mathbf{n}\,\frac{u}{R_n}\,\delta(l)\,, \\ R_v^{-1} = \left(\frac{\partial\mathbf{v}}{\partial l}\,\frac{\partial\mathbf{v}}{\partial l}\right)^{1/2}, &\qquad R_n^{-1} = \left(\frac{\partial\mathbf{n}}{\partial l}\,\frac{\partial\mathbf{n}}{\partial l}\right)^{1/2}.\end{aligned} \tag{2.8}$$

Here R_v and R_n are the radius of curvature and the radius of 'spiraling' of the dislocation line.

As follows from Eqn (2.8), the radius of spiraling is finite if the dislocation line evolves in space passing from the initial plane into a non-coplanar plane, with the unit vector normal to the slip plane changing in the direction of the dislocation line.

The 'relaxation' processes on the right-hand side of Eqn (2.8) have the following characteristic times: $\tau_{\mathrm{F}} = l_{\mathrm{F}}/u_{\mathrm{F}}$ is the action time of the Frank – Read source; $\tau_v = R_v/u$ is the time of formation of a dislocation segment with radius of curvature of R_v, or a circular loop with that radius; $\tau_n = R_n/u$ is the time in which the length of a segment increases as it goes into the noncoplanar plane.

As regards the relaxation time $\tau_l = (\partial u/\partial l)^{-1} = R_l/u$, it is connected with the change in the orientation of the dislocation line as it moves in the inhomogeneous fields of external and internal stresses. Indeed, since $u = u(\sigma^*)$, from Eqn (2.5) we have [141]

$$R_l^{-1} = \frac{\partial\ln u}{\partial l} = \frac{\partial\ln u}{\partial\sigma^*}\,\frac{\partial\sigma^*}{\partial l}\,, \quad b\,\frac{\partial\sigma^*}{\partial l} = n\cdot\frac{\partial\hat{\sigma}}{\partial l}\cdot b - \frac{\xi\dot{\hat{\sigma}}\dot{b}}{R_n}\,, \tag{2.9}$$

where R_l is a parameter that characterizes the inhomogeneity of the stress field.

Multiplying the first equation in Eqn (2.8) dyadically from the left by $\mathbf{b}$, we obtain the microscopic equation for the tensor density of dislocations

$$\frac{\partial\hat{\alpha}}{\partial t} + \nabla\cdot(\mathbf{u}\hat{\alpha}) = \frac{\mathbf{b}\mathbf{j}_{\mathrm{F}}}{l_{\mathrm{F}}} + \frac{u}{R_v}\,\hat{\alpha} + \frac{\mathbf{b}\mathbf{j}}{R_l} + \frac{\hat{J}}{R_n}\,. \tag{2.10}$$

Here $\mathbf{j} = \mathbf{u}\,\delta(l)$ is the flux of the scalar density of dislocations, $\mathbf{j}_{\mathrm{F}} = \mathbf{u}_{\mathrm{F}}\,\delta(l_{\mathrm{F}})$ is a similar flux from the Frank – Read source, $\hat{J} = \mathbf{b}\big(\mathbf{u}\times\delta(\mathbf{l})\big) = \mathbf{b}\mathbf{n}\mathbf{u}\,\delta(l)$ is the flux of tensor density of dislocations.

Now, when we multiply Eqn (2.8) from the right in scalar manner by the unit vector tangent to the dislocation line $\mathbf{v}$, we obtain the microscopic equation for the nondirectional dislocation line, that is, for its length (the scalar density of

dislocations):

$$\frac{\partial\delta(l)}{\partial t}+\nabla\cdot\mathbf{j}=\frac{\mathbf{j}_{\mathrm{F}}\cdot\mathbf{v}_{\mathrm{F}}}{l_{\mathrm{F}}}+\frac{u}{R_v}\,\delta(l)+(\mathbf{n}'\cdot\mathbf{v})\frac{u}{R_n}\,\delta(l)\,, \quad (2.11)$$

where $\mathbf{n}'$ is the unit vector normal to the noncoplanar slip plane where the dislocation segment goes to.

By contrast to the equations of the continuum theory of dislocations (2.2), equations (2.10) and (2.11) have a discrete character, and contain space-like (l_{F}, R_v, R_l, R_n) and time-like (τ_{F}, τ_v, τ_l, τ_n) parameters that define, depending on the structure of the crystal and loading conditions, the physical scales of evolution of the dislocation ensemble (see below). Together with the quasistatic equations of motion of dislocation (2.4) and (2.5), they describe the evolution of the ensemble on the microscopic level. To obtain equations that describe the kinetics of the ensemble on the mesoscopic and macroscopic levels, one has to carry out statistical averaging of the ensemble with due account for the interaction of dislocations with one another, and with various obstacles in the crystal that affect the kinetics.

2.3 Problem of averaging a dislocation ensemble

The problems encountered in the attempts to perform a consistent averaging of a dislocation ensemble have been more than once reported in the literature [16, 90–93, 97, 113]. These problems are related to the geometry of dislocations that behave as lines rather than points. Hence, come the numerous attempts to reduce the three-dimensional kinetic problem for the dislocation ensemble to the two-dimensional case by dissecting the ensemble with a certain representative plane, so as to treat is as an ensemble composed of pointlike particles.

However, from Eqns (2.8)–(2.11) we see that the characteristic and significant feature of the evolution of dislocations is the curvature of dislocations (the radius of curvature R_v), because this curvature is related to the fundamental property of dislocations and the dislocation ensemble as a whole — their ability to multiply. Obviously, the curvature of dislocations cannot be taken into account in the framework of a two-dimensional model.

Another feature of dislocations is that, as indicated above, the equations of motion of dislocations are dominated not by the dynamic terms, but rather by the quasi-static terms related to the force of friction of dislocations. Because of this, the kinetic energy of dislocations under the ordinary plastic deformation is many orders of magnitude less than the energy of interaction of dislocations. Accordingly, the problem of the 'temperature' and the thermodynamic equilibrium in the dislocation ensemble remains open.

Further on, owing to the diversity, complexity, and widely ranging scales of interactions, it is difficult to establish a universal hierarchy of small parameters that govern the evolution of the ensemble on the appropriate scales.

Interactions of dislocations with one another and with the obstacles in the crystal may be divided into two kinds: the long-range (Coulomb) interaction, and the short-range (contact, 'inelastic') one. The former is associated with the field of internal stresses from pileups of dislocations of the same sign, the effects of polarization of dislocations and misorientations of the lattice. The analysis of these effects requires knowing the distribution of the tensor density of dislocations $\hat{\alpha}(r,t)$ in the crystal.

The contact interaction of dislocations determines the processes of strain hardening and dynamic relaxation, whereas the interaction of dislocations with various obstacles in the crystal determines its resistance to deformation and the processes of multiplication and immobilization of dislocations. For analyzing these phenomena and the formation of various dislocation structures, one needs to know the distribution of the scalar density of dislocations $\rho(r,t)$ in the crystal.

In Appendix I we describe the procedure of statistical averaging of the dislocation ensemble that allows some of the features of dislocations indicated above to be taken into account. According to this procedure, the kinetic equation for the ensemble-averaged scalar density of dislocations $\rho(r,t)$ with Burgers vector b^a is

$$\frac{\partial\rho^a}{\partial t}+\nabla\cdot(u^a\rho^a)=n^a u^a+\sum_p\frac{u^a}{\lambda_p^a}\,\rho^a\,, \quad (2.12)$$

where λ_p is the characteristic free path of dislocations between the elementary acts of change (increase or decrease) of the length (density) of dislocations.

Into the right-hand side of Eqn (2.12) we have added a term describing the generation of dislocations from dislocation sources with the bulk density $n(r,t)$. In this form, Eqn (2.12) is similar in structure to Eqn (2.11) expressed from the kinematic relations (2.2) and (2.6). Averaging Eqn (2.11) with the aid of an appropriate distribution function of dislocations, we can obviously derive an equation of the type of Eqn (2.12).

Indeed, the radius of curvature of dislocation R_v in the case of a flat round loop is simply equal to its radius R. As the loop expands to the radius $R=\lambda_p$, the screw segments of the loop may overcome the obstacles they meet through the mechanism of double cross slip (DCS) [146, 147]. The act of DCS gives rise to a Frank–Read source in the adjacent parallel plane, which leads to an increase in the density of dislocations [148, 149].

The obstacles that initiate the DCS are the growth dislocations with density ρ_0 ($\lambda_p\propto\rho_0^{-1/2}$) [150], clusters of impurity atoms and inclusion particles [148, 149, 151], as well as forest dislocations with density ρ_{f} that intersect the slip plane ($\lambda_p\propto\rho_{\mathrm{f}}^{-1/2}$) [24, 148, 152, 153]. Thus, the characteristic scale of averaging of Eqns (2.11) and (2.12) must be greater than the above free paths of dislocations which, as indicated by the experiment, may vary over a rather broad range: from 10^{-5} to 10^{-3} m. As regards the third term on the right-hand side of Eqn (2.11), its contribution to the total density of dislocations in the case of DCS is small and can be disregarded.

In the next section, we present the kinetic equations for dislocations with due account for the results of this section and the mechanism of multiplication of dislocations through the double cross slip of screw dislocations.

2.4 Equations of evolution of the density of dislocations

As indicated by experiment, the plastic deformation of a crystal starts with the activation of surface and bulk sources of dislocations. The screw components of dislocation loops emitted by the sources that act through the DCS mechanism give rise to new sources of dislocations on the adjacent parallel slip planes if the distance h to these planes is greater than the critical distance

$$h_0=\frac{\mu b}{8\pi(1-\nu_{\mathrm{P}})(\sigma-\sigma_{\mathrm{f}})}\,, \quad (2.13)$$

required for having a clearance between the edge components of dislocation loops on the initial and the new slip planes [41]. Here μ is the shear modulus, and ν_P is Poisson's ratio. If the height of protrusion of the screw segment into the parallel slip plane is less than the critical value h_0, the Frank – Read source does not arise. Instead, there are two edge dipoles of height h and length $l_e \sim \lambda_s$, where λ_s is the free path of screw dislocations between the DCS acts.

In this way, the DCS mechanism in a crystal gives rise to new mobile dislocations, and to sessile dislocations in the form of edge dipoles [41, 148]. In addition, DCS transfers the plastic deformation in a direction transverse to the initial slip plane. Ejection of the screw segment into the parallel slip plane is a random process, and occurs with a certain probability [143 – 149, 154]

$$P(h) = h_c^{-1} \exp\left(-\frac{h}{h_c}\right). \tag{2.14}$$

This circumstance will be put to use in Section 4.

Taking into account the arguments developed above and in Section 2.3, we may write the following kinetic equations for the densities of mobile $[\rho_m(r,t)]$ and immobile (in the form of edge dipoles) $[\rho_i(r,t)]$ dislocations (superscript a dropped):

$$\frac{\partial \rho_m}{\partial t} + \nabla \cdot (u\rho_m) = nu + (\lambda_m^{-1} + \lambda_f^{-1})\, u\rho_m - (\lambda_{is}^{-1} + h_i\rho_i)\, u\rho_m - h_a u \rho_m^- \rho_m^+ , \tag{2.15}$$

$$\frac{\partial \rho_i}{\partial t} = \lambda_{ie}^{-1} u\rho_m - h_d u \rho_i \rho_m . \tag{2.16}$$

Here, λ_m and $\lambda_f = \delta_f \sum_c (\rho_f^c)^{-1/2}$ [24, 113, 148, 152, 153] are the free paths of screw dislocations between the acts of multiplication on obstacles of nondeformation (grown-in dislocations, inclusion particles) and deformation (forest dislocations, $\delta_f \approx 10^{-2}$) origin; λ_{is} is the free path of screw dislocations to annihilation or immobilization on the obstacles of nondeformation origin; h_i is the mean height of the edge dipoles, the interaction with which results in the immobilization of mobile dislocations; and h_a is the characteristic distance of annihilation of screw dislocations of opposite signs ($\rho_m^- = \rho_m^+ = \rho_m$). In Eqn (2.16), λ_{ie} is the free path of screw dislocations between the acts of DCS with the formation of edge dipoles; h_d is the mean height of edge dipoles being destroyed by mobile dislocations.

Equations (2.15) and (2.16) involve the most probable dislocation processes that affect evolution of the dislocation ensemble in the crystal subjected to plastic deformation given the homogeneous distribution of dislocations. The relative importance of individual processes depends on the structure of crystals and conditions of deformation. These equations were written under the assumption that the dislocation ensemble in the crystal is neutral both in the global sense (the sum of Burgers vectors of all dislocations is zero) and in the local sense [the density of dislocations is $\hat{\alpha}(r,t) = 0$]. We will use Eqns (2.15) and (2.16) for analyzing the curves of strain hardening of crystals. A more comprehensive version of these equations is considered in Sections 4 and 5.

3. Strain-hardening curves of crystals

Much like a voltage – current characteristic, the strain-hardening curve is the 'passport' of the crystal, showing its resistance to plastic deformation on the macroscopic level. This resistance is the result of interaction of moving dislocations with various obstacles in the crystal, and of interactions between dislocations. It is the interaction of dislocations with one another that underlies the process of strain hardening of a crystal, that is, the increase in the resistance of a crystal to plastic deformation with increasing extent of plastic deformation (Fig. 1).

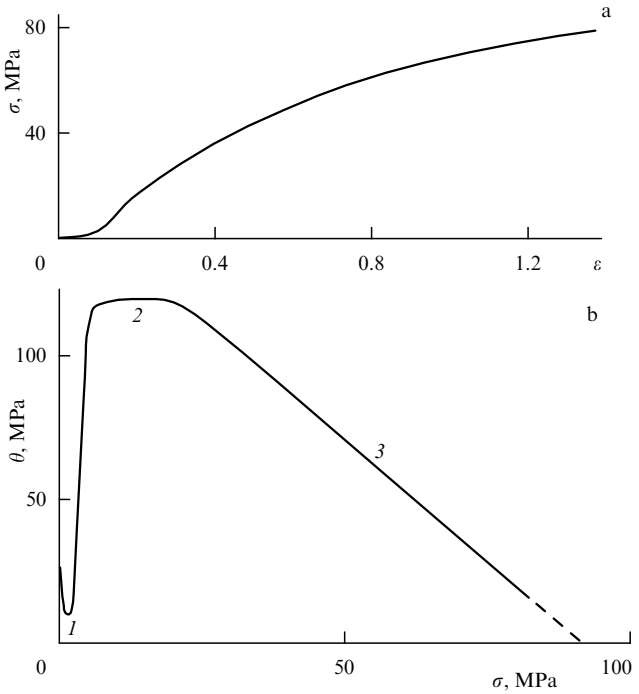

Figure 1. Strain-hardening curve $\sigma(\varepsilon)$ of a copper single crystal at 295 K [156] (a), and the strain-hardening coefficient of copper θ vs. the flow stress σ (b). Numbers mark the stages of hardening.

The problem of the mechanism of strain hardening and its multistage nature was one of the first questions attempted to be answered by the dislocation theory of the plasticity of crystals [17, 19 – 21]. Today, after extensive studies and discussions, many authors agree that at the first stage of hardening (the stage of easy slip) the predominant mechanism of hardening is the interaction of mobile dislocations with edge dipoles [20, 41, 148], and at the second stage, their interaction with the dislocations of secondary slip systems (with forest dislocations [24, 155, 156]). The third stage is the stage of dynamical recovery, and is associated with the annihilation of screw dislocations [24, 151, 157 – 164].

Much attention over the past two decades has been paid to the behavior of crystalline materials in the case of large (of the order of several units) plastic deformations [165 – 171]. Intensive studies led to the discovery of the fourth and fifth stages of hardening, the mechanism of which is actively discussed these days [172 – 175].

In this review, we confine ourselves to the theoretical analysis of strain-hardening curves within the first three stages of hardening. The dislocation structures typical of these stages are discussed in Sections 4 (single slip) and 5 (multiple slip).

For historical reasons, the mechanisms of strain hardening were studied separately for each segment of the stress–strain curve, out of connection with the other stages. At the

same time, the process of plastic deformation of a crystal is a continuous evolution of the dislocation ensemble, and the transition from one stage to the next occurs smoothly enough as the extent of plastic deformation increases.

Equations of evolution of dislocation density (2.15) and (2.16) give a satisfactory qualitative and quantitative description of this process and the typical three-stage strain-hardening curve with due account for various external and internal factors [176, 177].

3.1 Multistage nature of strain-hardening curves

To demonstrate this, let us rewrite Eqns (2.15) and (2.16) in the form

$$\rho_{\mathrm{m}}\,\frac{\mathrm{d}\rho_{\mathrm{m}}}{\mathrm{d}\varepsilon} = b^{-1}n + k_{\mathrm{m}}\,\rho_{\mathrm{m}} - (k_{\mathrm{is}} + k_{\mathrm{i}}\rho_{\mathrm{i}})\,\rho_{\mathrm{m}} + k_{\mathrm{f}}\sum_{c}(\rho_{\mathrm{f}}^{c})^{1/2} - k_{\mathrm{a}}\,\rho_{\mathrm{m}}^{2}\,, \tag{3.1}$$

$$\frac{\mathrm{d}\rho_{\mathrm{i}}}{\mathrm{d}\varepsilon} = k_{\mathrm{ie}} - k_{\mathrm{d}}\,\rho_{\mathrm{i}}\,, \tag{3.2}$$

taking advantage of the fact that, under the conditions of uniaxial tension or compression at a constant rate, we have $\partial\rho_{\mathrm{m}}/\partial t = (\partial\rho_{\mathrm{m}}/\partial\varepsilon)\dot{\varepsilon}$, where $\dot{\varepsilon} = bu\rho_{\mathrm{m}}$ is the rate of plastic deformation.

In Eqn (3.1), $k_{\mathrm{m}} = (b\lambda_{\mathrm{m}})^{-1}$ and $k_{\mathrm{f}} = \delta_{\mathrm{f}}\,b^{-1}$ are the coefficients of multiplication of dislocations, $k_{\mathrm{is}} = (b\lambda_{\mathrm{is}})^{-1}$ and $k_{\mathrm{i}} = h_{\mathrm{i}}/b$ are the coefficients of immobilization of mobile dislocations; $k_{\mathrm{a}} = h_{\mathrm{a}}/b$ is the coefficient of annihilation of screw dislocations. In Eqn (3.2), $k_{\mathrm{ie}} = (b\lambda_{\mathrm{ie}})^{-1}$ is the coefficient of immobilization of dislocations in edge dipoles; and $k_{\mathrm{d}} = h_{\mathrm{d}}/b$ is the coefficient of destruction of edge dipoles by mobile dislocations.

Equations (3.1) and (3.2) describe the change in the density of mobile dislocations and the density of edge dipoles with the increasing extent of plastic deformation. Let us look at the evolution at the initial stage of deformation, when there is no multiplication of dislocations on the dislocations of the secondary slip systems, and no annihilation of screw dislocations, while the destruction of dipoles by moving dislocations is negligible. Then we have the equations

$$\rho_{\mathrm{m}}\,\frac{\mathrm{d}\rho_{\mathrm{m}}}{\mathrm{d}\varepsilon} = b^{-1}n + k_{\mathrm{m}}\,\rho_{\mathrm{m}} - (k_{\mathrm{is}} + k_{\mathrm{i}}\,\rho_{\mathrm{i}})\,\rho_{\mathrm{m}}\,, \qquad \rho_{\mathrm{i}} = k_{\mathrm{ie}}\varepsilon\,. \tag{3.3}$$

At the very start of deformation (the stage of microdeformation), when only the sources with constant bulk density n are active and the first term on the right-hand side dominates in Eqn (3.3), for the density of movable dislocations we obtain $\rho_{\mathrm{m}} = (2n/b)^{1/2}\varepsilon^{1/2}$.

In the case of laminar flow of dislocations of different signs, the main mechanism of hardening is Taylor hardening: $\sigma = \alpha_0\mu b\rho_{\mathrm{m}}^{1/2}$ [19, 20], where $\alpha_0 \approx 0.2$ is the constant of interaction between dislocations. Accordingly, the stage of microdeformation ought to obey the law of deformation hardening $\sigma = \chi\varepsilon^{1/4}$, where $\chi/\mu = \alpha_0(2nb^3)^{1/4}$. The $\sigma \propto \varepsilon^m$ behavior, where $m = 0.25-0.35$, was reported in Refs [178–181] at deformations $\varepsilon = 10^{-5}-10^{-3}$.

The critical shear stress (yield stress) is the point where the dislocations in the crystal start multiplying through the DCS mechanism [41, 148, 149]. Here, there are two possibilities. If the density of surface and bulk dislocation sources is small (the distance between the sources is large), one or several slip bands are formed in the crystal, which expand by the DCS mechanism and fill the crystal. Such an inhomogeneous distribution of dislocations in crystal corresponds to a yield plateau on the stress–strain diagram. (The mechanism of formation and broadening of slip bands is discussed in Section 4.) If the number of sources is large, the deformation of the crystal occurs in a rather uniform way. The edge dipoles resulting from DCS serve as obstacles for moving dislocations, and the flow stress increases in proportion to the density of dipoles ρ_{e} [20, 41, 148]:

$$\sigma = \alpha_{\mathrm{d}}b\mu h_{\mathrm{d}}\rho_{\mathrm{e}} = \chi\varepsilon\,, \qquad \frac{\chi}{\mu} = \frac{\alpha_{\mathrm{d}}h_{\mathrm{d}}}{\lambda_{\mathrm{ie}}}\,, \tag{3.4}$$

where $\alpha_{\mathrm{d}} \approx 1-3$, $h_{\mathrm{d}}/\lambda_{\mathrm{ie}} \approx 10^{-4}$.

In a pure form, the dipole hardening can be observed in specially designed experiments with pure shear [148, 182], and in crystals carefully oriented to ensure single slip [21]. In ordinary experiments with uniaxial extension or compression, owing to the accommodation processes and activation of the secondary slip systems by the fields of internal stress caused by pileups of dislocations of the same sign, the edge dipoles are supplemented by other obstacles for moving dislocations such as forest dislocations [178, 183]. As a result, the hardening curves beyond the yield stress become quasi-linear, and the coefficient of strain hardening is greater than that for the purely dipole hardening [182].

In addition, dislocations of secondary slip systems are obstacles on which, like on the forest dislocations, the multiplication of primary dislocations may occur. Conversely, the dislocations of the primary system may serve as forest dislocations for the secondary dislocations. As a result, as indicated by experiment [183], their densities are very soon equalized. This means that, to a certain accuracy, we may assume that $\rho_{\mathrm{f}}^{a} \approx \rho_{\mathrm{m}}$ in Eqns (3.1) and (3.2), which then become

$$\rho_{\mathrm{m}}\,\frac{\mathrm{d}\rho_{\mathrm{m}}}{\mathrm{d}\varepsilon} = b^{-1}n + (k_{\mathrm{m}} - k_{\mathrm{im}})\,\rho_{\mathrm{m}} + k_{\mathrm{f}}\,\rho_{\mathrm{m}}^{3/2} - k_{\mathrm{a}}\rho_{\mathrm{m}}^{2}\,, \tag{3.5}$$

$$\frac{\mathrm{d}\rho_{\mathrm{i}}}{\mathrm{d}\varepsilon} = k_{\mathrm{ie}} - k_{\mathrm{d}}\rho_{\mathrm{i}}\,, \qquad k_{\mathrm{im}} = k_{\mathrm{is}} + k_{\mathrm{i}}\,\rho_{\mathrm{i}}\,. \tag{3.6}$$

These equations must be supplemented by the law of dislocation hardening because of the interaction of dislocations with one another

$$\sigma = \alpha b\mu\rho_{\mathrm{m}}^{1/2}\,. \tag{3.7}$$

To see how well the equation of evolution (3.5) agrees with experiment, we use the relation [184]

$$\sigma\,\frac{\mathrm{d}\sigma}{\mathrm{d}\varepsilon} = \frac{1}{2}(\alpha\mu b)^2\,\frac{\mathrm{d}\rho_{\mathrm{m}}}{\mathrm{d}\varepsilon}\,, \tag{3.8}$$

which follows from the law of hardening (3.7). Substituting Eqn (3.5) into (3.8), and noting that $\rho_{\mathrm{m}} \propto \sigma^2$, we find the coefficient of strain hardening $\theta = \mathrm{d}\sigma/\mathrm{d}\varepsilon$ as a function of the dimensionless flow stress $\bar{\sigma} = \sigma/\sigma_{\infty}$ [176]:

$$\theta = \theta_{\mathrm{m}}(Q_0\bar{\sigma}^{-3} - Q_{\mathrm{i}}\bar{\sigma}^{-1} + 1 - \bar{\sigma})\,, \tag{3.9}$$

where

$$\frac{\theta_{\mathrm{m}}}{\mu} = \frac{1}{2}\,\alpha bk_{\mathrm{f}}\,, \qquad \sigma_{\infty} = \alpha\mu b\rho_{\infty}^{1/2}\,, \qquad \rho_{\infty} = \left(\frac{k_{\mathrm{f}}}{k_{\mathrm{a}}}\right)^2\,,$$

$$Q_0 = \frac{n}{bk_{\mathrm{a}}\,\rho_{\infty}^{2}}\,, \qquad Q_{\mathrm{i}} = \frac{k_{\mathrm{im}} - k_{\mathrm{m}}}{k_{\mathrm{a}}\,\rho_{\infty}}\,. \tag{3.10}$$

Curves *1–3* in Fig. 2 are plotted from Eqn (3.9) with different values of parameters Q_0 and Q_i (see Table), of which the former accounts for the effects of the density of Frank – Read sources, and the latter for those of the immobilization of dislocations and dislocation sinks on the shape of $\theta(\sigma)$ curves and, hence, on the segmentation of the curves of deformation hardening. We see that the results for copper crystals, shown earlier in Fig. 1b, are in good agreement with curve *3* in Fig. 2.

Table. Values of the parameters Q_0, Q_i and g.

Parameter	Curve *1*		Curve *2*		Curve *3*	
	Fig. 2	Fig. 4	Fig. 2	Fig. 4	Fig. 2	Fig. 4
$Q_0 \times 10^6$	0.12	0.12	0.12	1.9	1.9	7.5
$Q_i \times 10^2$	0.12	0.12	0.5	2.25	2.25	3.56
g	1.0	1.0	0.06	0.04	0.04	0.07

Each term on the right-hand side of Eqn (3.9) is associated with a distinct hardening stage. Parameter Q_0 corresponds to the microdeformation stage; Q_i, to the first stage; and the next two terms determine the second and third stages, respectively. As follows from Figs 1b and 2, the coefficient of strain hardening at the third stage (the stage of dynamical recovery) decreases linearly with increasing flow stress [157, 167 – 174],

$$\theta = \theta_m \left(1 - \frac{\sigma}{\sigma_\infty}\right). \tag{3.11}$$

Relation (3.8) then assumes a purely parabolic form

$$\theta\sigma = \theta_m \sigma_\infty \left(1 - \frac{\sigma}{\sigma_\infty}\right) \frac{\sigma}{\sigma_\infty}, \tag{3.12}$$

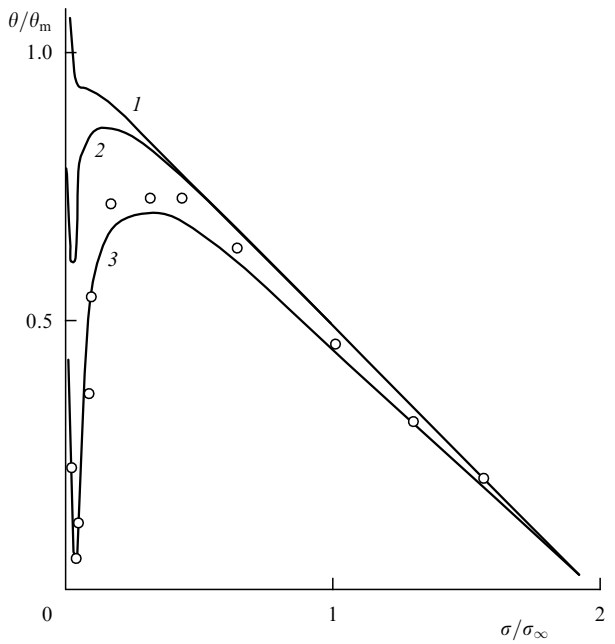

Figure 2. Coefficient of strain hardening θ vs. the stress σ according to Eqn (3.9) for different values of the parameters Q_0, Q_i, and g (see Table). Experimental points for Cu taken from Ref. [156].

and describes, according to Eqn (3.8), how the coefficient of dislocation multiplication changes with the stress (or strain) at the second and third stages [24, 157 – 161]:

$$\frac{d\rho_m}{d\varepsilon} = k_f \rho_m^{1/2} - k_a \rho_m . \tag{3.13}$$

Figure 3 shows the experimental strain-hardening curves for polycrystalline specimens of Al – 3 at.% Mg at different temperatures in the range of 77 – 473 K [160, 161] in the coordinates

$$y = \frac{\theta(\sigma - \sigma_0)}{\left[\theta(\sigma - \sigma_0)\right]_{max}}, \qquad x = \frac{\sigma - \sigma_0}{(\sigma - \sigma_0)_{max}}, \tag{3.14}$$

which point to good agreement between the parabolic law $y = x(2 - x)$ and the experiment, where σ_0 is the yield stress, and $\left[\theta(\sigma - \sigma_0)\right]_{max}$ and $(\sigma - \sigma_0)_{max}$ correspond to the tops of the parabolas. Similar agreement between the law (3.13) and the experiment was observed for the strain-hardening curves of Ag [160], Al [161], and Ni [159].

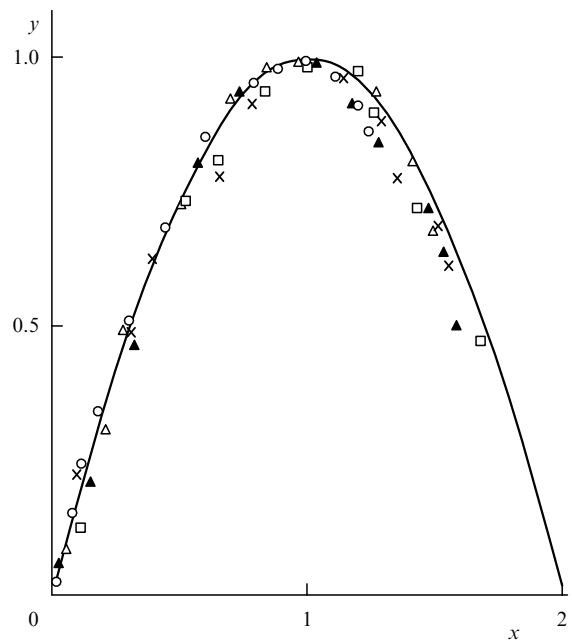

Figure 3. Quantity $\theta(\sigma - \sigma_0)$ vs. $\sigma - \sigma_0$ in the coordinates of Eqn (3.14). Experimental points are the values of $\theta(\sigma - \sigma_0)$ in the Al – 3.3 at.% Mg alloy at various temperatures in the range 77 – 473 K [160, 161].

To find the explicit form of the strain-hardening curve $\sigma(\varepsilon)$, we have to integrate Eqn (3.9):

$$\int_0^{\bar\sigma} \frac{d\bar\sigma}{Q_0 \bar\sigma^{-3} - Q_i \bar\sigma^{-1} + 1 - \bar\sigma} = \frac{\varepsilon}{\varepsilon_\infty}, \qquad \varepsilon_\infty = \frac{2}{k_a}. \tag{3.15}$$

The results of integration for different values of Q_0 and Q_i (see Table) are given in Fig. 4. Depending on the absolute and relative magnitude of these parameters, the curves $\sigma(\varepsilon)$ show the presence (curves *1* and *2*) or absence (curve *3*) of the first stage with a low coefficient of strain hardening.

To find the criterion of existence of the first stage of hardening, we differentiate Eqn (3.9) with respect to $\bar\sigma$. As a

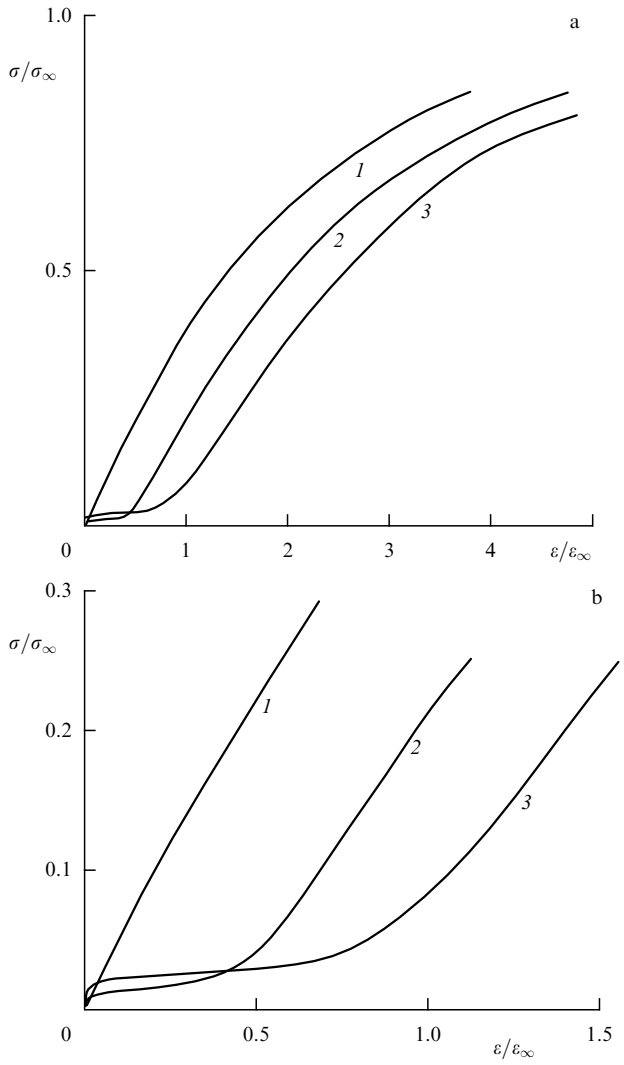

Figure 4. Strain-hardening curves $\sigma(\varepsilon)$ (a) and their initial portions (a) according to Eqn (3.15).

result, we find the stresses σ_2 and σ_1 at which the coefficient of strain hardening attains its maximum θ_2 (at the second stage) and minimum θ_1 (at the first stage) values:

$$\frac{\sigma_{1,2}}{\sigma_\infty} = \left(\frac{1}{2}\,Q_{\mathrm{i}}\right)^{1/2} \left[1 \mp (1-g)^{1/2}\right]^{1/2},$$

$$g = 12\,\frac{Q_0}{Q_{\mathrm{i}}^2} = \frac{12nk_{\mathrm{a}}}{b(k_{\mathrm{im}} - k_{\mathrm{m}})^2}\,. \tag{3.16}$$

From Eqn (3.16) we see that for the first stage to exist it is necessary that the processes of sinking and immobilization of dislocations should dominate over the processes of multiplication through the DCS mechanism ($k_{\mathrm{im}} > k_{\mathrm{m}}$). These processes must be of sufficient intensity to ensure that condition $g < 1$ is satisfied.

If $g \geqslant 1$, the first stage is absent, and the strain-hardening curve has two stages (curves *1* in Fig. 4). In such a case, the stage of microdeformation is immediately followed by the second stage, associated with the interaction between dislocations in the intersecting slip systems. The strain-hardening curve, according to Eqn (3.13), is described by expression

$$\sigma = \sigma_\infty \left[1 - \exp\left(-\frac{k_{\mathrm{a}}\varepsilon}{2}\right)\right], \tag{3.17}$$

from which it follows that for deformations $\varepsilon \ll 2/k_{\mathrm{a}}$ we have $\sigma \approx \theta_2\varepsilon$, where $\theta_2/\mu = \alpha b k_{\mathrm{f}}/2 \approx 2.5 \times 10^{-3}$ is the coefficient of strain hardening at the second (linear) hardening stage. Good agreement between Eqn (3.17) and the experiment is clear from the results presented in Figs 2 and 3.

If the processes of multiplication of dislocations through the DCS mechanism and the accumulation of dislocations owing to the presence of barriers that prevent dislocations from leaving the crystal dominate over the processes of immobilization of dislocations and their escape to sinks ($k_{\mathrm{m}} > k_{\mathrm{im}}$), then the deformation-hardening curve (after the stage of microdeformation) assumes a parabolic character:

$$\sigma = \sigma_\infty \left[1 - \exp(-k_{\mathrm{a}}\varepsilon)\right]^{1/2}, \tag{3.18}$$

where $\sigma_\infty = \alpha\mu b(k_{\mathrm{m}}/k_{\mathrm{a}})^{1/2}$. At $\varepsilon \ll 1/k_{\mathrm{a}}$, we have $\sigma \propto \varepsilon^{1/2}$, i.e., a parabolic hardening law, which is characteristic, for example, of polycrystalline aggregates, in which the free path of dislocations is limited by the grain size d, and therefore $k_{\mathrm{m}} = (bd)^{-1}$. As a result, we obtain the known Hall–Petch law $\sigma \propto d^{-1/2}$ for the flow stress as a function of the grain size [185–187].

The sensitivity of strain-hardening curves to the absolute and relative magnitude of the kinetic coefficients in the equation of evolution of dislocation density (3.5) also applies to the coefficient of annihilation of dislocations k_{a}. As shown in Refs [151, 159, 160], this coefficient is inversely proportional to the stress of lattice friction of dislocations, $k_{\mathrm{a}} \propto \sigma_{\mathrm{f}}^{-1}$ [162]. Because of this, everything that facilitates the increase in the stress of lattice friction must postpone the stage of dynamical recovery.

We know that in metallic crystals with a body-centered cubic (bcc) lattice at temperatures $T < 0.1T_{\mathrm{m}}$, where T_{m} is the melting point, the friction stress increases dramatically at low temperatures as dislocations move along the Peierls relief. Because of this, the strain-hardening curves [188, 189] cease to feature the third stage of hardening, and then the second, because the multiplication of screw dislocations by the DCS mechanism is hindered.

3.2 Size, orientational, and surface effects

As is known from experiment (see Refs [190–199] and literature cited in Ref. [177]), the very existence of the first stage of hardening and its parameters (yield stress σ_0, coefficient of strain hardening θ_1, length of stage $\varepsilon_2 - \varepsilon_1$) are very sensitive to the structural factors and loading conditions if the free path of dislocations (about 1 mm at the initial stage of deformation) is comparable to the transverse dimensions of the crystal under stress. The structural factors are all those factors that affect the free path of dislocations, and the loading conditions include all factors that facilitate or hinder the escape of dislocations from the crystal.

The buildup of dislocations in the crystal (and hence its hardening) is aided by impurities, inclusion particles, hard crystal orientations $\langle 111 \rangle$, specially hardened surface layers, oxide films, and coatings. The plasticization of the crystal and the appearance of the first stage of hardening are facilitated by factors such as the reduction of transverse dimensions of the crystal, soft orientations (e.g., $\langle 110 \rangle$), removal of oxide

film, chemical or electrolytic dissolution of crystal surface in the course of deformation, deformation of crystal in high vacuum.

The equation of evolution of the density of dislocations (3.5) provides for a quantitative assessment of the effects of the factors named above on the parameters of the first stage of hardening [177]. Indeed, as demonstrated in the previous section, the first stage owes its existence to the predominance of the processes of immobilization of dislocations and their escape to sinks (represented in thin crystals by the crystal surface) over the processes of multiplication and accumulation of dislocations in the crystal. Given this, we can express the coefficients of accumulation and immobilization of dislocations as [177]

$$k'_{\mathrm{m}} = \frac{1}{b\lambda_{\mathrm{m}}} + \frac{\beta_{\mathrm{m}}}{bL_{\mathrm{e}}}\,, \qquad k'_{\mathrm{im}} = \frac{1}{b\lambda_{\mathrm{is}}} + \frac{\beta_S}{bL_{\mathrm{e}}}\,, \tag{3.19}$$

where L_{e} is the distance covered by a dislocation in the slip plane to its egress on the surface; β_S and β_{m} are the coefficients of transparency of the surface for escape of dislocations from the crystal, and the efficiency of the surface barrier for the moving dislocations; λ_{m} and λ_{is} are the free paths of dislocations in the case of their multiplication by the DCS mechanism.

Further, we must take into account that, as the cross section of the crystal becomes smaller, the relative contribution of the surface dislocation sources with the density n_S to the total density of dislocation sources in the crystal increases [177]:

$$n = n_V + m_S L_{\mathrm{e}}^{-1} n_S\,, \tag{3.20}$$

where n_V is the density of bulk Frank – Read sources, and m_S is the orientation factor. Since $L_{\mathrm{e}} = m_{\mathrm{e}} d$, where $m_{\mathrm{e}} > 1$ is the orientation factor, and d is the thickness of the crystal, the total density of dislocation sources n increases as the thickness of the crystal under stress decreases.

Substituting Eqns (3.19) and (3.20) into (3.16), we express the critical parameter g as a function of the thickness of the crystal, its orientation, and the conditions of escape of dislocations to the surface of the crystal [177]:

$$g(L_{\mathrm{e}}) = g_\infty \frac{1 + k_1\lambda_{\mathrm{m}}/L_{\mathrm{e}}}{(1 + k_2\lambda_{\mathrm{m}}/L_{\mathrm{e}})^2}\,,$$

$$k_1 = \frac{l_S}{\lambda_{\mathrm{m}}}\,, \qquad k_2 = \frac{\beta_S - \beta_{\mathrm{m}}}{\beta_{\mathrm{i}} - 1}\,, \tag{3.21}$$

where $\beta_{\mathrm{i}} = \lambda_{\mathrm{m}}/\lambda_{\mathrm{is}}$, $l_S = m_S n_S/n_V$ is a parameter that accounts for the relative importance of surface sources in the generation of dislocations, and g_∞ is the parameter g in a thick ($L_{\mathrm{e}} \gg \lambda_{\mathrm{m}}$) crystal. At $\beta_S > \beta_{\mathrm{m}}$, $\beta_{\mathrm{i}} > 1$, $g_\infty > 1$, from Eqn (3.31) it follows that a reduction of crystal thickness ($L_{\mathrm{e}} < \lambda_{\mathrm{m}}$) will cause the appearance of the first stage of hardening that is not present in a thick crystal because $g \sim g_\infty L_{\mathrm{e}}/\lambda_{\mathrm{m}} < 1$. This is actually observed in experiment [194].

Condition $\beta_S > \beta_{\mathrm{m}}$ at $\beta_{\mathrm{i}} > 1$ implies that the surface of the crystal is an efficient sink for dislocations. This efficiency increases when the crystal is subject to chemical or electrolytic treatment in the course of deformation [195], or when its deformation takes place in high vacuum which prevents the formation of an oxide film [196].

In the case of chemical etching, the parameter β_S increases proportionally to the rate of removal of surface layers u_S: $\beta_S = 1 + u_S/u$, where u is the velocity of dislocations [177]. All these processes facilitate the appearance of the first stage of hardening, that is, plasticize the crystal. Conversely, if the critical parameter in the initial crystal is $g_\infty < 1$, the formation of a hardened surface layer or coating will eliminate the first stage of hardening [190 – 195].

From Eqns (3.5) and (3.19) it follows that the density of free dislocations in the beginning of the first stage of hardening is $\rho_{\mathrm{m0}} \approx n/b(k'_{\mathrm{im}} - k'_{\mathrm{m}})$. In this case, making use of Eqns (3.19) and (3.20), for the yield stress $\sigma_0 = \alpha\mu b\rho_{\mathrm{m0}}^{1/2}$ as a function of thickness of crystal d we obtain [177]

$$\sigma_0(L_{\mathrm{e}}) = \sigma_0(\infty)\left(\frac{1 + k_1\,\lambda_{\mathrm{m}}/L_{\mathrm{e}}}{1 + k_2\,\lambda_{\mathrm{m}}/L_{\mathrm{e}}}\right)^{1/2}, \qquad L_{\mathrm{e}} = m_{\mathrm{e}} d\,, \tag{3.22}$$

where $\sigma_0(\infty)$ is the yield stress of thick crystal.

From Eqn (3.22) we see that at $k_1 \ll 1$, $k_2 > 0$ the reduction of crystal thickness ought to bring down the yield stress. If $|k_2| \ll 1$, however, the thinning of the crystal will raise the yield stress [194]. A similar dependence of σ_0 on d is observed when the surface of the crystal is a barrier for the escape of dislocations ($k_2 < 0$).

Another consequence of Eqn (3.22) is the dependence of the yield stress σ_0 on the orientation of the crystal (orientational factor m_{e}). This circumstance underlies the known violation of Schmid's law in thin crystals and foils [197 – 199], which states that the active slip plane (system) is the plane with the highest Schmid factor [35], that is, with the maximum value of tangential stresses. As indicated by experiment, however, the operating slip plane in thin crystals is not that plane, but rather the plane with the least free path of edge dislocations to the surface of the crystal L_{e} [197], since this ensures lesser dislocation hardening as compared with the plane that has a higher tangential stress and a longer free path of dislocations L_{e}.

Indeed, the orientational factor in Eqn (3.22) is $m_{\mathrm{e}} \sim 1/\sin\varphi$ [197], where φ is the angle between the axis of deformation and the slip plane; therefore, at $k_1 \ll 1$ and $k_2 > 0$ the deviation of angle φ down from, for example, 45° will reduce the path of dislocation to the surface of crystal L_{e}. According to Eqn (3.22), this will bring down the yield stress of the crystal, that is, facilitate the start of its plastic flow (or rather the continuation of plastic flow following the stage of microdeformation).

The effects of these factors on other parameters of the first stage of deformation were analyzed in Refs [176, 177]. As regards the manifestation of these factors at the second and third segments of the deformation-hardening curve, their effects are insignificant, because the free path lengths of dislocations are much reduced at the second and third stages of hardening.

These results of the analysis of strain-hardening curves based on the kinetic equations (2.15) and (2.16) indicate that these equations fit in well with the experiment, and account for such fundamental properties of hardening curves as their multistage nature and sensitivity toward the structure of crystals and the conditions of deformation. In addition, on the basis of our analysis we may conclude that the strain-hardening curve is not purely static or quasi-static, but reflects the kinetic processes that take place in the dislocation ensemble of the crystal in the course of its deformation.

4. Slip lines and bands

One of the characteristic features of plastic deformation of crystals is its localization in the form of slip lines and bands [34–42, 200–209]. The discrete nature of slipping and its evolution along distinct crystallographic planes is not surprising by itself, and can be consistently explained within the framework of the dislocation mechanism.

What is surprising and calls for explanation is the emergence — in the course of plastic deformation of the crystal — of a hierarchic and spatially ordered system (stack) of slip lines [38, 40, 200, 201, 209] that points to the cooperative (fractal [206, 207], self-similar [208]) nature of the development of plastic deformation in the direction transverse to the principal slip plane of dislocations.

Figure 5 shows the distribution of slip lines with respect to distances Λ between them obtained with the replica technique at the end of the first stage of hardening in a crystal of Cu–8 at. % Mn alloy [209]. Similar histograms were obtained with different magnifications for Ni_3Fe alloy using optical and electron (replica technique) microscopy [208]. In Fig. 5 we see that the distances between the lines group with a certain probability around the mean value $\bar{\Lambda}$. This mean value does not remain constant and depends on the state of the crystal [208, 209] and strain (stress).

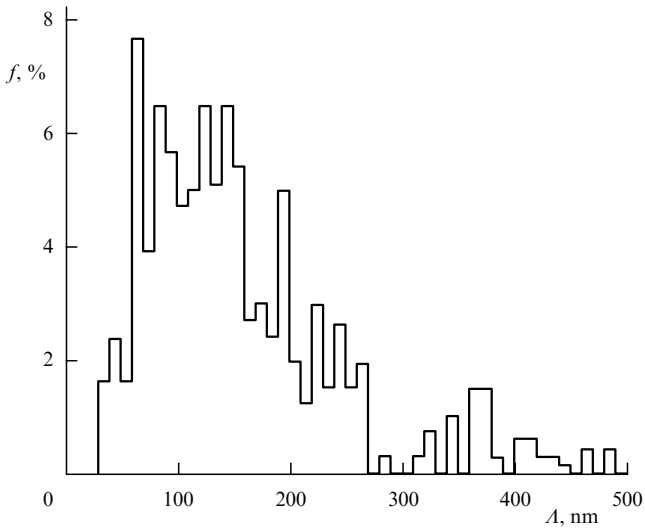

Figure 5. Histogram of distribution of distances Λ between slip lines in single crystals of Cu–8 at. % Mn alloy at the end of the first stage of hardening [209].

Figure 6 illustrates the mean distance between slip lines in copper single crystals stressed at 4.2 K as a function of stress that was varied within broad limits (the first and second stages of the copper hardening curve [201]). A similar result was reported in Ref. [202] for aluminum single crystals stretched at room temperature. The results can be approximated by the expression

$$\sigma = K_1 \left(\frac{\mu b}{\bar{\Lambda}}\right)^m , \tag{4.1}$$

where $K_1 = 1.2$, $m = 1.18\,(\mathrm{Cu})$, $m = 1.0\,(\mathrm{Al})$. Since $\sigma = \alpha \mu b \rho^{1/2}$, at $m \approx 1$ we find that the mean distance between slip lines $\bar{\Lambda}$ as a function of the mean density of

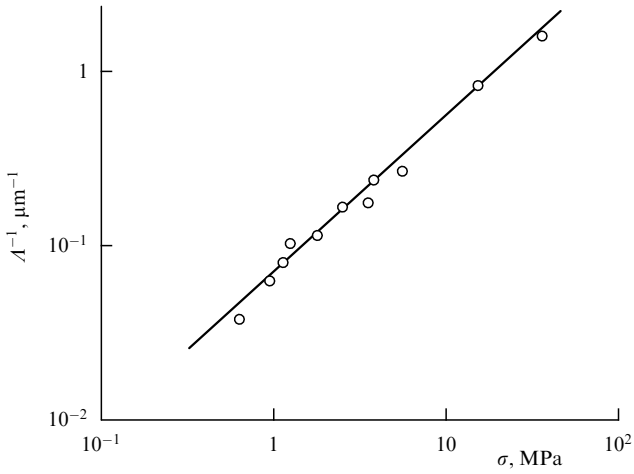

Figure 6. Inverse mean distance between slip lines $\bar{\Lambda}^{-1}$ in single crystals of copper vs. stress σ [201].

dislocations ρ is

$$\bar{\Lambda} = K_2 \rho^{-1/2} , \quad K_2 = K_1/\alpha . \tag{4.2}$$

Relations similar to Eqns (4.1) and (4.2) were found earlier for the cell size in the cellular dislocation structure (see Section 5).

Currently several possible mechanisms of formation of spatially ordered system of slip lines are being discussed. According to Ref. [210], slip lines result from consecutive activation of the dislocation sources closest to the slip plane in question by the fields of internal stress generated by moving groups of dislocations of the same sign.

Obviously, the mean distance between the slip lines $\bar{\Lambda}$ in this case must depend on the characteristic scale of the field of internal stress, and the distribution of slip lines with respect to distances must be determined by the distribution of dislocation sources. Since, as follows from experiment [200, 208, 209], the mean distance $\bar{\Lambda}$ depending on the scale of observation may vary widely (from 10 nm to 100 μm), the density of dislocation sources at, for instance, $\bar{\Lambda} = 10$–100 nm, in the form of Frank's grid must be of the order of $\bar{\Lambda}^{-3}$, and the density of growth dislocations is $\rho_0 \sim \bar{\Lambda}^{-2} \approx 10^{10}-10^{12}\ \mathrm{cm}^{-2}$. This density is several orders of magnitude greater than the density of growth dislocations in real crystals ($10^4-10^8\ \mathrm{cm}^{-2}$) [150, 183].

According to Refs [204, 205], the relay mechanism of formation of slip lines is due to the consecutive activation of the surface dislocation sources by the fields of internal stress from the 'outcropping' groups of like dislocations, and the resulting step on the surface which is a geometric concentrator of stress. This hypothesis draws similar comments to the previous one. Observe also that this mechanism is not universal, because the surface sources may be blocked when the surface layer is hardened in one way or another, and then, as noted in Ref. [204], plastic deformation starts with the activation of the bulk dislocation sources.

4.1 Correlation effects

In Ref. [211], the loss of spatial stability by the dislocation ensemble and the localization of deformation as a system of slip lines are associated with the formation of steady inhomogeneous fluctuations of dislocation density owing to the correlation effect in the spatial arrangement of disloca-

tions of one sign with respect to the dislocations of the other sign. The mechanism of shielding of the elastic field of dislocation by the elastic fields of dislocations of the opposite sign, resulting in the periodical clustering of dislocations, was used earlier for explaining the formation of cellular dislocation structure in the crystal [84]. It was further developed in Refs [139, 140, 211]. Given below are the results of calculations as relevant to our discussion.

The inclusion of the correlation effect when averaging the equations of motion of dislocations (2.4) gives rise to an additional correlation stress $\sigma_{ik}^{\mathrm{cor}}$ (see Appendix II):

$$n_i(\sigma_{ik}^{\mathrm{ext}} + \sigma_{ik}^{\mathrm{in}} + \sigma_{ik}^{\mathrm{cor}})\, b_k = b\sigma^{(\mathrm{f})}\,,$$
$$\sigma^{(\mathrm{f})} = \sigma^*(u, T) + \sigma_{\mathrm{f}} + \sigma_\mu(\rho)\,, \tag{4.3}$$

where

$$\sigma_{ik}^{\mathrm{cor}}(r, t) = -\int A_{iksp}(r' - r)\, b_k v_s\, \rho(r', t)\, g(r' - r, t)\, \mathrm{d}r'\,, \tag{4.4}$$

$g(r' - r, t)$ is the pair correlation function.

For illustrative purposes, we consider a two-dimensional model ensemble consisting of parallel screw dislocations of opposite sign in equal proportion [140]. The presence of correlation stress in the equation of motion (4.3) gives rise to the correlation drift flow $j^{\mathrm{cor}} = \rho\, u(\hat{\sigma}^{\mathrm{cor}})$ in Eqn (2.15) in addition to the flows of dislocations created by the external and internal stresses. For a relatively low correlation stress we have

$$j_p^{\mathrm{cor}} \approx \rho u M_{pq}^{\mathrm{cor}} \sigma_{qk}^{\mathrm{cor}} b_k\,, \qquad M_{pq}^{\mathrm{cor}} = \frac{\partial \ln u}{b\, \partial \sigma_{pq}^{\mathrm{cor}}}\,. \tag{4.5}$$

Expanding $\rho(r', t)$ in the integrand in Eqn (4.4) in a Taylor series with respect to $r' - r$ and carrying out integration, we obtain for the ensemble in question the following expression for the correlation flux:

$$\mathrm{J}_p^{\mathrm{cor}} = \rho(r, t) u M_{pq}^{\mathrm{cor}} (A_1 + A_2 \nabla^2 + \ldots) \nabla_q \rho\,, \tag{4.6}$$

where

$$A_1(t) = -\mu b^2 \int_0^\infty r\, g(r, t)\, \mathrm{d}r\,,$$
$$A_2(t) = -\frac{\mu b^2}{6} \int_0^\infty r^3\, g(r, t)\, \mathrm{d}r\,, \qquad r = |r' - r|\,. \tag{4.7}$$

The solution of the stationary kinetic equation for the correlation function is [140]

$$g(|r' - r|) = -\frac{\mu b^2}{2\pi E} K_0\left(\frac{|r' - r|}{r_{\mathrm{D}}}\right), \tag{4.8}$$

where $K_0(x)$ is the Bessel function of the imaginary argument of zero order; $r_{\mathrm{D}} = (E/\mu b^2)^{1/2} \rho^{-1/2}$ is the radius of 'Debye atmosphere' of dislocations of opposite sign; and E is a certain mechanical energy (the counterpart of the kinetic 'temperature' of the dislocation ensemble), which defines the finite value of the correlation radius of dislocations. As a result, we find that in the expression for the correlation flux (4.7) we have

$$A_1 = \frac{\mu b^2}{2\pi\rho}\,, \qquad A_2 = \frac{E}{3\pi\rho^2}\,. \tag{4.9}$$

Substitution of Eqn (4.7) into the kinetic equations for the densities of positive and negative dislocations of the type of (2.15) and the appropriate linear analysis of stability of the system of equations with respect to inhomogeneous fluctuations of the density of dislocations reveal [211] that this system of equations becomes unstable when the fluctuations reach their critical amplitudes of

$$\Lambda_{\mathrm{cr}} = 2\pi\left(\frac{2A_2}{A_1}\right)^{1/2} = K_2 \rho^{-1/2}\,, \qquad K_2 = 4\pi\left(\frac{E}{3\mu b^2}\right)^{1/2}. \tag{4.10}$$

In this way, the correlation interaction of dislocations in principle warrants the emergence of the spatially modulated clustering of dislocations in crystal with the characteristic length $\Lambda \propto \rho^{-1/2} \propto \sigma^{-1}$, in agreement with experiment (see Eqn (4.1) and Fig. 6). According to experiment, the constant $K_2 = K_1/\alpha$ must be of the order of 2.4 – 6.0, depending on the magnitude of the constant of interaction between dislocations α: $\alpha = 0.2$ for Taylor's interaction, and $\alpha = 0.5$ in the case of interaction with forest dislocations.

The relation between the mechanical energy of dislocations and the energy of their interaction $E/\mu b^2 \approx 0.1 - 0.7$ is then such that the correlation radius is $r_{\mathrm{D}} \leqslant l_\rho$, where $l_\rho = \rho^{-1/2}$ is the mean distance between dislocations in the ensemble. This means that even if the correlation effect does exist, it is not strong enough to account for the formation of slip lines in crystal. On top of that, like the relay mechanisms described above [204, 205, 210], the correlation mechanism is strictly deterministic and does not explain the existence of a multilevel and multiscale system of slip lines [200], which is self-similar [208] and suggests a branching fractal mechanism of development of plastic deformation in crystal.

These features are accounted for by the mechanism of multiplication of dislocations through double cross slip of screw dislocations. In the first place, this mechanism is essentially stochastic, because the ejection of a dislocation segment into the adjacent parallel plane is a random event [see Eqn (2.14)].

Second, some of these events are accompanied by the formation of Frank – Read sources, which generate dislocations and give rise to new slip lines. In turn, dislocations in slip lines may form new slip lines through the DCS mechanism. This means that the process of formation of slip lines has a branching (chain) multilevel nature. It is based on the same elementary act (pattern) — the ejection of a dislocation segment into the adjacent slip plane, giving rise to a slip line.

Third, the distance of ejection of a dislocation segment into the adjacent slip plane (2.13), which gives rise to a new slip line, decreases with increasing stress: $h_0 \propto \sigma^{-1}$, which gives at least a qualitative explanation to the observed decrease in the distance between slip lines as the plastic deformation develops (see Fig. 6).

4.2 Double cross slip and equations of evolution of dislocation density

The above equations of evolution of dislocation density (2.15) and (2.16) assume that generation of dislocations from the sources and multiplication of dislocations occur uniformly throughout the crystal. In this section we are going to take into consideration the stochastic and integral (chain) character of multiplication of dislocations by the DCS mechanism.

The elementary act of double cross slip of a screw segment of dislocations occurs with a certain probability

(2.14). Its result depends on the height h of ejection of the screw segment of dislocation into the parallel slip plane. If $h < h_0$, then an edge dipole is formed; if $h > h_0$, the Frank–Read dislocation source is formed that generates a finite number p of dislocation loops, whose screw portions take part in the acts of DCS and produce new sources of dislocations. The stochastic and integral nature of the process of multiplication of dislocations through the DCS mechanism relates not only to the coordinate y in the direction transverse to the slip plane, but also to the coordinate x in the direction of motion of screw portions of the loops.

Given this, the equations of evolution of the density of dislocations (2.15) and (2.16) assume the form

$$\frac{\partial \rho_{\mathrm{m}}}{\partial t} + \nabla \cdot (u\rho_{\mathrm{m}}) = n(r)u + p\lambda_{\mathrm{s}}^{-1} \int_x^{\infty} Q(x'-x)\,\mathrm{d}x' \times \int_{y+h_0}^{\infty} P(y'-y)\,u(\rho_{\mathrm{m}})\,\rho_{\mathrm{m}}(x',y',t)\,\mathrm{d}y' - (\lambda_{\mathrm{is}}^{-1} + h_{\mathrm{i}}\rho_{\mathrm{i}})u\rho_{\mathrm{m}} + \delta_{\mathrm{f}}\,\rho_{\mathrm{f}}^{1/2}u\rho_{\mathrm{m}} - h_{\mathrm{a}}u\rho_{\mathrm{m}}^2\,, \tag{4.11}$$

$$\frac{\partial \rho_{\mathrm{i}}}{\partial t} = \lambda_{\mathrm{s}}^{-1} \int_x^{\infty} Q(x'-x)\,\mathrm{d}x' \times \int_{y}^{y+h_0} P(y'-y)\,u(\rho_{\mathrm{m}})\,\rho_{\mathrm{m}}(x',y',t)\,\mathrm{d}y' - h_{\mathrm{d}}u\rho_{\mathrm{i}}\,\rho_{\mathrm{m}}\,, \tag{4.12}$$

where

$$Q(x'-x) = \lambda_{\mathrm{s}}^{-1} \exp\left(-\frac{|x'-x|}{\lambda_{\mathrm{s}}}\right), \qquad P(y'-y) = h_{\mathrm{c}}^{-1} \exp\left(-\frac{|y'-y|}{h_{\mathrm{c}}}\right), \tag{4.13}$$

$Q(x'-x)$ is the probability that the screw segment of the dislocation loop will cover the distance $x'-x > \lambda_{\mathrm{s}}$ after the DCS act; and λ_{s} is the path of screw segments to the appropriate obstacles. In writing these equations, we have taken into account the fact that the velocity of dislocations u, owing to deformation hardening (3.7), depends on the density of dislocations $\rho_{\mathrm{m}}(x,y,t)$.

Equations (4.11) and (4.12) are integrodifferential equations. For analyzing their stability with respect to inhomogeneous density fluctuations, it will be convenient to convert them to a purely differential form, by expanding the density of dislocations $\rho_{\mathrm{m}}(x',y',t)$ [or, more precisely, the flow of dislocations $u(\rho_{\mathrm{m}})\,\rho_{\mathrm{m}}$] into the double Taylor series with respect to variables $x'-x$, $y'-y$:

$$u(\rho_{\mathrm{m}})\,\rho_{\mathrm{m}}(x',y',t) = u\big[\rho_{\mathrm{m}}(x,y,t) + (1-M)\,R(x'-x,y'-y,t)\big]\,,$$

$$R(x'-x,y'-y,t) = \sum_{n=1} \frac{1}{n!}\left[(x'-x)\frac{\partial}{\partial x} + (y'-y)\frac{\partial}{\partial y}\right]^n \rho_{\mathrm{m}}(x,y,t)\,. \tag{4.14}$$

Substituting Eqn (4.14) into Eqns (4.11) and (4.12) and calculating the integrals, with due account for the symmetry and positivity of the integrands, we obtain

$$\frac{\partial \rho_{\mathrm{m}}}{\partial t} + \nabla \cdot (u\rho_{\mathrm{m}}) = n(r)u + (\lambda_{\mathrm{m}}^{-1} - \lambda_{\mathrm{is}}^{-1} - h_{\mathrm{i}}\,\rho_{\mathrm{i}})u\rho_{\mathrm{m}} + \delta_{\mathrm{f}}\,\rho_{\mathrm{f}}^{1/2}u\rho_{\mathrm{m}} - h_{\mathrm{a}}u\rho_{\mathrm{m}}^2 + \sum_{k=0}^{n} D^{(\mathrm{m})}_{(n-k)x,\,ky} \frac{\partial^n \rho_{\mathrm{m}}}{\partial x^k\,\partial y^{n-k}}\,, \tag{4.15}$$

$$\frac{\partial \rho_{\mathrm{i}}}{\partial t} = \lambda_{\mathrm{ie}}^{-1}u\rho_{\mathrm{m}} - h_{\mathrm{d}}u\rho_{\mathrm{i}}\,\rho_{\mathrm{m}} + \sum_{k=0}^{n} D^{(\mathrm{i})}_{(n-k)x,\,ky} \frac{\partial^n \rho_{\mathrm{m}}}{\partial x^k\,\partial y^{n-k}}\,. \tag{4.16}$$

Here,

$$\lambda_{\mathrm{m}}^{-1} = p\lambda_{\mathrm{s}}^{-1} \exp\left(-\frac{h_0}{h_{\mathrm{c}}}\right), \qquad \lambda_{\mathrm{ie}}^{-1} = \lambda_{\mathrm{s}}^{-1}\left[1 - \exp\left(-\frac{h_0}{h_{\mathrm{c}}}\right)\right],$$

$$M = -\frac{\partial \ln u}{\partial \ln \rho_{\mathrm{m}}} = \frac{V\sigma_{\mu}}{2kT}\,, \tag{4.17}$$

and $V = -\mathrm{d}H/\mathrm{d}\sigma^*$ is the activation volume.

The nonzero diffusion coefficients $D^{(\mathrm{m})}$ at even powers of space derivatives in Eqn (4.15) up to $n = 4$ (dropping the subscript m) are, respectively,

$$D_{2x} = p(1-M)\lambda_{\mathrm{s}}u\,, \qquad D_{2y} = \frac{1}{2}\,p(1-M)\frac{h_0^2}{\lambda_{\mathrm{s}}}\,u\,\varphi_2(q)\,,$$

$$D_{4x} = \lambda_{\mathrm{s}}^2 D_{2x}\,, \qquad D_{4y} = \frac{1}{24}\,p(1-M)\frac{h_0^2}{\lambda_{\mathrm{s}}}\,u\,\varphi_4(q)\,,$$

$$D_{2x,\,2y} = \lambda_{\mathrm{s}}^2 D_{2y}\,, \qquad \varphi_2(q) = (1 + 2q + 2q^2)\exp\left(-\frac{1}{q}\right),$$

$$\varphi_4(q) = (1 + 4q + 12q^2 + 24q^3 + 24q^4)\exp\left(-\frac{1}{q}\right), \quad q = \frac{h_{\mathrm{c}}}{h_0}\,. \tag{4.18}$$

In a similar way, one can find coefficients $D^{(\mathrm{i})}$ in Eqn (4.16). The estimates indicate, however, that $D^{(\mathrm{i})} \ll D^{(\mathrm{m})}$, and their role in the development of instabilities is not important. Because of this, the corresponding terms in Eqn (4.16) may be disregarded.

4.3 Slip lines

If in Eqn (4.15) and (4.16) the bulk density of dislocation sources n is large enough, and they are evenly distributed throughout the crystal, then the equations admit stationary homogeneous solutions

$$\rho_{\mathrm{i0}} = (h_{\mathrm{i}}\,\rho_{\mathrm{m0}})^{-1}\left[n + (\lambda_{\mathrm{m}}^{-1} - \lambda_{\mathrm{is}}^{-1} + \delta_{\mathrm{f}}\,\rho_{\mathrm{f}}^{1/2})\rho_{\mathrm{m0}} - h_{\mathrm{a}}\,\rho_{\mathrm{m0}}^2\right], \tag{4.19}$$

$$\rho_{\mathrm{i0}} = (\lambda_{\mathrm{ie}}h_{\mathrm{d}})^{-1}\,. \tag{4.20}$$

Curve *1* in Fig. 7 schematically depicts function (4.19) when $\rho_{\mathrm{f}} = \rho_{\mathrm{m}}$ (the second and third stages of hardening). The horizontal line *2* in this diagram corresponds to Eqn (4.20). We see that this system has three solutions. One of them (point a in Fig. 7) falls within the first stage of hardening, another (point b) is near the beginning of the second stage, and the third (point c) belongs to the third stage of the curve of hardening (cf. Fig. 1).

Let us investigate the stability of equations (4.15) and (4.16) in the neighborhood of point a with respect to fluctuations of density of the form $\delta\rho \propto \exp(\omega + \mathrm{i}q_x + \mathrm{i}q_y)$.

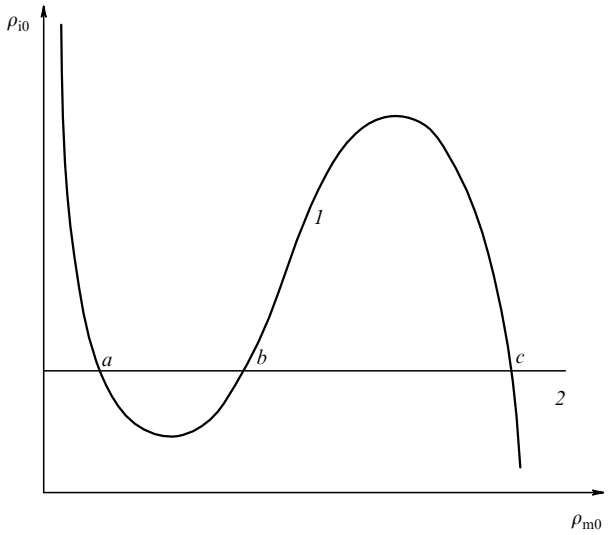

Figure 7. Curves of local linkage of densities of mobile ρ_{m0} and immobile ρ_{i0} dislocations according to Eqns (4.19) and (4.20).

At point a we have

$$\rho_{m0} = \frac{n\lambda_m}{\beta_i - 1}\,, \qquad \rho_{i0} = (h_d\lambda_{ie})^{-1}\,, \qquad \beta_i = \frac{\lambda_m}{\lambda_{is}} + \frac{h_i}{h_d}\,\frac{\lambda_m}{\lambda_{ie}} > 1\,. \tag{4.21}$$

Linear analysis indicates that the values of wave vectors corresponding to the criteria of instability of fluctuations

$$\frac{\partial\omega}{\partial q_x} = 0\,, \qquad \frac{\partial\omega}{\partial q_y} = 0\,, \qquad \omega(q_x, q_y) \geqslant 0\,, \tag{4.22}$$

are

$$q_x^{cr} \approx \left(\frac{D_{2x}}{2D_{4x}}\right)^{1/2}, \qquad q_y^{cr} \approx \left(\frac{D_{2y}}{2D_{4y}}\right)^{1/2}. \tag{4.23}$$

For the critical amplitudes of fluctuations $\Lambda_{x,y}^{cr} = 2\pi q_{x,y}^{-1}$, and the critical increment, we find, respectively,

$$\Lambda_x^{cr} = 2\sqrt{2}\,\pi\lambda_s\,, \qquad \Lambda_y^{cr} = \frac{2\pi}{\sqrt{6}}\left[\frac{\varphi_4(q)}{\varphi_2(q)}\right]_{q=1}^{1/2} h_0 \approx 9{,}2h_0\,, \tag{4.24}$$

$$\omega(q_x^{cr}, q_y^{cr}) = \frac{n\lambda_m}{\beta_i - 1}\,(h_i h_d)^{1/2} u > 0\,.$$

The magnitude of Λ_y^{cr} was estimated under the assumption that the quantity $q = h_c/h_0$ remains more or less the same in the course of deformation. According to Ref. [148], in LiF crystals we have $h_c/h_0 \approx 1$. This is because the mean distance of cross slip $\bar{h} = h_c$ decreases with increasing stress.

From the estimate for Λ_y^{cr} it follows that the amplitude of critical fluctuations is equal to several h_0 distances required for the DCS act to give rise to a Frank – Read source, which is an indication of the cooperative nature of the development of instability. Taking into account the dependence of distance h_0 on stress (2.13), we find the amplitude of critical fluctuations of the dislocation density as a function of stress:

$$\Lambda_y^{cr} = K_1\,\frac{\mu b}{\sigma - \sigma_f}\,, \qquad K_1 = \frac{1}{4\sqrt{6}\,(1 - \nu_P)}\left[\frac{\varphi_4(q)}{\varphi_2(q)}\right]_{q=1}^{1/2} \approx 0.5\,. \tag{4.25}$$

Now, let us consider the solution of Eqns (4.15) and (4.16) near point a, retaining in Eqn (4.15) only the first diffusional term with respect to coordinate y. We have the following equations:

$$\frac{\partial\rho_m}{\partial t} + \nabla\cdot(u\rho_m) = nu + (\lambda_m^{-1} - \lambda_{is}^{-1} - h_i\,\rho_i)u\rho_m + (1 - M)\lambda_y u\,\frac{\partial^2\rho_m}{\partial y^2}\,, \tag{4.26}$$

$$\frac{\partial\rho_m}{\partial t} = (\lambda_{ie}^{-1} - h_d\rho_i)u\rho_m\,, \qquad \lambda_y = \frac{1}{2}\,p\,\frac{h_0^2}{\lambda_s}\,\varphi_2(q)\,. \tag{4.27}$$

Near point a we may set $\partial\rho_m/\partial t = \partial\rho_i/\partial t = 0$. Then, the solution of Eqn (4.26) with zero drift flow is

$$\rho_m(y) = \rho_{m0}\left(1 + \cos 2\pi\,\frac{y}{\Lambda_y}\right),$$

$$\Lambda_y = 2\pi\left[\frac{M - 1}{\beta_i - 1}\right]^{1/2}(\lambda_m\lambda_y)^{1/2}\,. \tag{4.28}$$

Solution (4.28) describes a dislocation structure spatially modulated in the direction transverse to the slip plane of dislocations, with the period $\Lambda_y \propto h_0 \propto \sigma^{-1}$:

$$\Lambda_y = K_1\,\frac{\mu b}{\sigma - \sigma_f}\,,$$

$$K_1 = \frac{1}{4(1 - \nu_P)}\left[\frac{M - 1}{\beta_i - 1}\right]^{1/2}\left[\frac{1}{2}\exp\left(\frac{1}{q}\right)\varphi_2(q)\right]^{1/2}. \tag{4.29}$$

The existence of this structure requires that the relative coefficient of immobilization of dislocations β_i and the coefficient M that accounts for the effect of strain hardening on the velocity of dislocations should be greater than unity. For example, at room temperature in copper single crystals at the first stage of hardening, the coefficient of inversion of the dislocation flux is $M = M_1 = 20$ [113]. Setting $\beta_i = 2$, $q = 1$, $\nu_P = 0.25$ in Eqn (4.29), we obtain an estimate $K_1 = 2.3$, which in order of magnitude fits in with the experimental value of $K_1 = 1.2$. The mean distance between slip lines is 4.6 times greater than the amplitude of critical fluctuations of density (4.25).

We see that there are several levels (scales) of slipping. The smallest is the level of elementary slip associated with the DCS mechanism, $h_0 = 10 - 10^2$ nm. Next follows the level of critical fluctuations of dislocation density, $\Lambda_y^{cr} \approx 10h_0 = 0.1 - 1$ μm. The third level is represented by slip lines observable with an optical microscope, $\Lambda_y \approx 50h_0 = 0.5 - 5$ μm. At each level, the scale depends on the stress as $\Lambda \propto \sigma^{-1}$, which means that the deformation structures are self-similar [208]. Accordingly, the coefficients K_1 in Eqns (2.13), (4.25) and (4.29) are scaling coefficients. As follows from Eqns (4.26) and (4.27), the spatially periodic modulation of dislocation density is caused by the competing processes of generation of dislocations by sources, their immobilization in the form of dipoles, and inversion of diffusion flows because of strain hardening.

If the formation of slip lines is associated with the process of double cross slip of screw dislocations, then their distribution with respect to distances Λ (see Fig. 5) must be described by a function of the type of Eqn (2.14):

$$\frac{dN}{d\Lambda} = \Lambda_c^{-1}\exp\left(-\frac{\Lambda}{\Lambda_c}\right). \tag{4.30}$$

The broad spread of experimental points and the bimodal (with maxima near 100 and 375 nm) character of histograms in Fig. 5 for the Cu – Mn alloy make it difficult to compare Eqn (4.30) with the experimental findings. The spread of experimental points can be reduced if we consider not the differential distribution (4.30), but rather the integral distribution of slip lines with respect to distances Λ:

$$N(\Lambda) = N_0 \exp\left(-\frac{\Lambda}{\Lambda_c}\right), \tag{4.31}$$

where N_0 is the total number of slip lines.

The result of application of Eqn (4.31) to the unimodal histogram of distribution of slip lines in single crystals of Cu – 10 at. % Al [209] is shown in Fig. 8. We see that for this alloy the distribution of slip lines with respect to distances is well described by Eqn (4.31) with $\Lambda_c = 65$ nm. The exception is the region of the lowest values of Λ ($\Lambda < 60$ nm), where the experimental results deviate from Eqns (4.30) and (4.31). This may be caused by the inadequate sensitivity of the replica technique at $\Lambda < 60$ nm, or by the annihilation of screw dipoles that are formed in the act of DCS but do not have enough time to produce an active Frank – Read source.

The annihilation mechanism is borne out by the fact that the deviation from distributions (4.30) and (4.31) starts earlier for the Cu – Mn alloy (at $\Lambda = 100$ nm; see Fig. 5). The energy of stacking fault for the Cu – Mn alloy is four times as large as that for the Cu – Al alloy [209], which greatly increases the probability of dislocation annihilation [113, 162 – 163].

It should be noted that application of scanning tunneling microscopy to the study of structure of slip lines on the surface of deformed crystals [209, 212 – 214] opens up the scale of 1 to 10 nm. The first results of these studies point to the discrete nature of deformation not only in the direction transverse to the slip plane of dislocations, but also in the slip planes themselves [213].

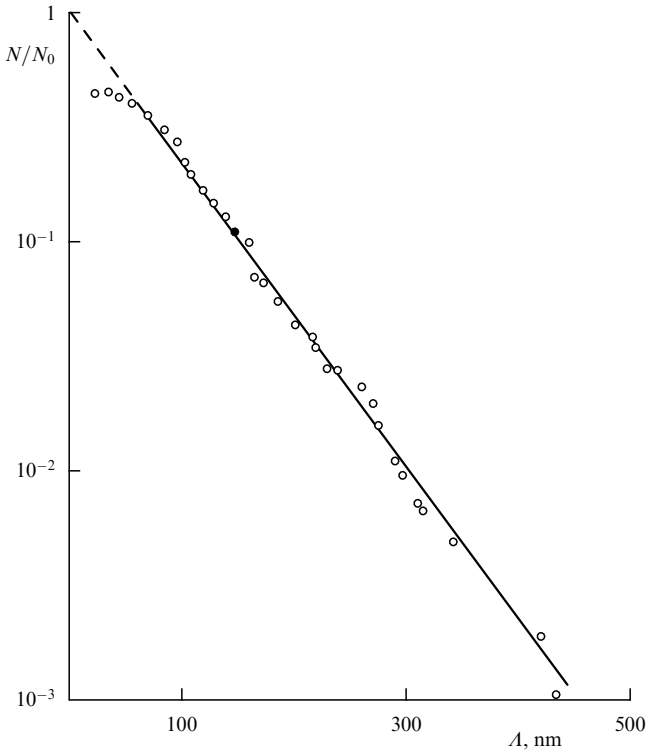

Figure 8. Curve of distribution of slip lines with respect to distances greater than Λ in single crystals of alloy Cu – 10 at. % Al [209].

4.4 Slip bands

Another characteristic feature of the initial stage of deformation of crystals is the formation and broadening of slip bands [39 – 42, 148, 200]. The steady movement of the front of multiplication of dislocations points to the concerted nature of the development of plastic deformation in the direction transverse to the slip plane of dislocations. The propagation of the front may be affected by the above mechanisms of formation of slip lines [200, 203 – 205] as a result of the action of internal stresses from pileups of dislocations of the same sign or the concentrator of stress in the form of a step on the surface of the crystal at the outcrop of the slip line. The action of these stresses may be associated with the drift flow of dislocations $j_y = \rho_m u_y$ in the direction transverse to the slip plane of dislocations.

Given this circumstance, equations (4.26) and (4.27) assume the form

$$\frac{\partial \rho_m}{\partial t} + u_y \frac{\partial \rho_m}{\partial y} + (M-1)\lambda_y u \frac{\partial^2 \rho_m}{\partial y^2} = nu - (\beta_i - 1)\lambda_m^{-1} u \rho_m ,$$

$$\frac{\partial \rho_i}{\partial t} = 0 .$$

Introducing in the notation of Eqn (4.21) the dimensionless density of dislocations $\rho = \rho_m/\rho_{m0}$ and the stationary coordinate $Z = (y - U_y t)/\Lambda_y$, where U_y is the rate of broadening of the band, we obtain the equation

$$\frac{d^2\rho}{dZ^2} - \omega \frac{d\rho}{dZ} = 1 - \rho , \qquad \omega = \frac{U_y - u_y}{(\beta_i - 1)u} \frac{\Lambda_m}{\Lambda_y} ,$$

$$\Lambda_y = \left(\frac{M-1}{\beta_i - 1}\right)^{1/2} (\lambda_m \lambda_y)^{1/2} , \tag{4.32}$$

which admits a solution of the form (curve *1* in Fig. 9)

$$\rho_m(Z) = \rho_{m0} \left\{1 - \exp\left[g(|Z| - Z_0)\right]\right\} , \qquad |Z| < Z_0 \tag{4.33}$$

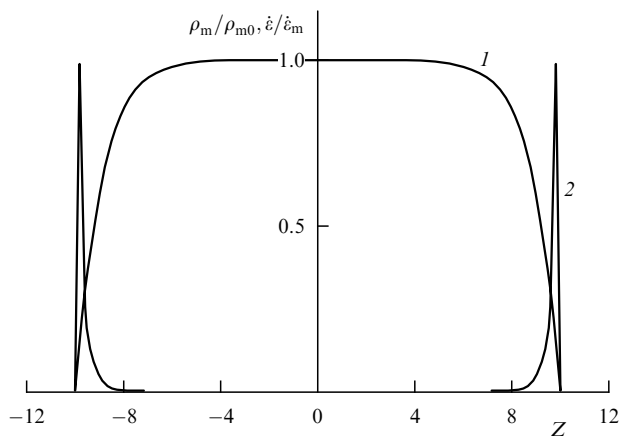

Figure 9. Distribution of dislocation density (*1*) and the rate of plastic deformation (*2*) across the width of the slip band.

under the conditions

$$g^2 - \omega g + 1 = 0\,, \qquad g_{1,2} = \frac{\omega}{2} \pm \sqrt{\frac{\omega^2}{4} - 1}\,. \tag{4.34}$$

For finding the parameter g, we have the equation of balance for the rate of plastic deformation in crystal where a two-way broadening of N slip bands takes place [148]:

$$\frac{\dot{\varepsilon}_0 l_0}{2N} = U_y \gamma\,, \tag{4.35}$$

where $\gamma = b\rho_{\mathrm{m}0}\lambda_{\mathrm{m}}$ is the deformation in the band [113], $\dot{\varepsilon}_0$ is the rate of plastic deformation set by the loading device, and l_0 is the length of crystal. In writing the equation of balance (4.35), we have noted that the rate of plastic deformation is the highest at the edges of the band because of strain hardening.

Curve *2* in Fig. 9 illustrates the distribution of the local deformation rate across the band $\dot{\varepsilon}(Z) = b\,\rho_{\mathrm{m}}(Z)\,u(\rho_{\mathrm{m}})$, where $\dot{\varepsilon}_{\max}$ is the maximum rate of deformation in the band, corresponding to the condition $M = 1$ [see Eqn (4.17)]. The calculation is based on the Arrhenius expression for the velocity of dislocations (2.5) with $H(\sigma^*) = H_0\left[1 - (\sigma^*/\sigma_{\mathrm{c}})^{1/2}\right]^2$ [24], $\sigma^* = \sigma - \sigma_{\mathrm{f}} - \alpha\mu b\rho_{\mathrm{m}}^{1/2}$, and $g = 1$, $Z_0 = 10$. For LiF crystals, the following values of parameters were used: $H_0/kT = 40$, $\sigma_{\mathrm{c}} = 8\sigma_{\mathrm{f}}$, $\sigma = 5\sigma_{\mathrm{f}}$, $\sigma_{\mathrm{f}} = 1$ MPa, $\alpha = 0.2$, $b = 0.3$ nm, $\mu = 4.3 \times 10^4$ MPa.

According to Eqn (4.34), the necessary condition for the formation and broadening of slip bands is $\omega > 2$. Making use of the notation of (4.32) and equation of balance (4.35), it may be represented as

$$\frac{\dot{\varepsilon}_0 l_0}{2Nnb\lambda_{\mathrm{m}}^2 u} > \frac{u_y}{u} + 2\,\frac{\lambda_y}{\lambda_{\mathrm{m}}}\,. \tag{4.36}$$

From condition (4.36) it follows that the formation and broadening of slip bands requires that their number N in the crystal should be not large, and the bulk density of dislocation sources n and the mobility of dislocations u be small. It is known that slip bands (Lüders bands) are formed in those crystals where, since the dislocations are strongly pinned by impurity atmospheres, or the surface quality is high, or the volume crystal is small (metallic 'whiskers' [39]), the number of dislocation sources and surface concentrators of stress N in crystal is not sufficient to warrant its uniform plastic deformation.

At the other extreme — when the bulk density of dislocation sources n and the number of surface concentrators of stress N in the crystal are large — condition (4.34) is not met ($\omega > 2$), and solution (4.33) of equation (4.26) makes way for solution (4.28). In other words, in place of one or a few slip bands, there are many of them.

Another circumstance that ought to be mentioned is the possibility of change (increase) of the number of slip bands in the course of plastic deformation because of the formation of new bands or the multiplication (branching) of existing bands.

The equation of balance for the rate of plastic deformation of crystal (4.35) can be written in the form

$$\dot{\varepsilon}_0 \approx 2N\dot{\varepsilon}_{\max}\,\frac{\Delta w}{l_0}\,, \tag{4.37}$$

where $\dot{\varepsilon}_{\max}$ and Δw are the rate of plastic deformation and the width of the region of localization of plastic deformation at the edges of the slip band (curve *2* in Fig. 9, respectively). When $\dot{\varepsilon}_{\max}$ is not large enough, or the region of localization of plastic deformation Δw is too narrow, the balance of deformation rates (4.37) may be achieved through increasing the number of slip bands N.

The processes of branching were observed with the propagation of Lüders bands [63] and Portevin – Le Châtelier bands [215], and also in inhomogeneously hardened or irradiated (layered) LiF crystals, when the slip bands pass from nonhardened to hardened (by doping or irradiation) crystal layers [216, 217]. The mechanism of branching of slip bands in layered crystals was theoretically treated in Ref. [218].

4.5 Annihilation channels

Bombardment of metallic crystals with neutrons or quenching from submelting temperatures produces a large number ($10^{15} - 10^{17}$ cm^{-3}) of vacancy and interstitial loops [57, 58]. Plastic deformation of irradiated or quenched crystals has special features associated not only with the hardening effects of radiation and quenching defects [219, 220], but also with the unsteady and nonuniform development of plastic deformation in such crystals.

Curve *2* in Fig. 10a schematically illustrates the stress – strain diagram for an irradiated or quenched crystal next to a conventional three-stage strain hardening curve *1* of well annealed metal. Plastic deformation of radiation-hardened or quenched crystals develops unevenly within the crystal as a Lüders front with small load jumps in the yield plateau (section *ab* in curve *2*). Load jumps are caused by the formation of coarse slip lines in the crystal with considerable local shifts (1 – 10) [57, 58, 221], which point to strong localization of deformation.

Transmission electron microscopic studies of deformation of preirradiated single crystals of copper [222, 223], and quenched aluminum crystals [224] reveal that the formation of coarse slip lines is associated with the formation of numerous defect-free channels (about 0.1 to 0.5 μm wide separated by 1 to 10 μm) in the defect structure of irradiated or quenched metals.

Figure 10b schematically shows the system of defect-free annihilation channels and their characteristic features. The

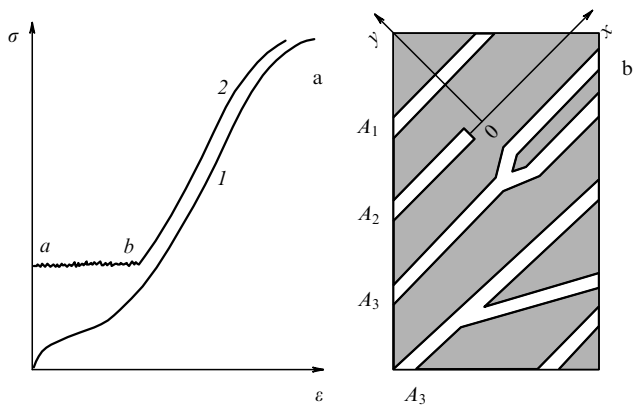

Figure 10. Stress – strain curves for annealed (*1*) and irradiated (*2*) crystals (a), and defect-free channels A_1, A_2, and A_3 in the defect structure of irradiated crystals after plastic deformation (b).

channels arrange along the slip planes, and can penetrate through the crystal (channels of type A_1). In some cases they have a dead end (channels of type A_2), or branch out (channels of type A_3). The existence of channels of types A_2 and A_3 is an indication of the relay mechanism of their formation. Such defect-free channels were found in many irradiated (Cu [57], Mo [225–227], Nb [228], Ni [229, 230], α-Fe [231, 232]) and quenched (Al [233], Au [234–236]) metallic crystals.

Another case of strong localization of strain in the shape of coarse slip lines with the formation of annihilation (dislocation-free) channels was observed in Refs [237–240] with plastic deformation of single-crystalline and polycrystalline molybdenum specimens at $T > 0.2T_m$ following predeformation at $T < 0.1T_m$. It was found that the flow stress of crystals predeformed at low temperature falls steadily after the start of flow; the stress–strain diagram, like in the case of irradiated or quenched specimens, shows small load jumps and coarse slip lines. When such crystals are strained further, the load jumps disappear, and the strain-hardening curve, like in the case of irradiated or quenched specimens (curve *1* in Fig. 10a), resumes its normal shape, typical of a given temperature of deformation.

Formation of dislocation-free channels in Mo was also observed in the experiments on fatigue [240, 241], electric spark erosion [242–244], and plastic deformation of Mo at the helium temperature of 4.2 K [240, 245]. In the latter two cases the formation of channels is due to the strong heating of regions of localization of deformation (slip lines) because of the dissipative processes that accompany electric spark erosion of metal and plastic deformation of crystals at low temperatures [246, 247].

The total or almost total absence of defects such as vacancy and interstitial loops and dislocations (in the case of molybdenum) in channels indicates that their formation is associated with the process of annihilation of dislocations that takes place at relatively low homological temperatures $(0.1-0.3)T_m$. Since it is only the screw components of dislocations that can annihilate at these temperatures, several mechanisms of conversion of vacancy and interstitial loops into conventional glissile dislocations were proposed — for example, through sweeping the loops by moving dislocations with the formation of jogs and kinks [248–250], or through the destruction of prismatic loops and sessile dislocation dipoles by the stress fields produced by the moving flat groups of dislocations of the same sign [251–253].

These studies did not touch upon the kinetic aspect of the problem, or the fact that the formation of a course slip line gives rise not to isolated defect-free or dislocation-free channels, but rather a system of such, with elements of self-organization. The latter is confirmed by the analysis [254, 255] of the published electron microscopic images of channels (Fig. 11). The diagram in Fig. 11a shows correlation between the width of channels $\Delta\Lambda_a$ and the mean distance between them Λ for a number of irradiated (Cu [223, 256], filled circles; Nb [228], empty circles; Ni [229], crosses) and quenched (Al [233], empty square; Au [234], empty triangle) metals. The experimental points group around a straight line with a slope of $\Delta\Lambda_a/\Lambda = 0.1$.

Figure 11b shows a similar correlation for the width of dislocation-free channels in single-crystal and polycrystalline Mo specimens. The filled circles in this diagram show the relationship between the width of channels and distance

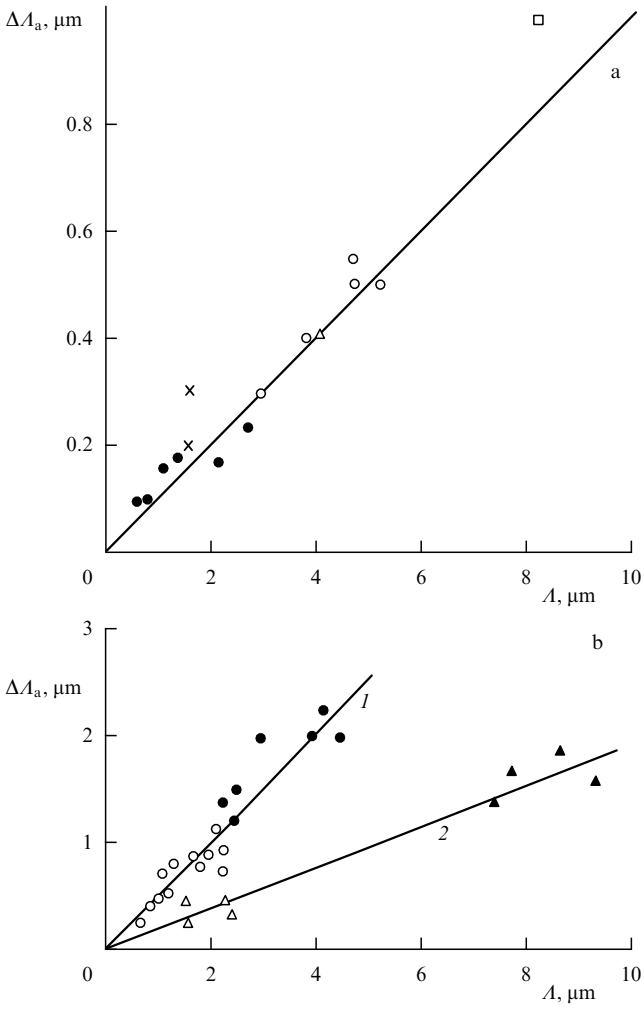

Figure 11. Correlation between the width $\Delta\Lambda_a$ of defect-free (a) and dislocation-free (b) channels and the distance between them [254, 255].

between them in the experiments on mechanical fatigue of Mo at a frequency of 36 Hz and temperature 293 K [240, 241]; the empty circles show the same relation in the case of plastic deformation of polycrystalline Mo at 493 K following predeformation at 293 K [239]. We see that these points group around the straight line *1* with a slope $\Delta\Lambda_a/\Lambda = 0.5$. The filled and empty triangles in Fig. 11b mark the results for dislocation-free channels in single-crystal and polycrystalline Mo specimens subjected to plastic deformation at 378 K after predeformation at 173 K [238]. In this case, the experimental points group around the straight line *2* with a slope $\Delta\Lambda_a/\Lambda = 0.2$.

From the arguments developed above it follows that the analysis of the formation of the system of channels must be based on the equations of dislocation kinetics taking due account of the fact that, after conversion of radiation and quenching defects into glissile dislocations, they further evolve in the conventional manner and take part in all processes that determine the evolution of the dislocation ensemble, for example, the process of double cross slip of screw dislocations.

The role of DCS in the formation of channels is confirmed by such evidence as the absence of annihilation channels in radiation damaged and subsequently deformed Cu–8 at. %

Al alloy, which has a low energy of stacking faults as compared with pure copper, or the presence of branching channels of type A_3 (Fig. 10b) in the defect structure of irradiated metals [232, 227], and in Mo predeformed at low temperature [237–240].

Before presenting the results of quantitative analysis of the mechanism of formation of annihilation channels based on the equations of evolution of dislocation density, let us make yet another remark concerning the initial defect structure of crystals that have been irradiated, quenched, or deformed at a low temperature. With the density of prismatic loops $N_0 = 10^{15}-10^{16}$ cm^{-3} and the average size $2R_0 = 10$ nm, the dislocation density after conversion into glissile dislocations is $\rho_0 = 2\pi R_0 N_0 \approx (0.3-3)\times 10^{10}$ cm^{-2}. This density is much greater than the density of dislocations 10^8 cm^{-2} typical of the initial stage of deformation of annealed crystals, and is close to the density of dislocations at the third stage of hardening.

A similar situation is observed with molybdenum — a metal with the bcc lattice. In the case of plastic deformation at temperatures $T < 0.1T_{\mathrm{m}}$ in metals with the bcc lattice, owing to the high stress of lattice friction of dislocations (Peierls stress), a uniform dislocation structure is formed that consists mainly of screw dislocations [46, 240, 259]. Subsequent deformation of Mo at a temperature $T > 0.15T_{\mathrm{m}}$ leads to annihilation of screw dislocations due to reduction of the stress of lattice friction of dislocations. As indicated by experiment, the annihilation decay of the initial defect structure 'overloaded' with dislocations in both cases occurs unevenly within the crystal, with the formation of defect-free or dislocation-free annihilation channels.

With due account for the convective (relay) mechanism of propagation of the front of annihilation of dislocations along the channels at the velocity u_x, we can write the equation of evolution of dislocation density in the form [254, 255, 260–262]:

$$\frac{\partial\rho}{\partial t} + u_x\frac{\partial\rho}{\partial x} + (M-1)\lambda_y u\frac{\partial^2\rho}{\partial y^2} = n_0 u - \lambda_{\mathrm{m}}^{-1}(\beta_{\mathrm{i}}-1)u\rho - h_{\mathrm{a}}u\rho^2 . \tag{4.38}$$

Because of the nonlinear term on the right-hand side of Eqn (4.38), the variables in the directions of the x and y axes (Fig. 10b) cannot be separated. Therefore, we consider an approximate solution of Eqn (4.38) under the assumption that the width of channels and the distance between them are determined primarily by the diffusion component of the flux of dislocations in the direction transverse to the slip plane of dislocations. (The motion of the front of annihilation of dislocations along the channel is discussed in Refs [260, 261].)

Introducing the dimensionless variables and parameters

$$\psi = \frac{\rho}{\rho_0}, \quad Y = \frac{y}{\Lambda_0}, \quad \Lambda_0 = \left[\frac{3(M-1)\lambda_y}{2bk_{\mathrm{a}}\rho_0}\right]^{1/2},$$
$$\psi_0 = \frac{3n_0}{bk_{\mathrm{a}}\rho_0^2}, \quad \psi_{\mathrm{m}} = \frac{3(\beta_{\mathrm{i}}-1)}{2bk_{\mathrm{a}}\lambda_{\mathrm{m}}\rho_0} > 0, \tag{4.39}$$

for the stationary case, we have the equation

$$\frac{\partial^2\psi}{\partial Y^2} = \frac{1}{2}\psi_0 - \psi_{\mathrm{m}}\psi - \frac{3}{2}\psi^2 . \tag{4.40}$$

Here, $\rho_0 = 2\pi R_0 N_0$ is the initial density of dislocations as defined earlier, confined in the radiation or quenching defects; $k_{\mathrm{a}} = h_{\mathrm{a}}/b$ is the coefficient of annihilation of screw dislocations.

Assuming the defects to be evenly distributed at the start of plastic deformation

$$\left.\frac{\partial N}{\partial y}\right|_{N=N_0} = 0, \quad \left.\frac{\partial\psi}{\partial Y}\right|_{\psi=1} = 0, \tag{4.41}$$

after integrating Eqn (4.40) once, we obtain

$$\left(\frac{\partial\psi}{\partial Y}\right)^2 = W(\psi) = (1-\psi)\left[(1+\psi_{\mathrm{m}}-\psi_0) + (1+\psi_{\mathrm{m}})\psi + \psi^2\right] . \tag{4.42}$$

The general solution to Eqn (4.42) is an elliptic integral of the first kind [254]

$$\delta^{-1}F(\theta,k) = \int\frac{\mathrm{d}\psi}{\sqrt{W(\psi)}} = \frac{y}{\Lambda_0} . \tag{4.43}$$

Its particular solutions $A-D$ depend on the absolute and relative magnitudes of the controlling (bifurcation) parameters ψ_0 and ψ_{m} in Eqn (4.40) (Fig. 12). They define the coefficient δ and the modulus k of the elliptic integral, and the roots of the cubic equation $W(\psi) = 0$:

$$\psi_1 = 1,$$
$$\psi_{2,3} = \frac{1}{2}\left[-(1+\psi_{\mathrm{m}}) \pm \sqrt{(1-\psi_{\mathrm{m}})^2 - 4(1-\psi_0)}\right]. \tag{4.44}$$

From Eqn (4.44) it follows that at

$$\psi_0 < 1 - \frac{1}{4}(1-\psi_{\mathrm{m}})^2 \tag{4.45}$$

equation $W(\psi) = 0$ has one real root. The integral (4.43) in this case describes a spatially periodical annihilation structure

$$\frac{1}{4}\frac{F(\theta,k)}{F(\pi/2,k)} = \frac{y}{\Lambda} \tag{4.46}$$

with the period $\Lambda = 4\delta^{-1}F(\pi/2,k)$ and the ratio of the width of annihilation channels to the distance between them

$$\frac{\Delta\Lambda_{\mathrm{a}}}{\Lambda} = 1 - \frac{1}{2}\frac{F(\theta_0,k)}{F(\pi/2,k)} , \tag{4.47}$$

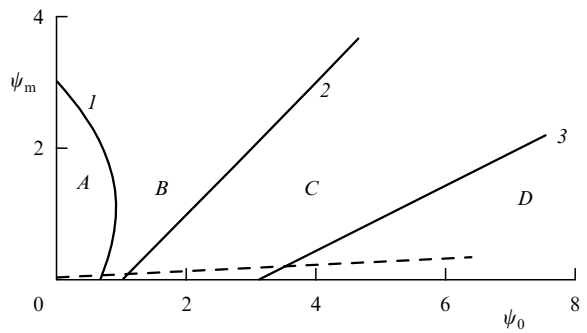

Figure 12. Regions $A-D$ of parameters ψ_0 and ψ_{m} corresponding to the existence of various annihilation and defect structures.

where

$$\cos\theta = \frac{\delta^2 - 1 + \psi}{\delta^2 + 1 - \psi}\,, \qquad \cos\theta\Big|_{\psi=0} = \cos\theta_0\,,$$

$$k^2 = \frac{1}{2} + \frac{1}{4}\,\frac{3 + \psi_{\rm m}}{\delta^2}\,, \qquad \delta^2 = (3 + 2\psi_{\rm m} - \psi_0)^{1/2}\,. \qquad (4.48)$$

Figure 13a shows the results of calculation of the annihilation structure (4.46) with $\psi_0 = 0.5$, $\psi_{\rm m} = 0$. The fraction of channels $\Delta\Lambda_{\rm a}/\Lambda$ in the structure being considered is 0.69. The relatively broad channels with $\Delta\Lambda_{\rm a}/\Lambda > 0.5$ are characteristic of the range of parameters ψ_0 and $\psi_{\rm m}$ marked in Fig. 12 with letter *A*. Curve *1* in this diagram corresponds to condition (4.45).

Outside region *A*, equation $W(\psi) = 0$ has three real roots. The character of the annihilation structure in this case depends on the relationship between the roots (4.44). At $\psi_3 < \psi_2 < \psi_1$, we have the annihilation structure

$$\frac{1}{2}\,\frac{F(\theta,k)}{F(\pi/2,k)} = \frac{y}{\Lambda}\,, \qquad \Lambda = \frac{4\Lambda_0}{\sqrt{1-\psi_3}}\,F\left(\frac{\pi}{2},\,k\right), \qquad (4.49)$$

$$\sin\theta = \left(\frac{1-\psi}{1-\psi_2}\right)^{1/2}, \qquad k = \left(\frac{1-\psi_2}{1-\psi_3}\right)^{1/2}.$$

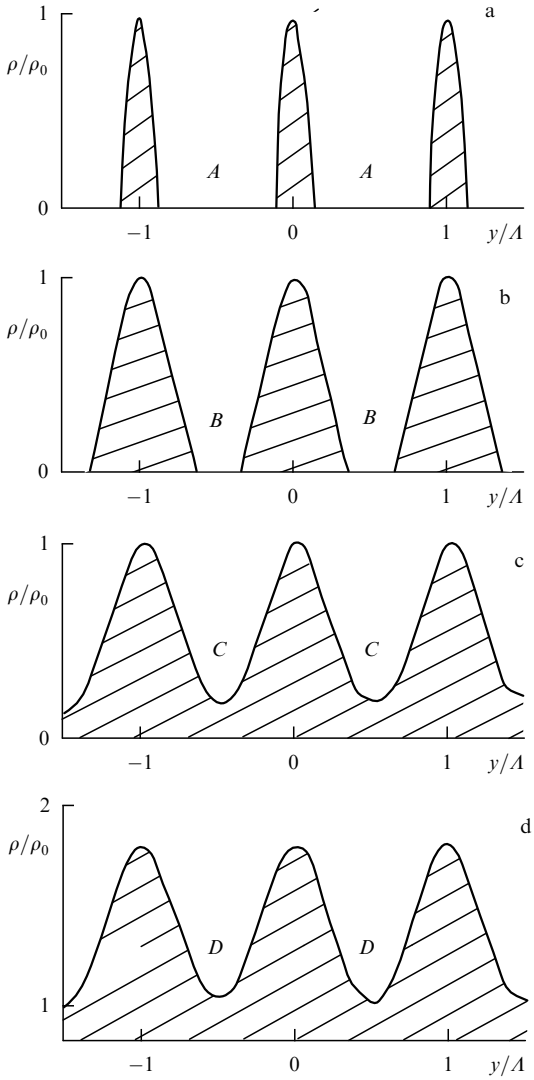

Figure 13. Character of annihilation structures corresponding to the regions *A* (a), *B* (b), *C* (c), and *D* (d) of parameters ψ_0 and $\psi_{\rm m}$ in Fig. 12.

If the condition $\psi_{\rm m} > \psi_0 - 1$ is satisfied (curve *2* in Fig. 12), the roots ψ_2 and ψ_3 become negative.

The annihilation structure shown in Fig. 13b corresponds to this condition ($\psi_0 = 0.9$, $\psi_{\rm m} = 0$). In Fig. 12, the condition $\psi_{\rm m} > \psi_0 - 1$ corresponds to the range of parameters *B*, within which the fraction of annihilation channels in the defect structure

$$\frac{\Delta\Lambda_{\rm a}}{\Lambda} = 1 - \frac{F(\theta_0,k)}{F(\pi/2,k)}\,, \qquad \sin\theta_0 = \frac{1}{\sqrt{1-\psi_2}} \qquad (4.50)$$

varies from 0 to 0.5. It is such a relation between $\Delta\Lambda_{\rm a}$ and Λ that is observed in the majority of experiments (see Fig. 11).

Upon transition to region *C*, the root ψ_2 becomes positive ($\psi_3 < 0$). This root is not greater than $\psi_1 = 1$ on condition that $\psi_{\rm m} > ((\psi_0 - 3)/2$ (curve *3* in Fig. 12). Annihilation channels in the range of parameters *C* are not entirely defect-free, but contain a finite density of defects (dislocations) $\rho_2 = \psi_2\rho_0 < \rho_0$ (channels of type *C* in Fig. 13c). Figure 14 shows the histogram of distribution of defects across the width of such a channel in neutron-irradiated (to a dose of 10^{18} cm^{-2}) copper [263]. The solid line in this diagram illustrates the distribution of defects as described by Eqn (4.49) with $\psi_0 = 1.47$.

At $\psi_2 = \psi_1 = 1$, the density of defects in the channels is equal to the initial density. This means that at $\psi_0 = 3$, $\psi_{\rm m} \approx 0$, the defect structure is stable against the process of annihilation decay. At $\psi_2 > \psi_1$, $\psi_0 > 3$ (region *D* in Fig. 12), the integral (4.43) describes the ordinary dislocation structure with the dislocation density $\rho > \rho_0$:

$$\frac{1}{2}\,\frac{F(\theta,k)}{F(\pi/2,k)} = \frac{y}{\Lambda}\,, \qquad \Lambda = \frac{4\Lambda_0}{\sqrt{\psi_2-\psi_3}}\,F\left(\frac{\pi}{2},\,k\right),$$

$$k\sin\theta = \left(\frac{\psi-1}{\psi-\psi_3}\right)^{1/2}, \qquad k = \left(\frac{\psi_2-1}{\psi_2-\psi_3}\right)^{1/2}. \qquad (4.51)$$

Figure 13d shows this structure with $\psi_0 = 6$, $\psi_{\rm m} = 0$.

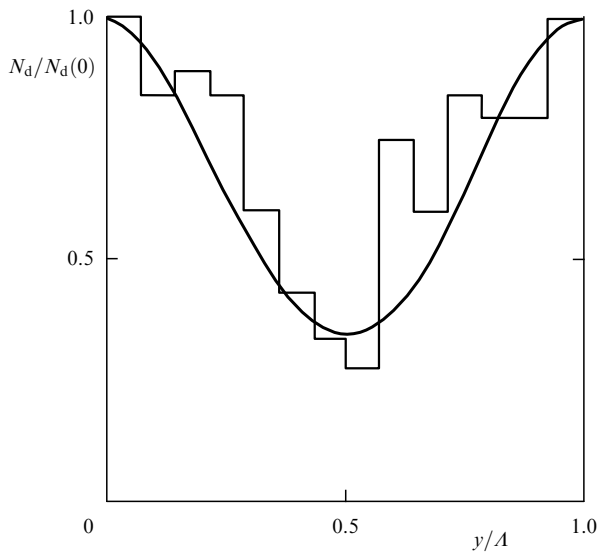

Figure 14. Histogram of the distribution of dislocation loops in the cross section of the annihilation channel in copper irradiated with neutrons [263]. Solid curve plotted from Eqn (4.49) with $\psi_0 = 1.47$, $\psi_{\rm m} = 0$.

In this way, the character of the dislocation structure that is formed because of plastic deformation in crystals that have been irradiated, quenched or predeformed at low temperature, depends essentially on the absolute and relative magnitude of the parameters ψ_0 and ψ_m. From definitions (4.39) it is clear that these parameters depend in turn on the initial density of defects $\rho_0 \propto N_0$ and on the coefficient of annihilation of screw dislocations k_a.

Some of the radiation and quenching loops, after recombination with gliding dislocations [248 – 250], can form Frank – Read dislocation sources with a density $n_0 = \beta_0 \rho_0^{3/2}$, where the coefficient β_0 defines the efficiency of loops as Frank – Read sources.

Given that the loops may also act as obstacles, on which dislocations multiply in the same way as on forest dislocations: $(b\lambda_m)^{-1} = \beta_f k_f \rho_0^{1/2}$, where β_f is the relevant efficiency, we find the parameters ψ_0 and ψ_m as functions of the initial density of defects:

$$\psi_0 = \frac{3\beta_0}{bk_a}\,\rho_0^{-1/2}\,, \qquad \psi_m = \frac{3(\beta_i - 1)}{2k_a}\,\beta_f k_f \rho_0^{-1/2}\,. \tag{4.52}$$

Since the density of loops varies with the irradiation dose as $N_0 \propto \Phi^n$, $n = 1/2 - 2/3$ [254], we find that the parameters ψ_0 and ψ_m decrease with the dose as $\psi_0 \propto \psi_m \propto \Phi^{-n/2}$. The ratio $\psi_m/\psi_0 = (\beta_i - 1)\,\beta_f(bk_f)/2\beta_0 \approx 10^{-2}$ [255] then remains approximately the same.

The dashed line in Fig. 12 schematically shows how the increase in the irradiation dose and the density of loops leads to a decrease in the parameters ψ_0 and ψ_m and a gradual transition from the dislocation structures of type *D* to the annihilation structures of types *C*, *B* and *A* (see Fig. 13). In nickel single crystals subjected to nonuniform bombardment with neutrons, for example, such a transition was observed when slip lines crossed the boundary between irradiated and unirradiated parts of the crystal. This transition was accompanied by a coarsening of slip lines and the formation of defect-free channels [230].

Another factor that strongly affects the values of the critical parameters ψ_0 and ψ_m is the coefficient of annihilation of dislocations k_a. Figure 15 shows the temperature dependence of annihilation coefficients for a number of bcc and fcc (face-centered cubic) metals derived from strain-hardening curves [159 – 164] of these metals at different temperatures using relation (3.11) between the coefficient of strain hardening θ and the flow stresses at the third stage of the hardening curve, which can also be represented in the form [157, 264]

$$\theta = \theta_m - \frac{1}{2}\,\kappa_a \sigma\,. \tag{4.53}$$

The slope of these lines (see Fig. 1) defines the coefficient of annihilation. In the case of fcc metals we have $k_a \propto \sigma_3^{-1}$ [160, 162], where σ_3 is the stress at the beginning of the third stage of strain hardening. Taking into account the temperature dependence of σ_3 [265], we obtain [113, 163]

$$k_a(T) = k_a(0)\exp\left(\frac{kT}{A}\ln\frac{\dot\varepsilon_0}{\dot\varepsilon}\right). \tag{4.54}$$

The temperature dependences of k_a in Fig. 15a are plotted in the coordinates $\ln k_a - T$. We see that with an increase in the stacking fault energy γ_D the slope of the lines increases, as the energy parameter *A* decreases with increasing γ_D [265]. As

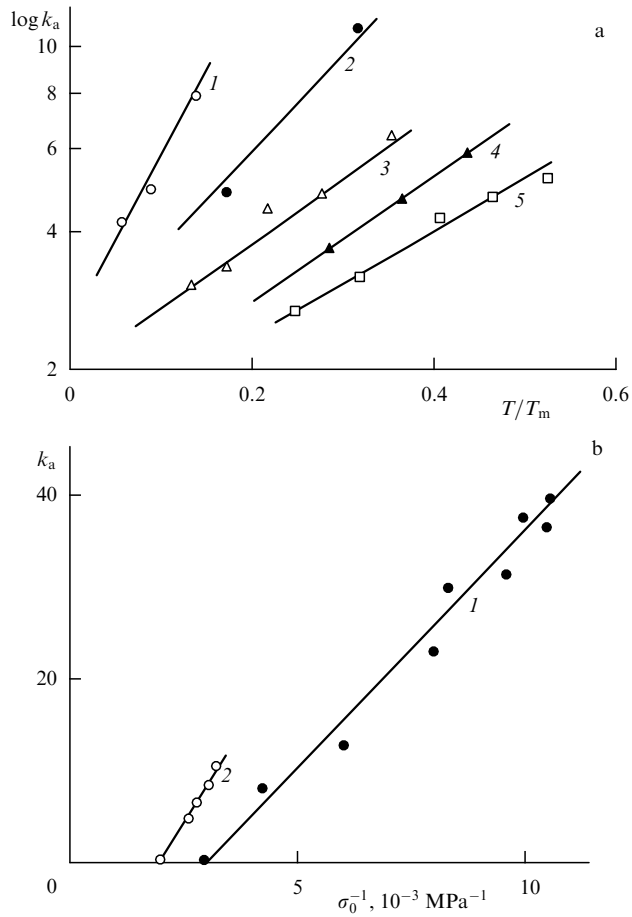

Figure 15. Coefficients of annihilation of screw dislocations: (a) in fcc metals (*1*, Al; *2*, Ni; *3*, Cu; *4*, Ag; *5*, Au [113, 162, 163]) vs. temperature; (b) in bcc metals (*1*, Mo; *2*, α-Fe [113, 261]) vs. inverse yield stress σ_0.

regards the bcc metals, the coefficient of annihilation of dislocations for them depends on the stress of lattice friction of dislocations (the Peierls stress): $k_a \propto \sigma_P^{-1}(T)$ [113, 162].

Figure 16b shows the dependence of k_a on the inverse yield stress $\sigma_0(T)$ for α-Fe and Mo [162] in the temperature range $(0.1 - 0.25)T_m$. At $T < 0.1T_m$, owing to the high stress of lattice friction of dislocations, the coefficient of annihilation of screw dislocations is practically zero, while at $T = 0.2T_m$ for Mo it approximately equals 40. Such a large value of the coefficient of annihilation of screw dislocations in Mo explains why defect-free [225, 226] and dislocation-free [237 – 245] channels form so easily in this metal. The formation of dislocation-free channels is caused by the dramatic reduction of the critical parameter $\psi_0 \propto k_a^{-1}(T)$ as the temperature increases, so that this parameter falls within the region of formation of dislocation-free channels *C*, *B*, and *A* (see Fig. 12).

Note in conclusion that the formation of dislocation-free channels in experiments on mechanical fatigue [60 – 62] may also be the result of annihilation decay of the system of deformation dipoles, which are easily formed under cyclic plastic deformation.

5. Cellular dislocation structure

As indicated by the electron microscopic studies [43 – 49], in upon plastic deformation of crystals, at the second and

third stages of strain hardening, the layered dislocation structures [46] typical of the first stage of hardening, give way to two-dimensional (network [49]) and three-dimensional (cellular [43–46]) dislocation structures. The formation of such structures depends on the operation of two or more slip systems. Attempts to establish the mechanism of their formation were based on the force [266], energy [84, 267], and kinetic considerations [83, 87, 114, 116, 268], as well as on the computer simulation of dislocation dynamics [269].

The first two approaches neglect the real features of the crystal structure (the presence of impurities, inclusions, and other obstacles in the way of moving dislocations), which, as indicated by experiment, are important for the formation of a cellular dislocation structure. The kinetic approach to the problem takes the crystal structure into account by including the structure-dependent processes of multiplication, immobilization, annihilation, and diffusion of dislocations into the initial kinetic equations. In most cases, the researchers confined themselves to qualitative analysis of the kinetic equations [83, 87, 268], or to the linear analysis of their stability with respect to the spatial fluctuations of density [114]. In this section we will discuss those works in which the analysis of the kinetics of formation of cellular structures goes as far as a direct quantitative comparison of experimental and theoretical results [116, 124, 270–273].

5.1 Equation of evolution of dislocation density in the case of multiple slip

The cellular dislocation structure starts to form at the second stage of hardening in the form of a network of individual dislocations [274], their bundles [43–46, 274], and tangles [46, 48]. Toward the end of the second stage of hardening, the bundles join together, forming a cellular structure with a high density of dislocations at the borders of the cells, and a low density of dislocations within the cells. When two slip systems have approximately the same orientation of slip planes with respect to the axis of extension (compression) of the crystal, the resulting dislocation structure has a network appearance (rectangular or square), with the cell boundaries aligned with the respective crystallographic slip planes [49, 175]. When many slip systems act simultaneously, the cells become rounded and lose coordination with the crystallographic planes.

Given this, the kinetic equation (4.15) for the densities of dislocations ρ_1 and ρ_2, when two slip systems are in action, can be written in the form [116]

$$\frac{\partial\rho_1}{\partial t}+(M-1)\lambda_D u\,\frac{\partial^2\rho_1}{\partial x^2}=(1-\beta_{\rm i})\lambda_{\rm m}^{-1}u\rho_1+\delta_{\rm f}\,\rho_2^{1/2}u\rho_1-h_{\rm a}u\rho_1^2\,, \tag{5.1}$$

$$\frac{\partial\rho_2}{\partial t}+(M-1)\lambda_D u\,\frac{\partial^2\rho_2}{\partial y^2}=(1-\beta_{\rm i})\lambda_{\rm m}^{-1}u\rho_2+\delta_{\rm f}\,\rho_1^{1/2}u\rho_2-h_{\rm a}u\rho_2^2\,, \tag{5.2}$$

where $\lambda_D\approx ph_0^2/\lambda_{\rm s}$ is the characteristic distance of diffusion of dislocation by the DCS mechanism in the direction transverse to the slip plane of dislocations (4.18).

Since the densities of dislocations in the primary and secondary slip systems at the second stage are practically the same ($\rho_1=\rho_2=\rho$ [183]), equations (5.1) and (5.2) can be reduced to one equation

$$\frac{\partial\rho}{\partial t}+(M-1)\lambda_D u\,\frac{\partial^2\rho}{\partial y^2}=(1-\beta_{\rm i})\lambda_{\rm m}^{-1}u\rho+\delta_{\rm f}\,\rho^{3/2}u\rho-h_{\rm a}u\rho^2\,. \tag{5.3}$$

Taking into account that $\beta_{\rm i}=\lambda_{\rm m}/\lambda_{\rm i}+h_{\rm i}\lambda_{\rm m}\rho_{\rm i0}$, and setting the right-hand side of Eqn (5.3) equal to zero, we obtain Eqn (4.19) at $n=0$. It has two solutions, represented by points b and c at the intersections of curve *1* with straight line *2* in Fig. 7. Analysis indicates that the former is an unstable focus, and the latter is a saddle.

Noting that $\partial\rho/\partial t=(\partial\rho/\partial\varepsilon)\dot\varepsilon$, where $\dot\varepsilon=b\rho u$ is the rate of plastic deformation, Eqn (5.3) can also be written in the form

$$\rho\,\frac{\partial\rho}{\partial\varepsilon}+(M-1)\,\frac{\lambda_D}{b}\,\frac{\partial^2\rho}{\partial y^2}=k_{\rm a}\rho\Big(\sqrt{\rho}-\sqrt{\rho_b}\Big)\Big(\sqrt{\rho}_c-\sqrt{\rho}\Big)\,, \tag{5.4}$$

where the densities of dislocations ρ_b and ρ_c, corresponding to the points b and c in Fig. 7, are, respectively,

$$\rho_{b,c}^{1/2}=\frac{k_{\rm f}\mp\left[k_{\rm f}^2-4(\beta_{\rm i}-1)k_{\rm a}k_{\rm m}\right]^{1/2}}{2k_{\rm a}}\,,\quad k_{\rm m}=(b\lambda_{\rm m})^{-1}\,. \tag{5.5}$$

Passing to the dimensionless variables

$$\psi=\frac{\rho}{\rho_c}\,,\qquad Y=\frac{y}{\Lambda_0}\,,\qquad \Gamma=k_{\rm a}\varepsilon\,,$$

$$\Lambda_0=\left[\frac{(M-1)\lambda_D}{bk_{\rm a}\,\rho_c}\right]^{1/2}\,, \tag{5.6}$$

we obtain the equation

$$\psi\,\frac{\partial\psi}{\partial\Gamma}+\frac{\partial^2\psi}{\partial Y^2}=\psi\Big(\sqrt{\psi}-\psi_0\Big)\Big(1-\sqrt{\psi}\Big)\,, \tag{5.7}$$

which contains one controlling parameter

$$\psi_0=\sqrt{\frac{\rho_b}{\rho_c}}=\frac{1-\sqrt{1-\eta}}{1+\sqrt{1-\eta}}\,,$$

$$\eta=4(\beta_{\rm i}-1)\,\frac{k_{\rm a}k_{\rm m}}{k_{\rm f}^2}\,,\qquad 0<\eta<1\,. \tag{5.8}$$

We see that this parameter depends on the combination η of kinetic coefficients that define the intensity of the processes of multiplication, immobilization, and annihilation of dislocations.

5.2 Cellular structure and its parameters

For a homogeneous distribution of dislocations, when $\psi(\Gamma)\equiv\vartheta(\Gamma)=\rho(\Gamma)/\rho_c$, Eqn (5.7) takes on the form

$$\frac{\partial\vartheta}{\partial\Gamma}=\Big(\sqrt{\vartheta}-\psi_0\Big)\Big(1-\sqrt{\vartheta}\Big)\,. \tag{5.9}$$

At $\vartheta\gg\psi_0^2$, it describes the evolution of the dislocation density

$$\rho(\varepsilon)=\rho_\infty\left[1-\exp\left(-\frac{1}{2}\,k_{\rm a}\varepsilon\right)\right]^2\,,\qquad \rho_\infty=\rho_c=\left(\frac{k_{\rm f}}{k_{\rm a}}\right)^2\,, \tag{5.10}$$

and flow stresses

$$\sigma(\varepsilon) = \alpha\mu b\rho^{1/2} = \sigma_\infty\left[1 - \exp\left(-\frac{1}{2}\,k_a\varepsilon\right)\right], \qquad \sigma_\infty = \alpha\mu b\rho_\infty^{1/2}, \tag{5.11}$$

at the second and third stages of the crystal strain-hardening curve.

The homogeneous distribution of dislocations, however, turns out to be unstable, and under certain conditions a spatially modulated cellular dislocation structure is formed in the crystal. At $\partial\psi/\partial\Gamma = 0$, that is, at the end of the third stage of hardening, Eqn (5.7) describes the equilibrium cellular dislocation structure [116, 270]

$$\rho(y) = \frac{\rho_{\max}^\infty}{\left[1 + (f_\infty - 1)\sin^2(\pi y/\Lambda_\infty)\right]^2},$$

$$\Lambda_\infty = 4\pi\left[\frac{(M-1)\lambda_D}{(\beta_i - 1)bk_m}\right]^{1/2}, \qquad f_\infty = \sqrt{\frac{\rho_{\max}^\infty}{\rho_{\min}}},$$

$$\rho_{\max}^\infty \approx \left(\frac{6}{5}\right)^2\rho_c, \qquad \rho_{\min} \approx \left(\frac{5}{4}\right)^2\rho_b, \tag{5.12}$$

where $\rho_{\max}^\infty$ and $\rho_{\min}$ are the densities of dislocations in the cell walls and inside the cells, under the following conditions:

$$(1+\psi_0)^2 - \frac{25}{6}\,\psi_0 > 0, \qquad 0 < \psi_0 < \frac{2}{3}, \qquad \eta < \frac{24}{25}. \tag{5.13}$$

Conditions (5.13) impose restrictions on the absolute and relative values of the kinetic coefficients.

Because Eqn (5.7) is nonlinear, the variables Y and Γ cannot be separated. In Ref. [270] a model expression was proposed for the solution of this equation, which at $\Gamma \to \infty$ tends to the steady solution (5.12)

$$\rho(y,\varepsilon) = \frac{\rho_{\max}(\varepsilon)}{\left[1 + \left(f(\varepsilon) - 1\right)\sin^2(\pi y/\Lambda_\infty)\right]^2}, \tag{5.14}$$

$$\rho_{\max}(\varepsilon) \approx \left(\frac{6}{5}\right)^2\rho_c\vartheta(\varepsilon), \qquad f(\varepsilon) = \sqrt{\frac{\rho_{\max}(\varepsilon)}{\rho_{\min}}}.$$

Obviously, as $\Gamma = k_a\varepsilon \to \infty$, the density of dislocations is $\rho(\varepsilon)/\rho_c = \vartheta(\varepsilon) \to 1$, and Eqn (5.14) becomes the same as (5.12). The conditions of formation of cellular structure then become dependent on the deformation:

$$(1+\psi_0)^2\vartheta^{1/2}(\varepsilon) - \frac{25}{6}\,\psi_0 > 0,$$

$$0 < \psi_0 < \frac{2}{3}, \qquad \eta < \frac{24}{25}. \tag{5.15}$$

The first of these conditions defines the critical deformation $\Gamma^{cr} = k_a\varepsilon^{cr}$ for the start of formation of the cellular structure

$$\varepsilon > \varepsilon^{cr} = \frac{2}{k_a}\ln\frac{(1+\psi_0)^2}{(2/3 - \psi_0)(3/2 - \psi_0)}. \tag{5.16}$$

It is smaller, the larger the coefficient of annihilation of dislocations k_a, and the smaller the parameter ψ_0. As $\psi_0 \to 2/3$, the critical deformation $\varepsilon^{cr} \to \infty$. Since the parameter ψ_0 is the larger, the stronger the immobilization of dislocations (by impurities, inclusion particles, grain boundaries, etc.), in some materials the formation of a cellular structure is hampered or not possible at all — for example, in bcc metals undergoing deformation in the temperature range below $0.1T_m$ [237, 238].

Figure 16a shows the evolution of the dislocation density in the cell walls as the extent of deformation increases in accordance with Eqn (5.14) at $\psi_0 = 0.1$ and $\Gamma^{cr} = 0.8$. The dashed line in the diagram marks the critical density of dislocations $\rho(\varepsilon^{cr})/\rho_{\max}^\infty \approx (25/12)^2\psi_0^2$ ($\psi_0 \ll 1$) at which the cellular structure starts to form. The density of dislocations in the cell walls increases according to the second expression in Eqn (5.14). This implies that the mean distance between the forest dislocations in the cell walls is

$$l(\varepsilon) = \left[\rho_{\max}(\varepsilon)\right]^{-1/2} = \frac{l_\infty}{1 - \exp(-k_a\varepsilon/2)}, \qquad l_\infty = \frac{5}{6\sqrt{\rho_c}}. \tag{5.17}$$

The curve in Fig. 16b depicts the theoretical dependence $l(\varepsilon)$, and the experimental points correspond to the thermo-activated path of dislocations λ_a as a function of strain in aluminum at 77 K at the second and third stages of strain-hardening curve measured with nuclear magnetic resonance [275]. Since it is the forest dislocations that are the main obstacles for thermally activated motion of dislocations at the second and third stages of strain hardening, we have $\lambda_a(\varepsilon) \propto l(\varepsilon)$, and therefore the free path must decrease with increasing strain, in accordance with Eqn (5.17), which is what is actually observed in experiment.

As indicated by experiment (Fig. 16d), the mean size of cells Λ in the course of plastic deformation does not remain constant: it gradually decreases, reaching its equilibrium value Λ_∞ by the end of the third stage [276–278]. A detailed study of the evolution of cell size in copper single crystals [276] revealed that, as the deformation proceeds further, the size of cells decreases through the formation of new boundaries inside the cells; that is, we are dealing with the process of division of cells. Since the formation of new dislocation boundaries requires a supply of fresh dislocations, the kinetics of multiplication of boundaries (division of cells) must be closely related to the kinetics of multiplication and annihilation of dislocations at the second and third stages of strain hardening. Indeed, since the density of cell boundaries per unit length is $\Lambda^{-1}(\varepsilon)$, and the dislocations concentrate mainly in the cell walls, the mean density of dislocations in the crystal is $\rho(\varepsilon) = \left[\Lambda(\varepsilon)\delta l(\varepsilon)\right]^{-1}$ and, with due account for Eqns (5.10) and (5.17), we have [270]

$$\Lambda(\varepsilon) = \frac{\Lambda_\infty}{1 - \exp(-k_a\varepsilon/2)}, \qquad \delta = \frac{1}{l_\infty\Lambda_\infty\rho_c}. \tag{5.18}$$

The curve in Fig. 16d is plotted according to Eqn (5.18). The experimental points in this diagram are taken from Ref. [270] and indicate the size of cells in copper rolled to different reductions at 4.2 (filled circles), 20 (empty circles), 77 (triangles), and 300 K (squares). The analysis of experimental curves $\Lambda(\varepsilon)$ for the pure metals Al [277], Ni [280], Cu [278] and the alloys Cu–Zn, Cu–Al [281] in the coordinates $\ln(1 - \Lambda_\infty/\Lambda) - \varepsilon$, performed in Refs [282, 283], reveals good agreement with Eqn (5.18). The coefficient of annihilation of dislocations k_a found from the slope of these lines increased steadily with the stacking-fault energy of metal or alloy in the same manner as shown in Fig. 15a.

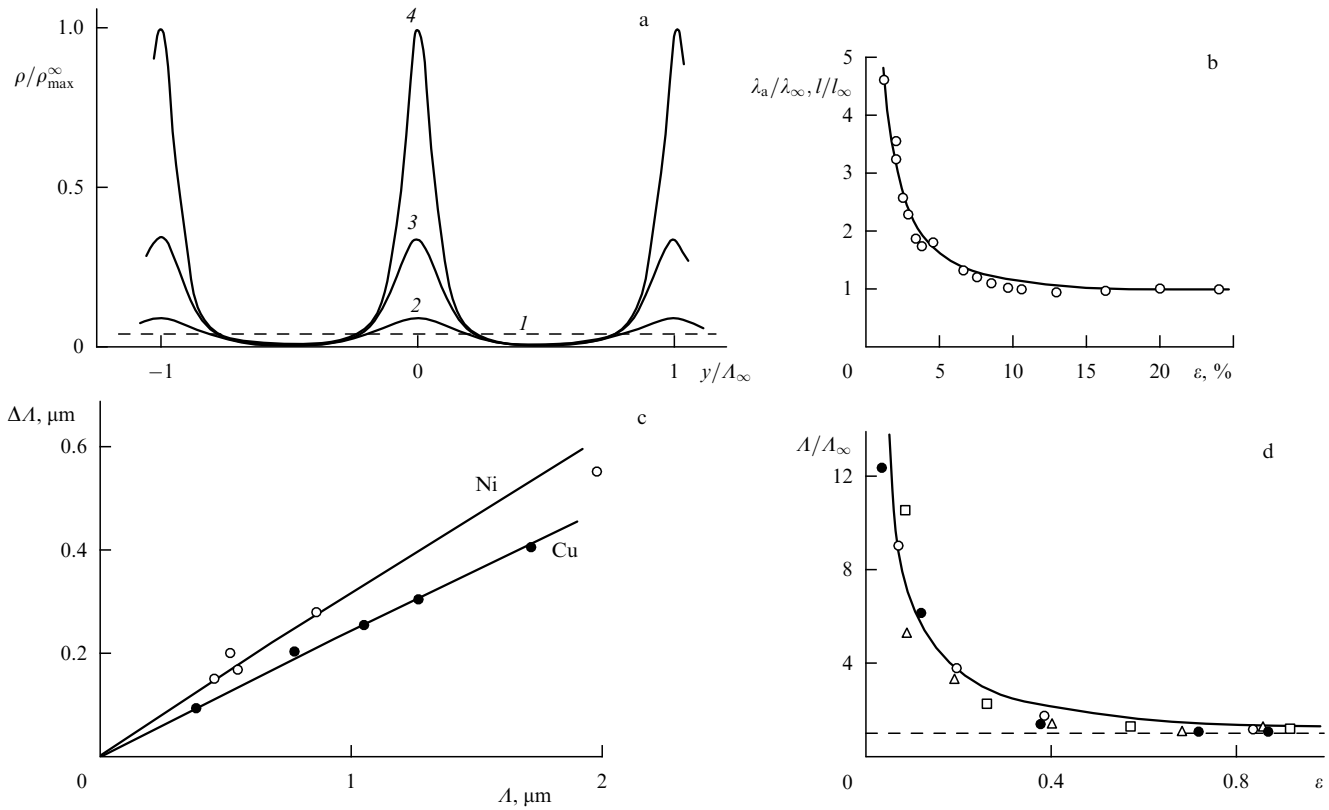

Figure 16. (a) Evolution of the density of dislocations in cell walls with increasing deformation (*1*, $\Gamma^{\rm cr} = 0.8$; *2*, 1.0; *3*, 2.0; *4*, ∞). (b) Free paths of dislocations $\lambda_{\rm a}$ within cells in Al [275] vs. degree of deformation. (c) Correlation between the width of boundaries and the cell size in Cu [279] and Ni [280]. (d) Cell size in copper [278] depending on the reduction of area upon rolling.

As the degree of plastic deformation increases, the width (thickness) of cell walls $\Delta\Lambda$ decreases, while the ratio $\Delta\Lambda(\varepsilon)/\Lambda(\varepsilon)$, as follows from Fig. 16c, remains constant. This ratio equals 0.23 for copper, 0.32 for nickel. Selecting the value $\Delta\Lambda_{1/2}$ for the boundary width corresponding to the density of dislocations within the boundary $\rho_{1/2} = (1/2)\rho_{\max}(\varepsilon)$, we obtain from Eqn (5.14) and Eqn (5.18)

$$\frac{\Delta\Lambda_{1/2}}{\Lambda} = \frac{2}{\pi}\left[\frac{\rho_{\max}(\varepsilon)}{\rho_c}\right]^{1/2} \arcsin\left(\frac{\sqrt{2}-1}{f(\varepsilon)-1}\right)^{1/2} . \qquad (5.19)$$

Calculation indicates [271] that the ratio (5.19) remains constant as the deformation increases from critical to $\varepsilon \to \infty$. At $\psi_0 \ll 1$, this ratio is $0.4\psi_0^{1/2}$.

From optical measurements [17, 21] we know that at the second stage of hardening of fcc metals the length of slip lines decreases with increasing deformation as $L = L_0(\varepsilon - \varepsilon_2)^{-1}$, where ε_2 is the deformation corresponding to the beginning of the second stage, and L_0 is a constant, which is, for example, 4 μm for copper single crystals and 6 μm for nickel [21].

Obviously, the length of slip lines depends on the free path of dislocations λ. When the moving dislocations interact with the forest dislocations, we have $\lambda_{\rm f} = 1/(bk_{\rm f}\,\rho_{\rm f}^{1/2})$. Since in the case of cellular structure the forest dislocations are concentrated in the cell walls, we find that the length of slip lines in the cellular structure ought to be $L = (1/2)bk_{\rm f}\,\rho_{\max}^{1/2}(\varepsilon)$. Using Eqns (5.10) and (5.14), we obtain [271]

$$L = \frac{L_\infty}{1-\exp(-k_{\rm a}\varepsilon/2)} , \qquad L_\infty = \frac{5}{12bk_{\rm f}\,\rho_c^{1/2}} . \qquad (5.20)$$

With deformations $\varepsilon \ll 2/k_{\rm a}$ (that is, at the second stage of hardening), given that $\rho_c = (k_{\rm f}/k_{\rm a})^2$, we obtain, in agreement with experiment,

$$L \approx \frac{L_0}{\varepsilon - \varepsilon_2} , \qquad L_0 = \frac{5b}{6(bk_{\rm f})^2} , \qquad L_\infty = \frac{1}{2}\,k_{\rm a}L_0 . \qquad (5.21)$$

Since $bk_{\rm f} \approx 10^{-2}$, the constant L_0 is on the order of a few microns. For copper, as reported in Ref. [17], we have $L_\infty/L_0 = 2.5$, and therefore at room temperature the coefficient of annihilation must be approximately equal to 5, which fits in with the results presented in Fig. 15a.

5.3 Self-similarity of cellular structures

As follows from the experimental and theoretical results presented above, the parameters of cellular structure exhibit a regular change with deformation at the second and third stages of the strain-hardening curve. These parameters, for example, the size of dislocation cells [284] and the flow stress, or the same parameters and the mean density of dislocations [276, 285, 286], are linked by the relations

$$\Lambda = K_1\,\frac{\mu b}{\sigma} , \qquad \Lambda = K_2\,\frac{1}{\sqrt{\rho}} , \qquad \sigma = K_3\alpha\mu b\sqrt{\rho} , \qquad (5.22)$$

which are invariant to plastic deformation, where K_1, K_2, K_3 are some coefficients that do not depend on plastic deformation.

These facts, as well as some other considerations, served as basis for formulating the principle of self-similarity of cellular dislocation structures [287]. This principle states that

an increase in strain and flow stress results in a decrease in the dimensions of the dislocation network within the cell limits l and the size of cells Λ, but the ratio Λ/l remains constant and does not depend on strain and stress, and this is actually observed in experiment [276].

Naturally, any theory of cellular dislocation structures must be consistent with this principle or at least not contrary to it. From the results presented in the preceding section we see that the solution (5.14) of equation (5.4) is in agreement with this principle. The expressions for the parameters of cells as functions of deformation (5.10), (5.11), (5.16) and (5.17) obtained with the aid of this equation permit the coefficients K_1, K_2, K_3, and $K_4 = \Lambda/l$ to be found.

Taking into account Eqn (5.18), in which, in accordance with the two-phase model of cellular structure [288],

$$\rho(\varepsilon) = \delta\rho_{\max}(\varepsilon) + (1-\delta)\,\rho_{\min}(\varepsilon)\,, \tag{5.23}$$

where δ is the volume fraction of dislocations confined in the cell walls, we obtain the following relations for the coefficients K [271]:

$$K_1 = \left(\frac{6}{5}\right)^2 \alpha\delta^{-1/2}\,, \qquad K_2 = \left(\frac{6}{5}\right)^2 \delta^{-1/2}\,,$$
$$K_3 = \frac{6}{5}\,\delta^{1/2}\,, \qquad K_4 = \left(\frac{6}{5}\right)^2 \delta^{-1}\,, \tag{5.24}$$

where $\delta = (6/5)(\Lambda_\infty\sqrt{\rho_c}\,)^{-1}$.

The relations (5.24) must be supplemented by the relation between the free path of dislocations in the cellular structure [the length of slip lines (5.20)] and the mean size of cells: $L = K_5\Lambda$, $K_5 = (25/72)(\delta/bk_{\rm f})$. With $\Lambda_\infty = 1$ μm, $\rho_c = 10^{10}$ cm^{-2}, we have $\delta = 0.12$, and therefore with $\alpha = 0.5$, $bk_{\rm f} = 10^{-2}$, the coefficients K are of the same order of magnitude as the experimental values. For example, the experimental value for aluminum found in Ref. [289] is $L/\Lambda = 3-4$, whereas the estimate gives $K_3 = 3.6$.

Figure 17a shows the flow stress versus the mean density of dislocations in single crystals of iron [290] oriented for single ([110], filled circles) and multiple ([100], empty circles) slip at two temperatures. The arrow marks the point where the cellular structure starts to form in the crystal. We see that at 77 K the formation of a cellular structure causes a change in the effective constant of interaction between dislocations $\alpha^* = K_3\alpha$ owing to the reduced density of dislocations inside the dislocation cells. Taking into account the coefficient K_3 in Eqn (5.24), we obtain the estimates for the volume fraction δ occupied in the crystal by the cell walls: 0.6 and 0.1 for the orientations [110] and [100], respectively. At 293 K, the cellular structure is formed for both orientations at a very early stage of deformation, and it is not possible to find the coefficient K_3.

Figure 17b shows similar results for pure Al and the solid solution Al–5.5 at. % Mg [291] at 293 K. The estimate gives $\delta = 0.13$ for pure aluminum, and $\delta = 0.53$ for the alloy. This means that the difference in the density of dislocations in the walls and inside the cells $\psi_0 = (\rho_b/\rho_c)^{1/2}$ in the alloy and in pure aluminum is not large. Indeed, taking into account Eqn. (5.12) and (5.24), we have

$$\delta \approx \frac{3}{10\pi}\left[\frac{bk_{\rm a}}{(M-1)\lambda_D}\right]^{1/2} \psi_0^{1/2} \sim \psi_0^{1/2}\,. \tag{5.25}$$

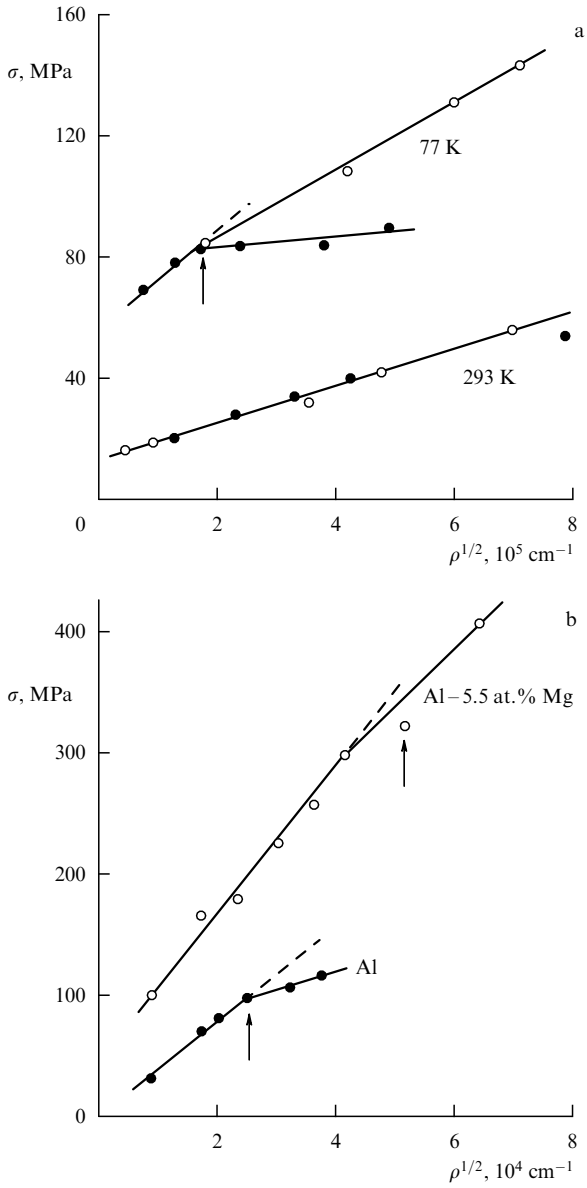

Figure 17. Flow stress vs. density of dislocations: (a) in single crystals of α-Fe [290]; (b) in polyscrystalline Al of 99.99% purity and in Al–5.5 at. % Mg alloy [291].

We also see that the formation of a cellular structure is hampered in the alloy and occurs at a higher density of dislocations ($\rho^{\rm cr} = 2.5\times10^9$ cm^{-2}) than in pure aluminum ($\rho^{\rm cr} = 6\times10^8$ cm^{-2}), because ($\psi_0 \ll 1$)

$$\rho^{\rm cr} \approx 3\rho_c\psi_0^2 \sim \psi_0^2\,, \qquad \text{or} \qquad \rho^{\rm cr} \approx 3\rho_b \approx 3(\beta_{\rm i}-1)k_{\rm f}k_{\rm m}\,. \tag{5.26}$$

5.4 Formation of a cellular structure in polycrystalline materials

Our treatment of the mechanism of formation of cellular dislocation structures would have been incomplete without discussing the features specific to polycrystalline materials. As indicated by experiment [47, 292], the size of grains d affects the critical strain when the cellular structure starts to form in the crystallites. The smaller the grain, the sooner the cellular structure will start to form in the polycrystalline material. There is a critical size $d^{\rm cr}$, such that at $d < d^{\rm cr}$ the

cellular structure would not form [293], whereas at $d > d^{cr}$ the size of dislocation cells increases with increasing grain size [47, 293].

According to the criterion of formation of a cellular structure (5.15), the decrease in the grain size raises the values of $\beta_i = \lambda_m/\lambda_{is} = \lambda_m/d$, which leads to violation of the condition $\eta < 1$, $\psi_0 < 2/3$. This explains the existence of the critical grain size d^{cr}. The increase in the threshold ε^{cr} as the grain size increases, $\varepsilon^{cr} \propto d$ [294], is associated with the fact that the cellular structure starts to form near the grain boundaries and then goes into the bulk. The smaller the grain, the sooner it will be occupied by the cellular structure as the strain increases. As regards the dependence of the cell size on the size of grain, we note that $\beta_i(d) \gg 1$ and obtain from Eqn (5.12) [116, 294]

$$\Lambda_\infty = 4\pi\left[(M-1)\lambda_D d\right]^{1/2} \propto d^{1/2}\,. \tag{5.27}$$

The diagram in Fig. 18 is based on the results of Ref. [293], and shows the size of dislocation cells in polycrystalline aluminum versus the grain size at the deformation $\varepsilon = 0.2$ and different temperatures as indicated in the diagram, according to Eqn (5.27) (see also Ref. [47]). Note that the lines $\Lambda \propto d^{1/2}$ cross at the critical values of $\Lambda^{cr} = 0.9$ μm and $d^{cr} = 3.6$ μm, below which, as reported in Ref. [293], cellular structures do not form in aluminum.

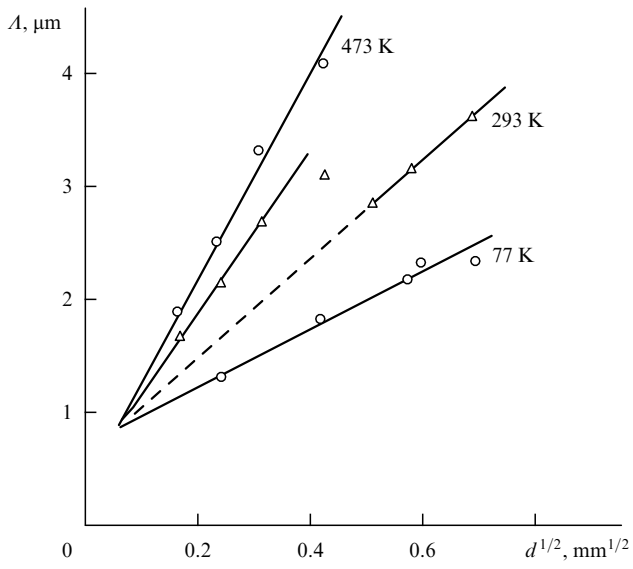

Figure 18. Dislocation cell size in Al of 99.99% purity vs. grain size at different temperatures [293].

6. Conclusion

The foregoing discussion of the mechanisms of formation of various dislocation structures in crystals subjected to plastic deformation indicates that the approach based on the equations of dislocation kinetics warrants adequate qualitative and quantitative treatment of these mechanisms, accounting for the effects of various external and internal factors on these structures.

Dislocation structures differ from structures formed in other active media in that they have a predominantly kinetic character, and are weakly linked with the conditions of thermodynamic equilibrium of the dislocation ensemble in the crystal. This means that, once formed, the dislocation structures 'freeze-in' in the crystal, and do not disappear after the removal of their cause, for example, an external force. This infinitely large time of relaxation of dislocation structures to their initial state is due to the existence at low and medium temperatures of the force of friction acting upon dislocations from the lattice (the Peierls relief), or from the point obstacles (impurity atoms, forest dislocations) that considerably limit the mobility of dislocations.

Under external stress, however, the mobility of dislocations is sufficient to let them rearrange and form new structures, which may cause misorientation and fragmentation of the lattice. As noted in the Introduction, space limitation has not allowed us to discuss the mechanism of formation of such structures within the framework of a unified kinetic approach, and the associated elastic and plastic rotations of the lattice [119, 120, 211, 295, 296].

The kinetic approach allows an answer to be found to such an important and not finally clarified question as the nature of the linkage between the stages of strain hardening of the crystal and the relevant dislocation structures [156, 180, 274]. A widespread view is that each hardening stage depends on the specific dislocation structure formed during this stage. The results discussed in Sections 2 and 5 (see Figs 4 and 17) indicate that both the hardening stages and the relevant dislocation structures are a regular result of the evolution of the dislocation ensemble and the associated elementary dislocation processes, such as the generation of dislocations from sources, their immobilization, multiplication, annihilation, and diffusion.

The formation of nonequilibrium dislocation structures is the consequence of spatial instability of the distribution of dislocations in the crystal, their self-organization and clustering through immobilization at obstacles ($\beta_i > 1$), and the inversion of the dislocation flow because of the correlation effects and the process of deformation (dislocation) hardening of the dislocation ensemble ($M > 1$). This means that the segmentation of hardening curves and the formation of structures have the same cause, namely, the space–time (deformation-related) evolution of the ensemble of dislocations in the crystal.

Note that the evolution of physical ensembles consisting of linear rather than pointlike elements ('particles') has many universal features and is often described by similar equations. For example, in Ref. [133], in connection with the study of the rate of formation of the normal phase as thermal vortices in superfluid helium, this rate was found to obey the kinetic equation

$$\frac{\mathrm{d}L}{\mathrm{d}t} = k_1 L^{3/2} - k_2 L^2\,, \tag{6.1}$$

where L is the total length of vortices per unit volume.

Introducing the dimensionless density of vortices $\bar{L} = L/L_0$, $L_0 = (k_1/k_2)^{1/2}$, we obtain

$$\frac{\mathrm{d}\bar{L}}{\mathrm{d}t} = \frac{k_1^2}{k_2}\,\bar{L}^{3/2}(1-\bar{L}^{1/2})\,. \tag{6.2}$$

Figure 19 shows the rate of formation of vortices versus their density according to Eqn (6.2). Equation (6.1) is similar to Eqns (3.5) and (5.3), which describe the rate of change of the density of dislocations at the second and third stages of strain

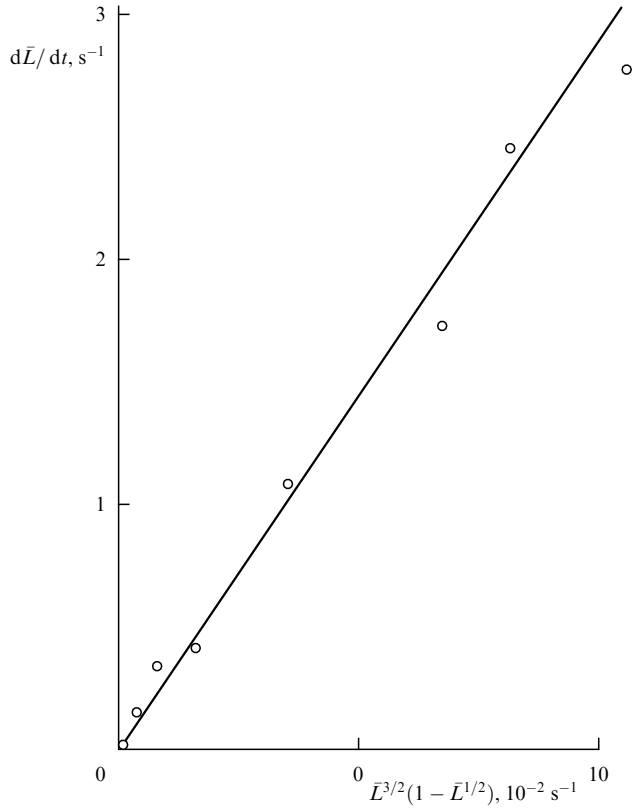

Figure 19. Rate of formation of thermal vortices in superfluid helium vs. density of vortices $\bar{L} = L/L_0$ according to Eqn (6.2) [133].

hardening of crystals because of multiplication of intersecting dislocations and annihilation of the screw components of dislocation loops. Similar processes also take place in the ensemble of vortex filaments in hard superconductors [131, 132].

It is clear that the macroscopic theory of plasticity of crystals must rely on the microscopic dislocation – disclination basis, since it is only at this level that the structure of the crystal affects the parameters of the strain-hardening curve and the distribution of dislocations in the crystal, as well as the emerging dislocation and deformation mesostructures, such as slip lines and bands, cellular and fragmented dislocation structures, pileups of dislocations of the same sign that define the fields of internal stress in the crystal undergoing deformation. A combination of microscopic and macroscopic approaches to plastic deformation is a priority for the merger of the physics of the strength and plasticity of crystals and deformation mechanics.

Finally let us note that, apart from the strength calculations as such, the dislocation kinetic equations are indispensable for the high technologies of today, such as the growth of perfect (defect-free) [297, 298] crystals and epitaxial films for microelectronics [299], or whenever the force acting on a solid produces mechanical tension.

The author is grateful to E V Kozlov, N A Koneva and A Luft for stimulating discussions of the mechanism of formation of cellular and annihilation structures, and to B I Smirnov and O V Klyavin for the discussion of the role of double cross slip of screw dislocations in the evolution of dislocation ensemble in the course of plastic deformation of crystals.

Appendices

I. Statistical averaging of a dislocation ensemble

For the purpose of statistical averaging of equations (2.10), (2.11) and the equation of motion of dislocations (2.4), we introduce the microscopic phase density $\varphi^a(l,t)$ for a dislocation segment of length l^a, having velocity $\mathbf{u}_l^a$, orientation v_l^a, and Burgers vector $\mathbf{b}^a$, and located at the point with coordinate $\mathbf{r}_l^a(t)$:

$$\varphi^a(l,t) = \frac{l^a}{\Omega}\,\delta\big(\mathbf{r}-\mathbf{r}_l^a(t)\big)\,\delta\big(\mathbf{u}-\mathbf{u}_l^a(t)\big)\,\delta\big(\mathbf{v}-\mathbf{v}_l^a(t)\big)\,, \quad \text{(I.1)}$$

where Ω is the volume of crystal, and $\delta(x-x_l)$ is the delta function. In the argument of function $\varphi^a(l,t)$, symbol l stands for the set of statistical parameters $\mathbf{r}$, $\mathbf{u}$, $\mathbf{v}$.

The total phase density of distribution of all segments with Burgers vector $\mathbf{b}^a$ in the nine-dimensional phase space is

$$N^a(l,t) = \sum_k \varphi^a(l_k,t)\,. \quad \text{(I.2)}$$

If the dislocation ensemble contains dislocations with different Burgers vectors, then the total phase density of the ensemble is

$$N(l,t) = \sum_a N^a(l,t)\,. \quad \text{(I.3)}$$

The phase densities (I.1) – (I.3) are normalized as follows:

$$\int \varphi^a(l,t)\,\mathrm{d}l = \frac{l^a(t)}{\Omega}\,, \qquad \int N^a(l,t)\,\mathrm{d}l = \Omega^{-1}\sum_k l_k^a(t) = \frac{L^a(t)}{\Omega}\,,$$

$$\int N(l,t)\,\mathrm{d}l = \Omega^{-1}\sum_a L^a(t) = \frac{L(t)}{\Omega}\,. \quad \text{(I.4)}$$

Here, L^a is the total length of dislocations with Burgers vector b^a, L is the total length of dislocations in the ensemble, and $\mathrm{d}l = \mathrm{d}r\,\mathrm{d}u\,\mathrm{d}v$ is the element of volume in the phase space. The normalizations (I.4) presume that the number of dislocations or the density of dislocations $\rho(t) = L(t)/\Omega$ do not remain constant, but change with time.

The Liouville equation for the microscopic phase density (I.1) then becomes (superscript a dropped)

$$\frac{\mathrm{d}\varphi(l,t)}{\mathrm{d}t} = \frac{\partial\varphi}{\partial t} + \nabla_r\cdot(\mathbf{u}_l\varphi) + \nabla_u\cdot(\dot{\mathbf{u}}_l\varphi) + \nabla_v\cdot(\dot{\mathbf{v}}_l\varphi) = \frac{\dot{l}}{l}\,\varphi\,, \quad \text{(I.5)}$$

where the dot denotes the time derivative. Since $\dot{\mathbf{u}} = \dot{\xi}\,u + \xi\,\ddot{u} \approx \dot{\xi}\,u$, further on for the independent statistical variable we will take not the velocity of dislocation $\mathbf{u}$, but the direction of its motion ξ.

Given this, for the phase density (I.2) we have the equation

$$\frac{\mathrm{d}N^a(l,t)}{\mathrm{d}t} = \frac{\partial N^a}{\partial t} + \nabla_r\cdot(\mathbf{u}^a N^a) + \nabla_\xi\cdot(\dot{\xi}^a N^a) + \nabla_v\cdot(\dot{\mathbf{v}}^a N^a) = \frac{\dot{L}^a}{L^a}\,N^a\,; \quad \text{(I.6a)}$$

and, similarly, for the phase density (I.3)

$$\frac{\mathrm{d}N(l,t)}{\mathrm{d}t} = \frac{\partial N}{\partial t} + \nabla_r\cdot(\mathbf{u}N) + \nabla_\xi\cdot(\dot{\xi}\,N) + \nabla_v\cdot(\dot{\mathbf{v}}\,N) = \frac{\dot{L}}{L}\,N\,. \quad \text{(I.6b)}$$

The rates of change of the statistical parameters in Eqns (I.1)–(I.3) are determined by the equations of motion of dislocations (2.4), (2.5) [141]:

$$\mathbf{u} = \boldsymbol{\xi} u\,, \qquad \dot{\mathbf{v}} = (\mathbf{v}\nabla)\mathbf{u} = \frac{\partial \mathbf{u}}{\partial l}\,, \qquad \dot{\boldsymbol{\xi}} = \frac{\partial}{\partial t}\left(R_v \frac{\partial \mathbf{v}}{\partial l}\right). \quad \text{(I.7)}$$

As a result, the set of equations (I.6), (I.7) is closed and self-consistent, since the velocity of dislocations, according to Eqn (2.5), depends on the stress $\hat{\sigma}^{\,\mathrm{in}}$, i.e., the total stress from all dislocations of the ensemble.

Using Eqn (I.1), we can express the microscopic values of tensor and scalar densities and their fluxes as

$$\hat{\alpha}^a(l,t) = (\mathbf{b}^a \mathbf{v}_l^a)\,\varphi^a(l,t)\,, \qquad \hat{J}^a(l,t) = (\mathbf{b}^a \mathbf{n}_l^a) u^a\,\varphi^a(l,t)\,,$$
$$\rho^a(l,t) = \varphi^a(l,t)\,, \qquad \mathbf{j}^a(l,t) = \boldsymbol{\xi}^a u^a\,\varphi^a(l,t)\,, \quad \text{(I.8)}$$

where $\mathbf{n} = \mathbf{v} \times \boldsymbol{\xi}$. Averaging the densities and fluxes (I.8) over the entire phase space, we obtain

$$\hat{\alpha}^a(l_1,t) = (\mathbf{b}^a \mathbf{v}_1^a) f_1^a(l_1,t)\,, \qquad \hat{J}^a(l_1,t) = (\mathbf{b}^a \mathbf{n}_1^a) u^a f_1^a(l_1,t)\,,$$
$$\rho^a(l_1,t) = f_1^a(l_1,t)\,, \qquad \mathbf{j}^a(l_1,t) = \boldsymbol{\xi}_1^a u^a f_1^a(l_1,t)\,, \quad \text{(I.9)}$$

where the one-particle distribution function is

$$f_1^a(l_1,t) = \int \varphi^a(l,t)\,N(l,t)\,\mathrm{d}l = \int N(l,t)\,\mathrm{d}l_2^c \ldots \mathrm{d}l_N\,. \quad \text{(I.10)}$$

The equation for the one-particle distribution function can be obtained by integrating Eqn (I.6) with respect to all parameters except l_1^a:

$$\frac{\mathrm{d}f_1^a(l,t)}{\mathrm{d}t} = \frac{\partial f_1^a}{\partial t} + \nabla_{r_1}\cdot(\overline{uN}) + \nabla_{\xi_1}\cdot(\overline{\dot{\xi}N}) + \nabla_{v_1}\cdot(\overline{\dot{v}N})$$
$$= \frac{\dot{l}_1^a}{l_1^a} f_1^a\,. \quad \text{(I.11)}$$

Expanding the ensemble averages in the first and second moments

$$\overline{\mathbf{u}N} = \mathbf{u}_1^a f_1^a + \overline{\delta\mathbf{u}\,\delta N}\,, \qquad \overline{\dot{\boldsymbol{\xi}}N} = \dot{\boldsymbol{\xi}}_1^a f_1^a + \overline{\delta\dot{\boldsymbol{\xi}}\,\delta N}\,,$$
$$\overline{\dot{\mathbf{v}}N} = \dot{\mathbf{v}}_1^a f_1^a + \overline{\delta\dot{\mathbf{v}}\,\delta N}\,, \quad \text{(I.12)}$$

and substituting these into Eqn (I.11), we obtain an equation for the one-particle distribution function of the form

$$\frac{\partial f_1^a}{\partial t} + \nabla_{r_1}\cdot(\mathbf{u}_1^a f_1^a) + \nabla_{\xi_1}\cdot(\dot{\boldsymbol{\xi}}_1^a f_1^a) + \nabla_{v_1}\cdot(\dot{\mathbf{v}}_1^a f_1^a)$$
$$= \Phi^a(f_1^a, f_2^a)\,, \quad \text{(I.13)}$$

where the 'collision integral'

$$\Phi^a(f_1^a, f_2^a) = \frac{f_1^a}{\tau_1^a} - \nabla_{r_1}\cdot(\overline{\delta\mathbf{u}\,\delta N}) - \nabla_{\xi_1}\cdot(\overline{\delta\dot{\boldsymbol{\xi}}\,\delta N})$$
$$- \nabla_{v_1}\cdot(\overline{\delta\dot{\mathbf{v}}\,\delta N}) \quad \text{(I.14)}$$

accounts for the interaction of dislocations with one another, and therefore contains the pair distribution function f_2.

The equation for f_2 can be expressed similarly to the equation for f_1. In Eqn (I.14) we have $(\tau_1^a)^{-1} = \dot{l}_1^a/l_1^a = \sum_p (\tau_1^a)_p^{-1}$, where $(\tau_1^a)_p$ are the characteristic times of elementary processes that may increase or decrease the length of dislocations. In the general case, $\tau_1^a = \tau_1^a(l_1^a, t)$.

Averaging (I.13) and (I.14) with respect to all ξ_1 and v_1, we obtain the kinetic equation for the scalar density of dislocations $\rho^a(r,t)$

$$\frac{\partial \rho^a}{\partial t} + \nabla_r\cdot(u^a\rho^a) = \sum_p \int \frac{u^a(l_1,t)}{\lambda_p^a(l_1,t)} f_1^a(l_1,t)\,\mathrm{d}\xi_1\,\mathrm{d}v_1\,. \quad \text{(I.15)}$$

Here, we have taken into account that the distribution functions vanish at the boundaries of the phase space. The collision integral on the right-hand side of Eqn (I.15) is expressed in terms of the free paths of dislocations between elementary acts that affect the dislocation length ($\lambda_p = u\tau_p$), rather than in terms of the relaxation times τ_p like Eqn (I.14). After carrying out integration in Eqn (I.15) with respect to all ξ_1 and v_1, we obtain Eqn (2.12) of Section 2.

In a similar way one can express the kinetic equations for the tensor density of dislocations $\hat{\alpha}(r,t)$ and its flux $\hat{J}(r,t)$.

II. Correlation stress

To account for the correlation effects, we multiply the equation of motion of dislocations (2.4) by the microscopic function of distribution of dislocations (I.1) $\varphi^c(l',t)$. Noting that the integrand $\sigma_{ik}^{\mathrm{in}}$ in Eqn (2.1) contains the distribution function $\varphi^a(l,t)$, after averaging over the entire ensemble we obtain the averaged equations of motion

$$n_i(\sigma_{ik}^{\mathrm{ext}} + \sigma_{ik}^{\mathrm{in}} + \sigma_{ik}^{\mathrm{cor}}) b_k^a = b^{\mathrm{a}}\sigma^{(\mathrm{f})}\,, \quad \text{(II.1)}$$

where this time

$$\sigma_{ik}^{\mathrm{in}} = -\sum_a \int A_{iksp}(\mathbf{r}' - \mathbf{r})\, b_s^a v_p^a\, f_1^a(l_1,t)\,\mathrm{d}l_1\,, \quad \text{(II.2)}$$

$$\sigma_{ik}^{\mathrm{cor}} = -\sum_c \int A_{iksp}(\mathbf{r}' - \mathbf{r})\, b_s^c v_p^c\, f_1^c(l_1,t)\, g^{ac}(l_1,l_2)\,\mathrm{d}l_1\,\mathrm{d}l_2\,, \quad \text{(II.3)}$$

$$g^{ac}(l_1,l_2,t) = \frac{f_2^{ac}(l_1,l_2,t)}{f_1^a(l_1,t) f_1^c(l_2,t)} - 1\,, \quad \text{(II.4)}$$

$f_2^{ac}(l_1,l_2,t)$ is the pair distribution function, $g^{ac}(l_1,l_2,t)$ is the pair correlation function, and $\sigma_{ik}^{\mathrm{cor}}$ is the correlation stress.

The functions f_2^{ac} or g^{ac} can be found from solution of the self-consistent kinetic equation for the density of dislocations. Since in the general case this is a formidable problem, we consider a more specialized case [140], namely, a dislocation ensemble consisting of an equal number of parallel screw dislocations of opposite signs with the same type of Burgers vector. The correlation function for such an ensemble is

$$g^{ac}(l_1,l_2,t) = \delta_{ac}\, g(r' - r, t)\,\delta(\xi^a - \xi^c)\,\delta(v^a - v^c)\,,$$

where δ_{ac} and $\delta(x)$ are delta functions. Substituting this into Eqn (II.3) and noting that $f_1(r,t) \equiv \rho(r,t)$, we obtain Eqn (4.4) of Section 4.

References

1. Orowan E *Z. Phys.* **8** 605 (1934)
2. Taylor G I *Proc. R. Soc. London Ser. A* **145** 362 (1934)
3. Griffith A A *Philos. Trans. R. Soc. London Ser. A* **221** 163 (1921)
4. Ioffe A F *Fizika Kristallov* (Physics of Crystals) (Moscow, Leningrad: GIZ, 1929)
5. Frenkel' Ya I *Vvedenie v Teoriyu Metallov* (Introduction to the Theory of Metals) (Moscow: GONTI, 1958)

6. De Wit R, in *Nat. Bur. Stand.* (US), *Spec. Publ. 317* **1** 651 (1970); *J. Res. Nat. Bur. Stand.* **77A** 49, 359, 607 (1973) [Translated into Russian *Kontinual'naya Teoriya Disklinatsiĭ* (Continuum Theory of Disclinations) (Moscow: Mir, 1977)]
7. Likhachev V A, Khaĭrov R Yu *Vvedenie v Teoriyu Disklinatsiĭ* (Introduction to the Theory of Disclinations) (Leningrad: Izd. LGU, 1975)
8. Vladimirov V I, Romanov A E *Disklinatsii v Kristallakh* (Disclinations in Crystals) (Moscow: Nauka, 1986)
9. Read W T *Dislocations in Crystals* (New York: McGraw-Hill, 1953) [Translated into Russian (Moscow: Metallurgizdat, 1957)]
10. Cottrell A H *Dislocations and Plastic Flow in Crystals* (Oxford: Clarendon Press, 1953) [Translated into Russian (Moscow: Metallurgiya, 1958)]
11. Van Bueren H G *Imperfections in Crystals* (Amsterdam: North-Holland, 1960) [Translated into Russian (Moscow: IL, 1962)]
12. Eshelby J D *Solid State Phys.* **3** 79 (1956); *Proc. R. Soc. London Ser. A* **241** 376 (1957); **252** 561 (1959); Eshelby J D, Frank F C, Nabarro F R N *Philos. Mag.* **42** 351 (1951); de Wit R *Solid State Phys.* **10** 249 (1960); Head A K, Thomson P F *Philos. Mag.* **7** 439 (1962); Eshelby D "The continuum theory of lattice defects", in *Solid State Physics* Vol 3 (New York: Academic, 1956) p. 79 [Translated into Russian (Moscow: IL, 1963)]
13. Friedel J *Dislocations* (Oxford: Pergamon Press, 1964) [Translated into Russian (Moscow: Mir, 1967)]
14. Kröner E "Allgemeine Kontinuumstheorie der Versetzungen und Eigenspannungen" *Arch. Rat. Mech. Anal.* **4** (4) 18 (1960) [Translated into Russian (Moscow: Mir, 1965)]
15. Hirth J P, Lothe J *Theory of Dislocations* (New York: McGraw-Hill, 1968) [Translated into Russian (Moscow: Atomizdat, 1972)]
16. Kosevich A M *Dislokatsii v Teorii Uprugosti* (Dislocations in Theory of Elasticity) (Kiev: Naukova Dumka, 1978)
17. *Dislocations and Mechanical Properties of Crystals. An International Conf.* (*Lake Placid, 1956*) (New York: John Wiley and Sons, 1957) [Translated into Russian (Moscow: IL, 1960)]
18. *Fracture. Proc. of an Intern. Conf. on the Atomic Mechanisms of Fracture, Swampscott, Mass., 1959* (New York: John Wiley and Sons, 1960) [Translated into Russian (Moscow: Fizmatgiz, 1963)]
19. Mitchell T E *Prog. Appl. Mater. Res.* **6** 119 (1964)
20. Nabarro F R N, Basinski Z S, Holt D B "The plasticity of single crystals" *Adv. Phys.* **13** (50) (1964) [Translated into Russian (Moscow: Metallurgiya, 1967)]
21. Berner R, Kronmüller G *Plastische Verformung von Einkristallen* (Plastic Deformation of Single Crystals) (Moderne Probleme der Metallophysik, Ed. A Seeger) (Berlin: Springer, 1965) [Translated into Russian (Moscow: Mir, 1969)]
22. Honeycombe R W K *The Plastic Deformation of Metals* (London: Edward Arnold, 1968) [Translated into Russian (Moscow: Mir, 1972)]
23. Orlov A N (Ed.) *Aktual'nye Voprosy Teorii Dislokatsiĭ* (Actual Problems in the Theory of Dislocations) (Moscow: Mir, 1968) [A collection of papers (1965–1967), translation from English]
24. Kocks U F, Argon A S, Ashby M F *Thermodynamics and Kinetics of Slip* (New York: Pergamon Press, 1975)
25. Nabarro F R N (Ed.) *Dislocation in Solids* Vols 1–9 (Amsterdam: North-Holland Publ. Co., 1979–1991)
26. Nadgornyĭ E M et al. *Usp. Fiz. Nauk* **67** 625 (1959) [*Sov. Phys. Usp.* **2** 282 (1959)]
27. Indenbom V L, Orlov A N *Usp. Fiz. Nauk* **76** 557 (1962) [*Sov. Phys. Usp.* **5** 272 (1962)]
28. Kosevich A M *Usp. Fiz. Nauk* **84** 579 (1964) [*Sov. Phys. Usp.* **7** 837 (1964)]
29. Kosevich A M, Boĭko V S *Usp. Fiz. Nauk* **104** 201 (1971) [*Sov. Phys. Usp.* **14** 286 (1971)]
30. Kaganov M N, Kravchenko V Ya, Natsik V D *Usp. Fiz. Nauk* **111** 655 (1973) [*Sov. Phys. Usp.* **16** 878 (1974)]
31. Kosevich A M *Usp. Fiz. Nauk* **114** 509 (1974) [*Sov. Phys. Usp.* **17** 920 (1975)]
32. Al'shits V I, Indenbom V L *Usp. Fiz. Nauk* **115** 3 (1975) [*Sov. Phys. Usp.* **18** 1 (1975)]
33. Tyapunina N A, Belozerova E P *Usp. Fiz. Nauk* **156** 683 (1988) [*Sov. Phys. Usp.* **31** 1060 (1988)]
34. Schmid E, Boas W *Kristallplastizität, mit Besonderer Berücksichtigung der Metalle* (Plasticity of Crystals with Special Reference to Metals) (Berlin: J. Springer, 1935) [Translated into Russian (Moscow, Leningrad: GONTI, 1938)] [Translated into English (London: F.A. Hughes, 1950)]
35. Klassen-Neklyudova M V *Plasticheskie Svoĭstva i Prochnost' Kristallov* (Plastic Properties and Strength of Crystals) (Leningrad, Moscow: GTTI, 1933)
36. Stepanov V A *Osnovy Prakticheskoĭ Prochnosti Kristallov* (Fundamentals of Practical Strength of Crystals) (Moscow: Nauka, 1974)
37. Yakutovich M V et al. *Izv. Akad. Nauk SSSR Ser. Fiz.* **15** 383 (1951)
38. Diehl J, Mader S, Seeger A *Z. Metallkd.* **46** 650 (1955)
39. Brenner S S *J. Appl. Phys.* **28** 1023 (1957)
40. Clarebrough L M, Hargreaves M E *Prog. Metals Phys.* **8** 1 (1959)
41. Gilman J J, Johnston W G *Phys. Status Solidi* **13** 147 (1962)
42. Klyavin O V et al. *Phys. Status Solidi* **35** 427 (1969)
43. Steeds J W *Proc. R. Soc. London Ser. A* **292** 343 (1966)
44. Essmann V *Phys. Status Solidi* **12** 707 (1965)
45. Fujita H *J. Phys. Soc. Jpn.* **23** 1349 (1967)
46. Foxall R A, Duesbery M S, Hirsch P B *Can. J. Phys.* **45** 607 (1967)
47. Conrad H, Fenerstein S, Rice L *Mater. Sci. Eng.* **2** 157 (1967)
48. Furubayashi E *J. Phys. Soc. Jpn.* **27** 130 (1969)
49. Kawasaki Y *J. Phys. Soc. Jpn.* **36** 142 (1974)
50. Clauer A H, Wilcox B A, Hirth J P *Acta Metall.* **18** 381 (1970)
51. Takeuchi S, Argon A S *J. Mater. Sci.* **13** 11 1542 (1976)
52. Gilman J J *J. Met.* **6** 621 (1954)
53. Kelly A *Acta Crystallogr.* **7** 554 (1954)
54. Urusovskaya A A, Thyagarajan R *Phys. Status Solidi* **10** 349 (1965)
55. Siethoff H *Acta Metall.* **21** 1523 (1973)
56. Malin A S, Hartherly M *Metal Sci.* **13** 463 (1979)
57. Sharp J W *Philos. Mag.* **16** 77 (1967)
58. Bapna M S, Meshii M *Mater. Sci. Eng.* **16** 181 (1974)
59. Luft A et al. *Mater. Sci. Eng.* **20** 113 (1975)
60. Woods P J *Philos. Mag.* **28** 155 (1973)
61. Winter A T *Philos. Mag.* **37** 457 (1978)
62. Laird C, in *Dislocations in Solids* Vol. 6 (Ed. F R N Nabarro) (Amsterdam: North-Holland, 1983) p. 55
63. Van Rooyen G T *Mater. Sci. Eng.* **7** 37 (1971)
64. Irisibar R, Mazza J *Scr. Metall.* **9** 1045 (1975)
65. Cuddy L J, Leslie W C *Acta Metall.* **20** 1157 (1972)
66. Van Westrum J S, Wijler A *Acta Metall.* **21** 1079 (1973)
67. Zuev L B, Danilov V I, Kartasheva N V *Pis'ma Zh. Eksp. Teor. Fiz.* **60** 538 (1994) [*JETP Lett.* **60** 553 (1994)]
68. Zuev L B, Danilov V I *Fiz. Tverd. Tela* **39** 1399 (1997)
69. Basinski Z S *Proc. R. Soc. London Ser. A* **240** 2299 (1957)
70. Erdmann J C, Jahoda J A *J. Appl. Phys.* **39** 2793 (1968)
71. Rogers H *Ann. Rev. Mater. Sci.* **9** 283 (1979)
72. Timothy S P *Acta Metall.* **35** 301 (1987)
73. Berezhkova G V et al. *Fiz. Tverd. Tela* **26** 1074 (1984)
74. Bobrov V S, Lebedkin M A *Fiz. Tverd. Tela* **35** 1881 (1993)
75. Lebyedkin M A et al. *Acta Mater.* **44** 4531 (1996)
76. Lebyodkin M A, Dunin-Barkovskiĭ L R *Zh. Eksp. Teor. Fiz.* **113** 1816 (1998) [*JETP* **86** 993 (1998)]
77. Akulov N S *Dislokatsii i Plastichnost'* (Dislocations and Plasticity) (Minsk: Izd. AN BSSR, 1961)
78. Orlov A N *Fiz. Met. Metalloved.* **20** 1338 (1965)
79. Webster G A *Philos. Mag.* **14** 1303 (1966)
80. Hahn G T *Acta Metall.* **10** 727 (1962)
81. Gillis P P, Gilman J J *J. Appl. Phys.* **36** 3380 (1965)
82. Bergstrom Y *Mater. Sci. Eng.* **5** 193 (1970)
83. Orlov A N *Fiz. Met. Metalloved.* **24** 817 (1967)
84. Holt D L *J. Appl. Phys.* **41** 3197 (1970)
85. Vladimirov B I, Pegel B *Phys. Status Solidi B* **56** K105 (1973)
86. Vladimirov V I, Kusov A A *Fiz. Met. Metalloved.* **39** 1150 (1975)
87. Vladimirov V I, Kusov A A *Fiz. Met. Metalloved.* **41** 951 (1976)
88. Malygin G A *Phys. Status Solidi B* **61** K45 (1974)
89. Malygin G A *Fiz. Met. Metalloved.* **40** 21 (1975)
90. Zorski H *Int. J. Solid Structures* **4** 959 (1968)
91. Meshcheryakov Yu I, Prokuratova E I, in *Fizicheskaya Mekhanika* Vyp. 2 (Physical Mechanics) Vol. 2 (Leningrad: Izd. LGU, 1976) p. 118

92. Malygin G A, in *Tezisy Vsesoyuznoĭ Konferentsii po Fizike Plastichnosti Kristallov* (These of All-Union Conference on Physics of Plasticity of Crystals) (Kharkov: FTINT AN USSR, 1976) p.61
93. Khannanov Sh Kh *Fiz. Met. Metalloved.* **46** 708 (1978)
94. Likhachev V A, Volkov A E, Shudegov V E *Kontinual'naya Teoriya Defektov* (Continuum Theory of Defects) (Leningrad: Izd. LGU, 1986)
95. Bottani C E, in *Mechanical Properties and Behaviour of Solids: Plastic Instabilities* (Eds V Balakrishnan, C E Bottani) (Singapore: World Scientific, 1986) p. 169
96. Bottani C E *Nuovo Cimento* **11** 865 (1989)
97. Meshcherayakov Yu I, Prokuratova E I *Int. J. Solid Structures* **32** 1711 (1995)
98. Nicolis J, Prigogine I *Self-Organization in Non-Equilibrium Systems: From Dissipative Structures to Order Through Fluctuations* (New York: Wiley, 1977) [Translated into Russian (Moscow: Mir, 1979)]
99. Haken H *Synergetics* (Berlin: Springer-Verlag, 1978) [Translated into Russian (Moscow: Mir, 1980)]
100. Swift J, Hohenberg P C *Phys. Rev. A* **15** 319 (1977)
101. Zhabotinskiĭ A M *Kontsentratsionnye Avtokolebaniya* (Concentration Self-Oscillations) (Moscow: Nauka, 1974)
102. Meinhardt H *Models of Biological Pattern Formation* (New York: Academic Press, 1982)
103. Belintsev B N, Livshits M A, Volkenstein M V *Z. Phys. B* **44** 345 (1981)
104. Belintsev B N *Usp. Fiz. Nauk* **141** 55 (1983) [*Sov. Phys. Usp.* **26** 775 (1983)]
105. Aifantis E C, in *The Mechanics of Dislocations. Proc. Int. Symp.* (Eds E C Aifantis, J P Hirth) (Ohio: ASM Metals Park, 1985) p. 127
106. Walgraef D, Aifantis E C *Int. J. Eng. Sci.* **23** 1351 (1985)
107. Aifantis E C *Mater. Sci. Eng.* **81** 653 (1986)
108. Kubin L P, Lepinoux J, in *Strength of Metals and Alloys Proc. of the Int. Conf., Timpere, Finland, 1988* (ICSMA-8) (Eds P O Kettunen, T K Leppisto, M E Lehtonen) (Oxford: Pergamon Press, 1989) p. 35
109. Zasimchuk E E, in *Kooperativnye Deformatsionnye Protsessy i Lokalizatsiya Deformatsii* (Cooperative Deformation Processes and Localization of Deformation) (Kiev: Naukova Dumka, 1988) p. 58
110. Krupkin P L et al. *Fiz. Met. Metalloved.* **66** 979 (1988)
111. Aifantis E C *Nonlinear Phenomena in Material Science* (Eds G Martin, L Kubin) *Solid State Phenomena* **23/24** 355 (1992)
112. Kubin L P, in *Material Sci. and Technol.* Vol. 6 (Ed. H Mughrabi) (GRG: VCH-Weinberg, 1993) p. 138
113. Malygin G A *Fiz. Tverd. Tela* **37** 3 (1995)
114. Walgraef D, Aifantis E C *J. Appl. Phys.* **58** 688 (1985)
115. Schiller C, Walgraef D *Acta Metall.* **36** 563 (1988)
116. Malygin G A *Fiz. Tverd. Tela* **31** 43 (1989)
117. Malygin G A *Fiz. Met. Metalloved.* **6** 33 (1991)
118. Nagornykh S N, Sarafanov G F *Metallofizika* **13** (9) 93 (1991)
119. Malygin G A *Fiz. Tverd. Tela* **31** 43 (1989)
120. Malygin G A *Fiz. Tverd. Tela* **32** 1102 (1990)
121. Gaĭkov A L, Romanov A E *Fiz. Tverd. Tela* **33** 2772 (1991)
122. Nagornykh S N, Sarafanov G F *Metallofizika* **14** (5) 67 (1992)
123. Khannanov Sh Kh *Fiz. Met. Metalloved.* **74** (4) 34 (1992) [*Phys. Met. Metallogr.* **74** (4) 334 (1992)]
124. Malygin G A *Fiz. Met. Metalloved.* (7) 16 (1991)
125. Khannanov Sh Kh *Fiz. Met. Metalloved.* **49** 59 (1980)
126. Vladimirov V I, Romanov A E, in *Kooperativnye Deformatsionnye Protsessy i Lokalizatsiya Deformatsii* (Cooperative Deformation Processes and Localization of Deformation) (Kiev: Naukova Dumka, 1988) p. 101
127. Birkovskiĭ A A, Romanov A E *Fiz. Tverd. Tela* **33** 1589 (1991)
128. Romanov A E *Mater. Sci. Forum* **123/125** 617 (1993)
129. Kossecka E, de Wit R *Arch. Mech.* **29** 633 (1977)
130. Kossecka E, de Wit R *Arch. Mech.* **29** 749 (1977)
131. Clem J R *Phys. Rev. B* **26** 2463 (1982)
132. Savel'ev S E, Fisher L M, Yampol'skiĭ V A *Zh. Eksp. Teor. Fiz.* **112** 936 (1997) [*JETP* **85** 507 (1997)]
133. Vinen W F *Proc. R. Soc. London Ser. A* **240** 443 (1957)
134. Nemirovskii S K *Rev. Mod. Phys.* **67** 37 (1992)
135. Klimontovich Yu L *Kineticheskaya Teoriya Neideal'nogo Gaza i Neideal'noĭ Plazmy* (Kinetic Theory of Nonideal Gas and Nonideal Plasma) (Moscow: Nauka, 1975) [Translated into English (Oxford: Pergamon Press, 1982)]
136. Lifshitz E M, Pitayevskiĭ L P *Fizicheskaya Kinetika* (Physical Kinetics) (Moscow: Nauka, 1979) [Translated into English (Oxford: Pergamon Press, 1981)]
137. Shelest A V *Metod Bogolyubova v Dinamicheskoĭ Teorii Kineticheskikh Uravneniĭ* (Method of Bogolyubov in the Dynamical Theory of Kinetic Equations) (Moscow: Nauka, 1990)
138. Klimontovich Yu L *Usp. Fiz. Nauk* **158** 59 (1989) [*Sov. Phys. Usp.* **32** 416 (1989)]
139. Khannanov Sh Kh *Fiz. Met. Metalloved.* **74** (4) 34 (1992) [*Phys. Met. Metallogr.* **74** (4) 334 (1992)]
140. Sarafanov G F *Fiz. Tverd. Tela* **39** 1575 (1997)
141. Malygin G A *Fiz. Tverd. Tela* **38** 2418 (1996)
142. Kunin I A "Teoriya Dislokatsiĭ" (Theory of Dislocations), in Skhouten Ya A *Tenzornyĭ Analiz dlya Fizikov* (Tensor Analysis for Physicists) (Moscow: Nauka, 1965) p. 373
143. Wiedersich H *J. Appl. Phys.* **33** 854 (1962)
144. Orlov A N, Perevesentsev V N, Smirnov B I *Phys. Status Solidi A* **32** 351 (1975)
145. Gilman J J *Philos. Mag. A* **76** 329 (1997)
146. Appel F, Betghe H, Messerschmidt U *Phys. Status Solidi A* **42** 61 (1977)
147. Appel F et al. *Mater. Sci. Eng.* **56** 211 (1982)
148. Smirnov B I *Dislokatsionnaya Struktura i Uprochnenie Kristallov* (Dislocation Structure and Strengthening of Crystals) (Leningrad: Nauka, 1981)
149. Klyavin O V *Fizika Plastichnosti Kristallov pri Gelievykh Temperaturakh* (Physics of Plasticity of Crystals at Helium Temperatures (Moscow: Nauka, 1987)
150. Reid C N, Gilbert A, Rosenfield A K *Philos. Mag.* **12** 409 (1965)
151. Popov L E, Kobytev V S, Kovalevskaya T A *Plasticheskaya Deformatsiya Splavov* (Plastic Deformation of Alloys) (Moscow: Metallurgiya, 1984)
152. Appel F *Philos. Mag. A* **63** 71 (1991)
153. Miura Y, Higuchi F *Philos. Mag. A* **71** 1363 (1995)
154. Zimkin I N et al. *Fiz. Tverd. Tela* **22** 852 (1980)
155. Thorton P R, Mitchell T E, Hirsch P *Philos. Mag.* **7** 337, 1349 (1962)
156. Basinski S J, Basinski Z S, in *Dislocation in Solids* Vol. 4 (Ed. F R N Nabarro) (Amsterdam: North-Holland, 1979) p. 263
157. Kocks U F *J. Eng. Mater. Tech.* (ASME-H) **98** 76 (1976)
158. Estrin Y, Mecking H *Acta Metall.* **32** 57 (1984)
159. Malygin G A *Fiz. Tverd. Tela* **29** 2067 (1987)
160. Malygin G A *Phys. Status Solidi A* **119** 423 (1990)
161. Vladimirova G V, Malygin G A, Ryvkina D G *Fiz. Met. Metalloved.* **67** 380 (1989)
162. Malygin G A *Fiz. Tverd. Tela* **34** 2882 (1992)
163. Malygin G A *Fiz. Tverd. Tela* **34** 3200 (1992)
164. Malygin G A *Fiz. Tverd. Tela* **35** 1604 (1993)
165. Gil Sevillano J, Aernoudt E *Prog. Mater. Sci.* **25** (2/4) 69 (1980)
166. Rybin V V *Bol'shie Plasticheskie Deformatsii i Razrushenie* (Large Plastic Deformations and Fracture) (Moscow: Metallurgiya, 1986)
167. Gil Sevillano J, Aernoudt E *Mater. Sci. Eng.* **86** 351 (1987)
168. Aernoudt E, Gil Sevillano J, Van Houtte "Constitutive Relations and their Physical Basis", in *Proc. 8th Int. Symp. on Metallurgy and Mater. Sci.* (Eds S I Andersen et al.) (Ris, Denmark, 1987) p. 1
169. Rollet A D, Kocks U F, Doherty R D, in *Formability and Metallurgical Structure* (Eds A K Sachdev, J D Embury) (Warrendale, PA: The Society, 1987) p. 211
170. Zehetbauer M, Trattner D, in *Strength of Metals and Alloys* (ICSMA-7) (Eds H J McQueen et al.) (Oxford: Pergamon Press, 1986) p. 105
171. Zehetbauer M, Seumer V *Acta Metall. Mater.* **41** 577, 589 (1989)
172. Haasen P *J. Phys.* (Paris) **50** 2445 (1989)
173. Zehetbauer M et al. *Phys. Status Solidi A* **151** 305 (1995)
174. Kassner M E et al. *Acta Metall. Mater.* **42** 3223 (1994)
175. Hansen N, Hughes D A *Phys. Status Solidi B* **149** 155 (1995)
176. Malygin G A *Fiz. Tverd. Tela* **35** 1328 (1993)
177. Malygin G A *Fiz. Tverd. Tela* **35** 1698 (1993)
178. Argon A S, Brydges W T *Philos. Mag.* **18** 817 (1968)
179. Man J, Holzmann M, Vlach B *Phys. Status Solidi* **19** 543 (1967)
180. Nabarro F R N, in *Strength of Metals and Alloys* (ICSMA-7) Vol. 3 (Eds H J McQueen et al.) (Oxford: Pergamon Press, 1986) p. 1667

181. Lebedev A B *J. Phys. IV* Coll. **C8** 325 (1996)
182. Franzbecker W *Phys. Status Solidi* **57** 545 (1973)
183. Mecking H, Bulian G *Acta Metall.* **24** 249 (1976)
184. Mecking H, Lucke K *Z. Metallkd.* **60** 185 (1969)
185. Conrad H *Acta Metall.* **11** 75 (1963)
186. Al-Haidary J T, Petch N J, Rios E R *Philos. Mag. A* **47** 869 (1983)
187. Narutani T, Takamura J *Acta Metall. Mater.* **39** 2037 (1991)
188. Mitchell T E, Foxall R A, Hirsch P B *Philos. Mag.* **8** 189 (1963)
189. Mitchell T E, Spitzig W A *Acta Metall.* **13** 1169 (1965)
190. Kramer I R *Adv. Mech. Phys. Surface* **3** 109 (1986)
191. Nabarro F R N, in *Surface Effects in Crystal Plasticity* (NATO Advanced Study Institutes Series, Ser. E, no 17, Eds R M Latanision, J T Fourie) (Leyden: Noordhoff, 1977) p. 49
192. Belikov A M et al. *Plasticheskaya Deformatsiya Nitevidnykh Kristallov* (Plastic Deformation of Whiskers) (Voronezh: Izd. VGU, 1991)
193. Iskanderova Z A, Radzhapov T D, Rakhimova G R *Poverkhnost* (8) 5 (1992)
194. Suzuki H, Ikeda S, Takeuchi S *J. Phys. Soc. Jpn.* **11** 382 (1956)
195. Kramer I R, Demer L J *Prog. Mater. Sci.* **9** 131 (1961)
196. Kramer I R, Podlaseck S *Acta Metall.* **11** 70 (1963)
197. Wu L, Smoluchovski R *Phys. Rev.* **78** 468 (1950)
198. Lohne O *Phys. Status Solidi A* **25** 709 (1974)
199. Kolkman H J *Scr. Metall.* **8** 45 (1974)
200. Neuhauser H, in *Dislocation in Solids* Vol. 6 (Ed. F R N Nabarro) (Amsterdam: North-Holland Publ., 1983) p. 319
201. Basinski Z S, Basinski S J *Philos. Mag.* **9** 51 (1964)
202. Rosi F D, Mathewson C H *Trans. AIME* **188** 1159 (1950)
203. Mendelson S *J. Appl. Phys.* **33** 2175, 2182 (1962)
204. Mitchell J W *Phys. Status Solidi A* **135** 455 (1992)
205. Indenbom V L *Kristallografiya* **42** 3985 (1994)
206. Kleiser Th, Bocek M *Z. Metallkd.* **77** 582 (1986)
207. Gil Sevillano J I, Bouchaud E *Scr. Metall. Mater.* **25** 355 (1991)
208. Teplyakova L A, Kunitsyna T S, Kozlov E V *Izv. Vyssh. Uchebn. Zaved. Fiz.* (4) 51 (1998)
209. Welzel G, Plessing J, Neuhauser H *Phys. Status Solidi A* **166** 791 (1998)
210. Hazzledine P M *Can. J. Phys.* **45** 765 (1967)
211. Khannanov Sh Kh *Fiz. Met. Metalloved.* **78** (2) 31 (1994) [*Phys. Met. Metallogr.* **78** (2) 142 (1994)]
212. Vettegren' V I, Rakhimov S Sh, Svetlov V N *Fiz. Tverd. Tela* **37** 913, 3635 (1995)
213. Vettegren' V I, Rakhimov S Sh, Svetlov V N *Fiz. Tverd. Tela* **39** 1560 (1997)
214. Vettegren' V I et al. *Fiz. Tverd. Tela* **40** 668 (1998)
215. Dubiec H *Scr. Metall.* **23** 1997 (1989)
216. Nikiforov A V, Klyavin O V *Fiz. Tverd. Tela* **38** 2744 (1996)
217. Smirnov B I, Orlova T S *Fiz. Tverd. Tela* **38** 2431 (1996)
218. Malygin G A *Fiz. Tverd. Tela* **41** 252 (1999)
219. Blewitt T A, Coltmann R R, Jamisson R E *J. Nucl. Mater.* **2** 277 (1960)
220. Okada A et al. *J. Nucl. Mater.* **115/157** (Part B) 1301 (1988)
221. Kitajima S, Shinodara K, Kurishita H *J. Nucl. Mater.* **108/109** 397 (1982)
222. Greenfield I G, Wilsdorf H G F *J. Appl. Phys.* **32** 827 (1961)
223. Seeger A *J. Phys. Soc. Jpn.* **18** 59 (1963)
224. Shin P W, Meshii M *J. Met.* **15** 80 (1963)
225. Mastel B et al. *J. Appl. Phys.* **34** 3637 (1963)
226. Hasson D F et al. *Metall. Trans.* **5** 374 (1974)
227. Suzuki M et al. *Philos. Mag. A* **64** 395 (1991)
228. Tucker R P, Wechsler M S, Ohr S M *J. Appl. Phys.* **40** 400 (1969)
229. Saka H et al. *Phys. Status Solidi A* **31** 139 (1975)
230. Okada A, Kanao K, Yoshii T *Trans. Jpn. Inst. Metal.* **30** 265 (1989)
231. Eyre B L, Bartlett A F *Philos. Mag.* **12** 261 (1965)
232. Mughrabi H, Strohle D, Wilkens M *Z. Metallkd.* **72** 300 (1981)
233. Mori T, Meshii M *Acta Metall.* **17** 167 (1969)
234. Bapna M S, Mori T, Meshii M *Philos. Mag.* **17** 177 (1968)
235. Bapna M S, Meshii M *Metal. Trans.* **3** 3205 (1972)
236. Bapna M S, Meshii M *Mater. Sci. Eng.* **16** 181 (1974)
237. Luft A et al. *Mater. Sci. Eng.* **20** 113 (1975)
238. Ritschel Ch, Luft A, Schulze D *Krist. Tech.* **13** 791 (1978)
239. Brenner B, Luft A *Mater. Sci. Eng.* **52** 2299 (1982)
240. Luft A *Prog. Mater. Sci.* **35** 91 (1991)
241. Bega R D et al. *Metallofizika* **2** (1) 71 (1980)
242. Dubovitskaya N V, Larikov L N, Zakharov S M *Fiz. Khim. Obrab. Mater.* (3) 39 (1979)
243. Dubovitskaya N V, Zakharov S M, Larikov L N *Fiz. Met. Metalloved.* **47** 659 (1979)
244. Dubovitskaya N V, Larikov L N *Fiz. Met. Metalloved.* **52** 891 (1981)
245. Luft A, Kaufmann H J, in *Proc. Symp. on the Structure and Properties of Crystal Defects, Liblice, Czecheslovakia, 1983* Vol. 1 (Amsterdam: Elsevier, 1984) p. 55
246. Malygin G A *Fiz. Nizk. Temp.* **5** 1338 (1979)
247. Malygin G A, Klyavin O V *Fiz. Tverd. Tela* **40** 1479 (1998)
248. Saada G, Washburn J *J. Phys. Soc. Jpn.* **18** 43 (1963)
249. Makin M J *Philos. Mag.* **10** 695 (1964)
250. Foremann A J, Sharp J V *Philos. Mag.* **19** 931 (1969)
251. Vladimirov V I, Kusov A A *Fiz. Met. Metalloved.* **43** 1127 (1977)
252. Vladimirov V I, Kusov A A *Fiz. Met. Metalloved.* **53** 367 (1982)
253. Zaiser M, Hahner P *Philos. Mag. A* **74** 287 (1998)
254. Malygin G A *Fiz. Tverd. Tela* **32** 3253 (1990)
255. Malygin G A *Fiz. Tverd. Tela* **33** 1069 (1991)
256. Sharp J W *Philos. Mag.* **16** 77 (1967)
257. Brimhall J L, Mastel B *Appl. Phys. Lett.* **9** 127 (1966)
258. Brimhall J L *Trans. Metall. Soc. AIME* **233** 1737 (1965)
259. Noskova N I et al. *Fiz. Met. Metalloved.* **64** 554, 583 (1987)
260. Malygin G A *Fiz. Tverd. Tela* **33** 1855 (1991)
261. Malygin G A *Latvian J. Phys. Tech. Sci.* (4) 23 (1991)
262. Malygin G A *Fiz. Tverd. Tela* **34** 3605 (1992)
263. Johnson E, Hirsch P B *Philos. Mag. A* **43** 150 (1981)
264. Voce E *J. Inst. Metals* **74** 537 (1948)
265. Seeger A, Berner R, Wolf H *Z.Phys.* **155** 247 (1959)
266. Bassim M N, Kuhlmann-Wilsdorf D *Phys. Status Solidi A* **17** 379 (1973)
267. Hansen H, Kuhlmann-Wilsdorf D *Mater. Sci. Eng.* **81** 141 (1986)
268. Kratochvil J *Scr. Metall.* **24** 891 (1990)
269. Amodeo R J, Ghoniem N M *Phys. Rev. B* **41** 6968 (1990)
270. Malygin G A *Fiz. Met. Metalloved.* (5) 22 (1990)
271. Malygin G A *Fiz. Met. Metalloved.* (11) 46 (1990)
272. Malygin G A, in *Strukturnaya i Khimicheskaya Mikroneodnorodnost' v Materialakh* (Structural and Chemical Microinhomogeneity in Materials) (Kiev: Naukova Dumka, 1991) p. 44
273. Malygin G A *Fiz. Tverd. Tela* **33** 3267 (1991)
274. Koneva N A, Kozlov E V *Izv. Vyssh. Uchebn. Zaved. Fiz.* (2) 89 (1990)
275. Schlagowski U et al. *Acta Metall.* **36** 865 (1988)
276. Prinz F, Argon A S *Phys. Status Solidi A* **57** 741 (1980)
277. Tabata T, Yamanaka Sh, Fujita H *Acta Metall.* **26** 405 (1978)
278. Gindin I A, Starodubov Ya D, Aksenov V K *Metallofizika* (2) 49 (1980)
279. Knoesen D, Kritzinger S *Acta Metall.* **30** 1219 (1982)
280. Rubtsov A S, Rybin V V *Fiz. Met. Metalloved.* **44** 611 (1977)
281. Kornienko L A, Bakach G P, Dudarev V F *Plasticheskaya Deformatsiya Splavov* (Plastic Deformation of Alloys) (Tomsk: Izd. TGU, 1986)
282. Malygin G A *Fiz. Met. Metalloved.* (7) 16 (1991)
283. Malygin G A *Fiz. Tverd. Tela* **31** 298 (1989)
284. Langford G, Kohen M *Trans. Quart. ASM* **62** 623 (1969)
285. Staker M R, Holt D L *Acta Metall.* **20** 569 (1972)
286. Keh A S *Philos. Mag.* **12** 9 (1965)
287. Kuhlmann-Wilsdorf D *Mater. Sci. Eng.* **55** 29 (1982)
288. Mughrabi H A *Mater. Sci. Eng.* **85** 15 (1987)
289. Thompson A W, Baskes M I, Flanagan W F *Acta Metall.* **21** 1017 (1973)
290. Ikeda S *J. Phys. Soc. Jpn.* **27** 1564 (1969)
291. Guyot P, Raynaud G M *Acta Metall.* **39** 317 (1991)
292. Brovkov V A et al. *Fiz. Met. Metalloved.* **64** 1183 (1987)
293. Fujita H, Tabata T *Acta Metall.* **21** 355 (1973)
294. Malygin G A *Fiz. Tverd. Tela* **33** 3267 (1991)
295. Khannanov Sh Kh *Fiz. Met. Metalloved.* **49** 715 (1980)
296. Khannanov Sh Kh *Fiz. Met. Metalloved.* **84** (3) 12 (1997) [*Phys. Met. Metallogr.* **84** (3) 208 (1997)]
297. Tsai C T, Yao M W, Chait A *J. Cryst. Growth* **125** 69 (1992)
298. Moosbrugger J C *Int. J. Plasticity* **11** 799 (1995)
299. Romanov A E et al. *Phys. Status Solidi B* **199** 33 (1997)